Politecnico di Milano

SCHOOL OF INDUSTRIAL AND INFORMATION ENGINEERING

Master of Science – Energy Engineering – Energy for Development (track)

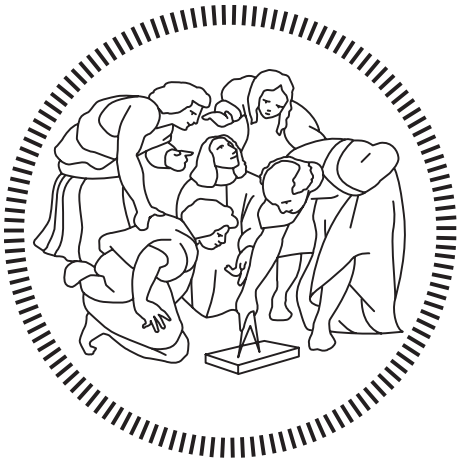

Assessment of the potential CO_2 geological storage capacity of saline aquifers under the North Sea

Supervisor

Professor M. J. Blunt

Candidate

Panagiotis KARVOUNIS – 912513

Academic Year 2020 – 2021

To my forever friend, who happens to have four legs.

AKNOWLEGMENTS

In the 7th century BC, Homer described the journeys of Odyssey from the war zone of Troy to its beloved country Ithaca. No matter the difficulties on the way, no matter, even, the destination, it is that very journey, the people that accompany you, the experiences you gain, the endless hours of mental and physical interactions that you spend, this is what is of outmost importance. After three years in Politecnico di Milano, I can relate with Odyssey. I don't know yet where the next stop will be, what I can tell for now, is that I met incredible people, I came across a tremendous amount of knowledge and I 've learnt to appreciate more my companions to this journey. I owe a special 'thank you' to my supervisor and mentor, professor Blunt, that has spent countless hours reviewing my thesis, correcting my paper drafts and most of all providing rivers of knowledge. At this point, I want to say that, apart from friends and family that played a vital role in the fulfilment of this master, I owe this successful trip to my forever compañera, Sofia. It is this bright spirit of determination and joyfulness that keeps inspiring me for the days to come. A final gratitude to all my fellows in the university, as without their support, this dream would have never been completed (in time).

Karvounis Panagiotis, Milano, 2021

SOMARIO

L'ampio sfruttamento delle risorse della terra, insieme all'aumento dell'attività industriale e alla crescita della popolazione negli ultimi decenni, ha portato a un rapido aumento dell'anidride carbonica rilasciata nell'atmosfera. Ciò è associato all'aumento della temperatura in diverse parti del mondo che porta a un grave cambiamento climatico che dovrebbe influenzare la vita umana e la biodiversità del pianeta. Per mitigare molti di questi effetti, possono essere adottate diverse misure che riducano la dipendenza dai combustibili fossili e promuovano lo sviluppo sostenibile nei prossimi decenni. La cattura e il sequestro del carbonio è una di tali misure che riduce l'impronta di carbonio dell'attività umana poiché la CO_2 emessa dall'industria viene raccolta, trasportata e infine depositata nel sottosuolo. Sebbene tutti i passaggi secondari di questo processo siano importanti, la parte vitale è la selezione di un sito di stoccaggio adeguato, sia per motivi di sicurezza, ma anche in termini di capacità. In questo studio vengono analizzati potenziali siti di stoccaggio nel sottosuolo del Mare del Nord, al fine di ottenere una stima della capacità di stoccaggio di CO_2 disponibile. Sono analizzati in totale 441 siti in cinque paesi (Regno Unito, Danimarca, Norvegia, Paesi Bassi e Germania), in termini di caratteristiche geofisiche e capacità potenziale. Il modo più comune per stimarlo è un approccio basato sul volume, cioè basato sullo spazio poroso disponibile della roccia, che produce una soluzione sovrastimata a causa del fatto che non viene considerato l'accumulo di pressione. Pertanto, in questo studio, l'aumento di pressione in ciascun pozzo di iniezione è il fattore limitante della velocità di iniezione e la capacità di stoccaggio viene rilevata in base al numero di pozzi che possono essere collocati in ciascun potenziale sito di stoccaggio. I siti di stoccaggio designati considerati sono terreni di petrolio e gas esauriti che il livello di conoscenza delle caratteristiche geofisiche è adeguato, così come altre formazioni che includono Bunter, Brent e altri. Lo studio ha rivelato un enorme potenziale di stoccaggio di CO_2 che si avvicina a 440 Gt con un possibile tasso di iniezione di 22 000 Mt yr-1. Il Regno Unito può immagazzinare potenzialmente più di 230 Gt di CO_2 in 30 anni, un valore 20 volte superiore alle sue emissioni attuali, mentre le stesse scale valgono per i Paesi Bassi con un potenziale di 147 Gt di CO_2. I tredici terreni di petrolio e gas esaminati in Danimarca sono in grado di immagazzinare circa 4 Gt di CO2 in tre decenni a un tasso di 127 Mt anno-1 coprendo più del doppio delle attuali emissioni della nazione, mentre la Norvegia può immagazzinare 48 Gt solo in 10 grandi falde acquifere saline del Mare del Nord. Tali risultati ci forniscono un risultato chiaro, nonostante le potenziali incertezze ed errori sulla raccolta e manipolazione dei dati, l'applicazione estensiva dello stoccaggio geologico dell'anidride carbonica, ha la capacità non solo di mettere la CO2 nel sottosuolo riducendo l'impronta di carbonio dell'attività umana, ma ci fornirà il tempo essenziale per attuare pienamente altre strategie di mitigazione che evitino l'aumento della temperatura di oltre 1,5 oC nel prossimo decennio e, con esso, le implicazioni del cambiamento climatico.

Parole chiave

Cattura del carbonio chiave, Deposizione geologica, Cambiamento climatico, Capacità di stoccaggio

CONTENTS

LIST OF TABLES

LIST OF FIGURES

ABSTRACT

Extensive exploitation of earth's resources along with increased industrial activity and population growth in the past decades has led to a rapid rise of the carbon dioxide released in the atmosphere. This is associated with temperature increases in several parts of the world leading to severe climate change that is expected to affect human life and biodiversity of the planet. To mitigate several of such effects, different measures can be adopted that reduce dependency on fossil fuels and foster sustainable development in the forthcoming decades. Carbon capture and sequestration is one of such measures that reduces the carbon footprint of human activity as the CO_2 emitted from the industry is collected, transported and eventually deposited in the subsurface. Though all the sub steps of this process are important, the most vital part is the selection of a proper storage site, both for safety reasons but in terms of capacity as well.

In this study, potential storage sites in the subsurface of North Sea are analyzed, in order to retrieve an estimation of the available CO_2 storage capacity. In total 441 sites in five countries (United Kingdom, Denmark, Norway, Netherlands and Germany) are analyzed in terms of geophysical characteristics and potential capacity. The most common way to estimate it is a volume-based approach, that is based on the available pore space of the rock, that produces an overestimated solution due to the fact that no pressure build up is considered. Therefore, in this study, pressure increase in each injection well is the limiting factor of the injection rate and storage capacity is found according to the number of wells that can be placed in each potential storage site. The designated storage sites considered, are depleted oil and gas fields that the level of knowledge of the geophysical characteristics is adequate, as well as other formations that include Bunter, Brent and others. The study reviled a tremendous potential of CO_2 storage approaching 440 Gt with a possible injection rate of 22 000 Mt yr^{-1}. United Kingdom can potentially store more than 230 Gt of CO_2 over 30 years, a value 20 times higher than its current emissions, while same scales apply for Netherlands with 147 Gt CO_2 potential. The thirteen oil and gas fields examined in Denmark are able to store around 4 Gt of CO_2 in three decades in a rate of 127 Mt yr^{-1} covering more than twice the current emissions of the nation, while Norway can store 48 Gt only in 10 large saline aquifers of North Sea. Such results, provide us with a clear outcome, despite the potential uncertainties and errors on the data collection and manipulation, extensive application of carbon dioxide geological storage, has the ability not only to put CO_2 underground reducing the carbon footprint of human activity, but it will provide us with essential time to fully implement other mitigation strategies that avert the temperature increase more than 1.5 ^oC in the next decade and with it, the implications of climate change.

Keywords

Carbon Capture, Geological Deposition, Climate Change, Storage Capacity

EXTENDED SUMMARY

Are renewable sources of energy, electrification of end uses, consumption reduction and cutback of fossil fuel dependency, enough to avert the planet entering the vicious cycle of climate change? If true, what is the time span essential for such transformation and are there any other mitigation techniques that will buy us time for the above much needed social and technological switch? In this case, the solution is literally lying beneath our feet. In the next few pages, I will guide you through the concept of carbon capture and geological deposition and highlight its importance and role in reducing the concentration of CO_2 in the atmosphere. Then, we will go deeper and in fact, several kilometers below the surface, to assess the quantity of CO_2 that can be stored as well as the best way to do so. This report, presents a first order estimation of the potential storage capacity in several designated saline aquifers of North Sea and what does this mean in terms of carbon dioxide removed from the ambient and stored in subsurface. Last but not least, a benchmark is done with the current emissions of the associated nations those saline aquifers belong to. But first things first.

We find ourselves in the first quarter of 2021, six years after the COP15 and the unanimous adoption of the Paris Agreement's set of seventeen sustainable development goals, SDGs. These SDGs bind the nations to adopt certain measures to mitigate climate change, in order for the planet to avert a temperature increase of more than 1.5 ^{o}C by 2050. Despite a small regression due to the pandemic, carbon dioxide emissions keep increasing annually and are expected to reach 35 Gt of CO_2 in 2022. Since the signing of the Paris accord, renewable sources have increased their penetration in the national and European energy mix from 9% on average in 2004 to 20% in 2020. On top of that, worldwide energy consumption is still fossil fuel dominated with around 70% of the total energy coming from coal, oil and gas. Now, taking into account the population increase along with a greatest share of people getting access to electricity, the effort to reach the goals should be continued in a faster pace. It is true, that the energy sector is the most dominant one regarding CO_2 emissions. The energy use in industry alone is responsible for 24% of the associated carbon release while the transportation and buildings sector contribute accordingly. With existing measures in place EU is very far away of reaching the short-term target of 40% reduction by 2030 and even further from the near-neutrality in 2050. On top of that, fossil fuel extraction, at an international level, has been merely constrained so far while future projections demonstrate that, a continuation of such unconstrained extraction of earth's natural resources, will lead in the consumption of the available carbon budget two decades earlier than supposed. But it is not all black. Climate change mitigation strategies are being implemented throughout the world, with countries taking measures to reduce the carbon intensity of their productive activities and inform people of the potential risks. To be honest though, the pace of this essential transformation is smaller than the circumstances require. Therefore, the international community has started to appreciate the benefits of carbon capture and storage, CCS, a mitigation strategy with a binary nature. It is not only assisting in the reduction of concentration of CO_2 in the environment, but secures much needed time in the implementation of other measures that would avert global warming. CCS requires a few steps in order to be conducted properly and maximum results are obtained. First step is the carbon capture from the source. It is done using cyclone filters at the outlet of the exhaust gas stream that capture a percentage of the carbon dioxide under a chemical reaction. Other than that, recently, other techniques are used to directly capture CO_2 from the

ambient with the use of large fans. As soon as CO_2 is captured, it is required to be transported to the injection facility. Transportation takes place using pipelines and/or ships. Using a pipeline network, not only is cheaper but less carbon intensive, reducing the overall environmental footprint of the process, therefore it is essential for the carbon capture to take place in a relatively short distance from the injection facility. In Europe, industrial activity has been traditionally placed in the north. The Netherlands, Germany, Belgium, Denmark and the United Kingdom were among the leaders and with it, comes greenhouse emissions. An effective storage site, in terms of vicinity to the sources would be the North Sea. But is any kind of geological formation capable to store CO_2? Can we just drill and inject anywhere and at any rate?

The North Sea covers a massive area bounded by the national waters of several countries. To properly assess the amount of CO_2 able to be stored in a certain rock type and place, we need to be aware of several of its geophysical characteristics. Moving into the subsurface and several kilometers below sea level, the acquisition of such data comes with great uncertainties. The way to retrieve information about rocks porosity, permeability, and other important values, is through log (downhole) measurements at several locations in a bounded area. These are able to provide us with a range of values that in most cases have to be rounded in a single one, in order to perform calculations. Apart form saline aquifers, that refer to a number of sedimentary rock types saturated with brine, potential storage sites can be depleted oil and gas fields but also functioning ones. The latter come with the advantage that, geophysical characteristics of the rock are well known, as they were previously operated for several years. Before continuing with the ways to calculate the capacity of an aquifer or oil and gas field, I would like to stress out another interesting way to utilize captured CO_2. The extraction industry, end specifically the oil and gas sector, are able to use large amounts of CO_2 in a process called Enhanced Oil Recovery by injecting them in the subsurface and enable greater production as the fluid displaces the hydrocarbons trapped in the pore spaces of the rock. This technique is used as a last step before abandoning the field and enables the recovery of 50-70%.

To conduct a proper assessment of the storage capacity in a designated field, we need a set of parameters to be determined beforehand. Data about the shallowest and mean depth of the reservoir, its thickness and its total area are essential to determine the gross rock volume while permeability, porosity, rock compressibility and pore pressure assist in the illustration of rock characteristics. Apart from those, CO_2 properties (density and viscosity) may vary in subsurface but for the shake of competency we considered them constant. In a number of studies encountered in the international literature, capacity is a linear function of gross rock volume implying that all void space in a rock can be filled with CO_2. Such methodology usually overestimates the potential capacity as it doesn't include any pressure build up in the reservoir. In this report a new methodology of estimating storage volume is considered, taking into consideration the plume pressure at each injection well. Especially in closed reservoirs or saline aquifers, as the injected fluid displaces brine from the pore space, the pressure dissipation is really slow resulting in rapid pressure build up and therefore small capacities. The ultimate storage capacity is estimated using the maximum injection rate of each well, which is a function of pressure increase and technological constraints. The software created, results a number of scenarios of injection rate and inter-well distances (which then is used to determine the number of wells in the designated area of the reservoir) and picks the optimal one.

In total 441 potential storage sites were analyzed in the North Sea territory, covering both saline aquifers, oil and gas fields. The fields were listed based on the national boundaries belonging at. In United Kingdom, 154 fields were considered 71 of which are saline aquifers belonging in the Bunter sandstone, Chalk and Brent formations as well as others, while the rest are oil and gas fields. Results demonstrated an enormous potential of capacity with a total of 238 Gt of CO_2 in a 30-year span. This corresponds to approximately 8000 Mt per year injection rate, a number almost twenty times higher than the annual emissions of the country. Enormous saline aquifers of Bunter sandstone are able to store alone more than 100 Gt of CO_2 using 1340 wells, while the average efficiency is close to 4% in all the fields studied ranging from 3.6% (chalk formations) to 4.4% (oil & gas fields). In Denmark, thirteen oil and gas fields are able to store 3.8 Gt of CO_2 with an average of 127 Mt per year employing around 35 wells and under 2.0% efficiency, while in this way, Denmark can offset more than two times its annual emissions. In Norway, ten massive saline aquifers were analyzed proving the capability to store around 48 Gt of CO_2 in 30 years using 450 wells and under 2.7% efficiency and therefore placing underground thirty-six times its annual emissions. It is worth clarifying, that this amount refers only to saline aquifers and doesn't take into account any oil and gas fields, which are many due to the increased extraction activity of the country. In the Netherlands, a huge number of 247 oil and gas fields, depleted or not, were examined resulting in 147 Gt of CO_2 employing 1440 injection wells and on average of 4.0% efficiency. Under that results, a country with a great environmental footprint, due to its industrial activity, can offset more than thirty times its current emissions by putting around 5000 Mt of CO_2 underground, per year. In German territory, only three fields were examined, due to the lack of available data, including two Bunter sandstone formations and the Mittelplate oil field. The total capacity estimated under the implementation of 14 wells, is 1.6 Gt of CO_2.

Even considering the great uncertainties we face in the studies, due to scarce availability of solid data sources, it is more than clear, that carbon capture and geological sequestration is a powerful weapon in the battle against global warming. For instance, the Northern Lights project in Norway is a fully functioning CCS facility that provides the scientific community with information about the proper function and monitoring of a storage project. The European Union, since 2009 has set the guidelines of implementation of large-scale CCS initiatives within its territory, by publishing the directive for carbon capture and storage (DIRECTIVE 2009/31/EC) that provides essential guidelines in order for such projects to become reality, urging the 27 nations to initiate studies and evaluate their storage capacity potential. Ultimately, after this introduction, we can draw the conclusion, that CCS has the capacity to assist us in the, so called, sustainable transition, and avert the planet entering the uncharted waters of climate change. Following in the text, all the topics touched before, are going to be discussed in more detail, and give a better insight on the cause and effect of carbon dioxide geological sequestration, with attention paid in the software that enabled us conduct the study, the physical mechanisms that govern the porous scale environment as well as the results obtained.

Peer reviewed papers based on this project work-thesis

Panagiotis Karvounis, Martin J. Blunt, (2021), **Assessment of CO2 geological storage capacity of saline aquifers under the North Sea**. International Journal of Greenhouse Gas Control, *accepted publication*

ABREVIATIONS

CCS	Carbon Capture Storage
CCT	Carbon Capture Technology
EOR	Enhanced Oil Recovery
ETS	Emission Trading System
IEA	International Energy Agency
LNG	Liquefied Natural Gas
SDG	Sustainable Development Goals

OIL INDUSTRY ABREVIATIONS & CONVERSION FACTORS

Oilfield units	**Conversion Factor**	**SI units**
acres	4 046	square meters [m^2]
barrels	0.14	Tones
cubic feet [ft^3]	0.028	cubic meters [m^3]
darcy	0.98×10^{-12}	square meters [m^2]
feet [ft]	0.3	meters [m]

API	Oil gravity American Petroleum Institute degrees
bbl	Barrel
bcf	Billion cubic feet
GIIP	Gas initially in place
GOC	Gas – oil contact
GOR	Gas – oil ratio
mD	milli Darcie
scf	Standard cubic feet
STB	Stock tank barrel
STOIIP	Stock tank oil initially in place

INTRODUCTION

According to the Intergovernmental Panel for Climate Change (IPCC), human activities are estimated to have caused approximately 1.0 ^{o}C of global warming above pre-industrial levels. This amount is expected to reach 1.5 ^{o}C between 2030 and 2052 (Figure.1), with the continuation of current growth rates. This temperature increase is expected to lead to extreme natural phenomena including extensive droughts, hot days and cold nights near the equators and substantial sea level rise [1]. All the previous are accompanied by severe health issues to the human population and biodiversity loss.

At the Conference of the Parties (COP21) in Paris, 2015 all nations agreed for common action to combat temperature increase and therefore climate change. To that extent, several mitigation strategies have been proposed in literature for the past five years, and nations through the "Nationally Determined Contributions" (NDCs) have proposed their own goals to tackle climate change.

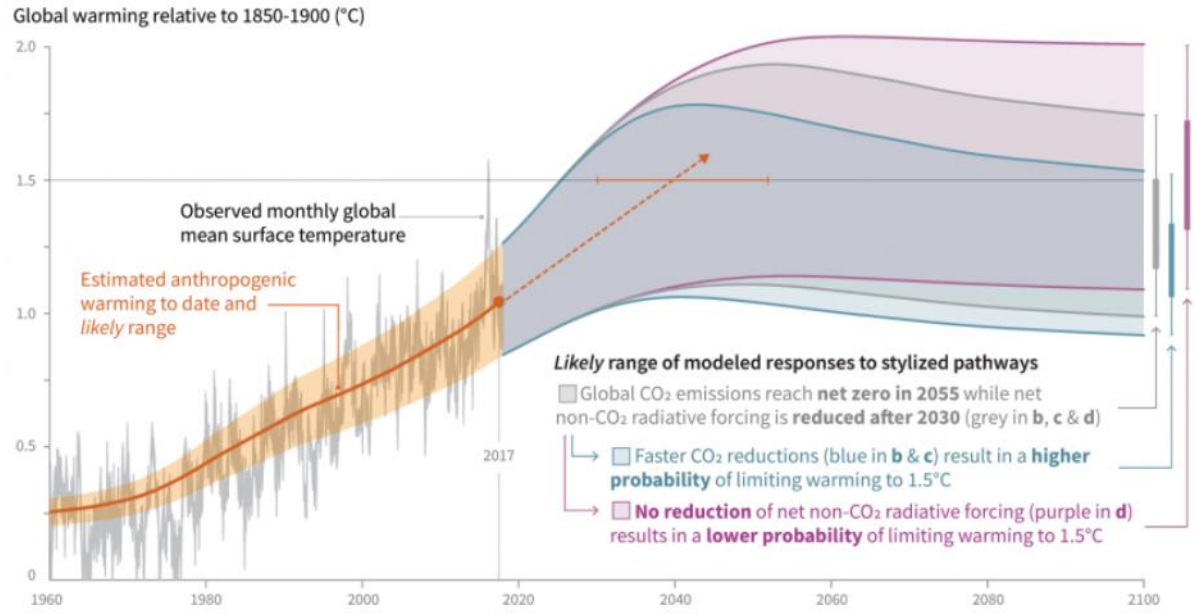

Figure 1.Global warming relative to pre-industrial levels – both past changes and projections under different scenarios [1]

According to the Shared Socioeconomic Pathways [2], an increase of two billion in the population is almost inevitable over the next few decades. According to such a scenario, demand for energy and other resources is projected to increase with a consequent increase in greenhouse gas emissions (Figure. 2 (left)). Considering the latter, greenhouse gas emissions, are expected to rise substantially [12], in all cases up until 2060 at least (Figure. 3), while carbon capture and sequestration is expected to be one of the game changers on the efforts to combat climate change. Even in the most pessimistic scenarios for the growth of emissions (SSP5, SSP2), CCS is well established with more than 5 Gt per year to be deposited underground in the next 50 years.

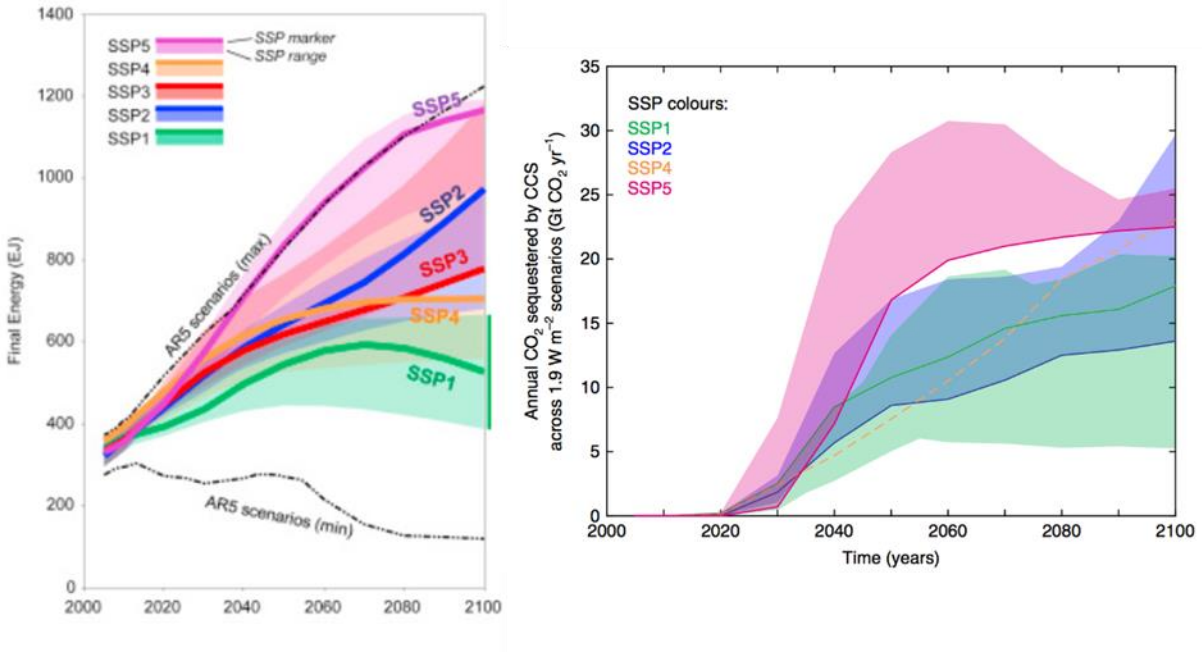

Figure 2. Total Final Energy demand according to the SSPs projections (left) and annual sequestration by carbon capture by 2100 (right) [2].

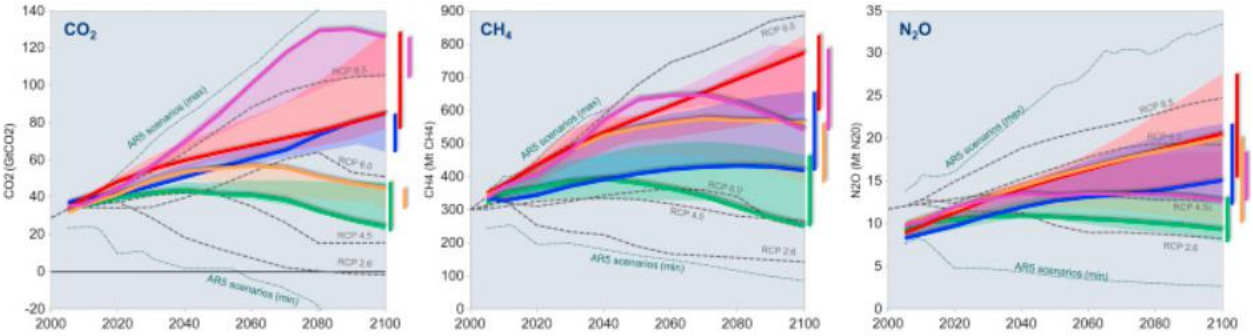

Figure 3. Greenhouse gas emissions under projected SSPs [2].

According to the International Energy Agency (IEA), the energy sector is expected to be one of the leading sources of carbon emissions, to cover constantly increasing demand [3] as more and more people are connected to the grid and developed nations keen to electrify end uses [4].

Carbon capture and storage is considered to play an important role in mitigating climate change effects [5]. In order to achieve the much-needed net zero CO_2 emissions by 2050, large amounts of CO_2 must be removed from the atmosphere and deposited underground. A first estimate from IEA, [6] suggests that carbon capture and sequestration accounts for 12% of the cumulative emissions reductions needed for carbon neutrality in the next three decades. This accounts for more than 100 Gt of CO_2 between 2016 and 2050, while under the Sustainable Development Scenario [7] this amount increases to 1300 Gt [8]. In the pre-pandemic context, CCS

was gaining momentum with 8 new projects to be announced in US and other 20 to be under development worldwide. Still, only 2 facilities are fully operating, with a cumulative capacity of 2.4 Gt far behind the targets.

Figure 4. Global CCS projects. With light blue representing the commercial projects with full carbon capture, transportation and storage, dark blue the pilot projects and red ones are designated as CCS hubs and are future projects.

Figure 4 is a representation of CCS projects around the world. From the twenty awarded facilities, two in North America are fully operating. The one in US is the Petra-Nova coal fired power plant with an average cost of carbon capture and utilization of $65/tonne of CO_2 a price 30% reduced compared to the Boundary Dam facility in Canada that has been operating since 2014. A recent study from the International CCS Knowledge Center [13], proposed that the CCS cost from a coal power plant is around $45/tonne CO_2. China, Japan and Korea, are among the adopters of CCS in Asia, that is masted from enormous coal-based power production, embedding them in their climate strategies for 2050.

The Covid-19 pandemic context paused a decade of development and deployment of CCS. Projects that have been scheduled to take off by 2020 were postponed and funding has also been postponed. However, from March up until October 2020, the prospects of CCS have been boosted by a series of new funding announcements [8]. The UK is among the most active, pledging almost a billion dollars for funding in CCS projects. The US government has awarded almost $200million in grants from April to September. Also, in September, the Norwegian government proposed $1.8billion plan to employ full scale CCS projects increasing the total investment to $2.7billion. The downturn of the oil prices is almost certain that will cause delays and cancelations in the private sector adoption and further investment on CCS. By May 2020, Petra-Nova CCS has halted the carbon capture scheme that fed with 1.4Mt per year to EOR processes in West Rach oil field in Houston. It is estimated that crude oil prices greater than $60/barrel are required to sustain operating and transportation costs.

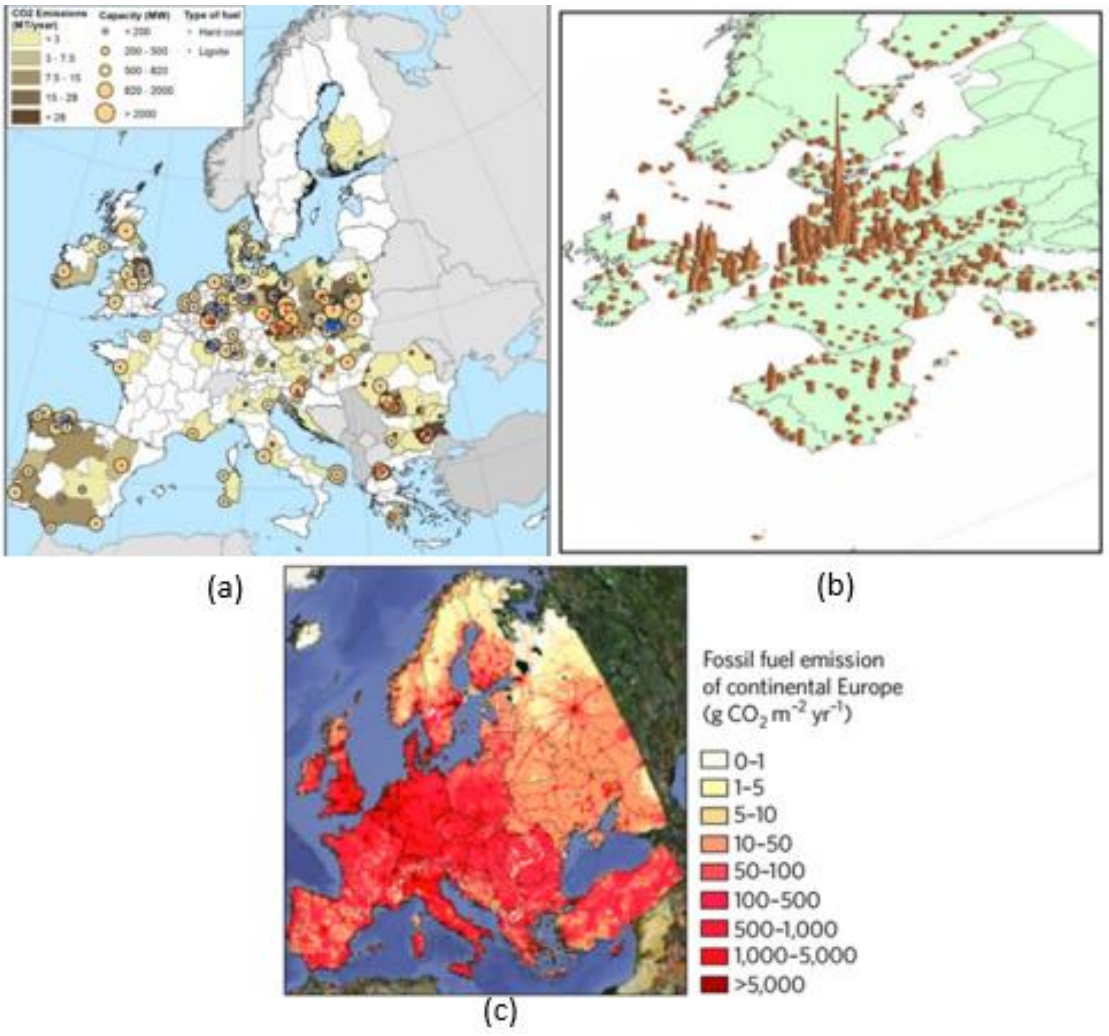

Figure 5. Point sources of CO2 emissions in Europe. Three maps showing the concentration of emissions in different metrics [9] for (a) [10] for (b), [11] for (c).

According to Figure 5, the main concentration of CO_2 emissions in Europe is observed in the northern part of the continent, in countries with increased industrial activity, with the UK, Germany, the Netherlands and Denmark possessing the lion's share. In the context of carbon capture and sequestration, such localization of emissions, requires proximal deposition options to minimize transportation costs. North Sea, provides adequate place for sequestration with its large aquifers that can absorb a great amount of the associated emissions.

This project is going to focus on the assessment of the available capacity of CO_2 storage in deep saline aquifers, oil and gas fields in the North Sea territory. The assessment begins with the collection of data off geophysical characteristics for oil and gas fields, as well as saline aquifers. Since great uncertainty defines these characteristics in the subsurface, several assumptions need to be made in the case of non-solid data. Previous works assess the available capacity in terms of gross rock volume, while this doesn't take into account any pressure build-up. In this study, we use an integrated assessment model, that considers pressure dissipation in the reservoir, a major constraint parameter.

Sono arrivato a credere che il mondo intero sia un enigma, un innocuo enigma reso terribile dal nostro folle tentativo di interpretarlo come se avesse una verità nascosta.

I have come to believe that the whole world is an enigma, a harmless enigma that is made terrible by our own mad attempt to interpret it as though it had an underlying truth.

Umberto Eco

CHAPTER I

1.1 European Union Directive on Carbon Capture and Storage.

The European Union is among the leaders on adoption and implementation of carbon capture and storage technologies (CCS) [14]. According to the 2030 climate and energy policy framework [15] "significant emissions cuts are needed in EU's carbon intensive industries. As theoretical efficiency limits are being reached and process-related emissions are unavoidable in some sectors, CCS is the only option available to reduce direct emissions from industrial processes." The newly signed (2019) European Green Deal [16] introduces the intentions of European council to include the deployment of carbon capture and sequestration among the leading ways to achieve climate neutrality. Moreover, CCS is also a strategic security question for Europe, along with reducing dependency of external energy sources.

This chapter is an explanation of the EU's directive for geological storage of carbon dioxide DIRECTIVE 2009/31/EC. According to the text, EU considers CCS a binding technology that consists of CO_2 capture from industrial installations, transportation to the storage site and injection into a suitable underground geological formation for permanent storage. This process, on the other hand, should not be taken as a further incentive to enlarge the share of commercial power plants, but instead as a mitigation strategy, to avoid negative environmental impacts.

The objective of the regulatory framework is to ensure that the deployment of carbon capture and storage technology is done in an environmentally safe way and to ensure that no future concerns will emerge. The aim is to make CCS widely accepted and a key contributor to climate change mitigation efforts. The directive requires a flow model existence to assess storage capacity and risks. Later in this report, we will use a flow model to provide a storage assessment in potential storage sites. Below several articles and chapters of the framework, were selected to be communicated in this project.

Chapter #2

Article #4

Selection of storage sites

Each member state is responsible to assess its own storage capacity inside its territory, and possesses the right to ban CO_2 deposition on the underground. Any geological formation, may be used as a storage site, if and only if, there are no risks of leakage and no important environmental and health concerns are present.

Chapter #3

Article #8

Conditions for storage permits

A storage permit is issued under the following considerations:

(a) The contractor is financially sound and possesses the adequate technical capacity and trained staff to fully complete the project.

(b) In the existence of more than one storage sites in the same hydraulic unit, contractor, needs to make sure that potential pressure build up, allows for both sites to meet the requirements of this framework.

(c) CO_2 stream meets the requirements for storage.

(d) Adequate monitoring is in place.

Chapter #4

Article #12

CO_2 stream acceptance criteria

A CO_2 stream must consist only of carbon dioxide, not containing other waste or species. However, trace substances that are used in the monitoring phase and may indicate the CO_2 migration, are allowed in concentrations that do not alter the composition of the stream and/or pose environmental risks. To that extend, it is obligatory that the operator, accepts and injects CO_2 streams, that are analyzed and corrosive species are absent while environmental risks are minimum.

Article #13

Monitoring

Monitoring is essential, in order to assess various properties of CO_2 and make sure that the environmental and health standards are met. A proper monitoring unit must:

(a) Compare the real and simulated behavior CO_2 and formation water in the storage site.

(b) Detect irregularities.

(c) Detect CO_2 leakage.

(d) Detect possible negative effects on the surrounding environment.

(e) Detect CO_2 migration.

(f) Update the assessment of the safety and integrity of storage complex in both, short and long term.

Article #14

Reporting

At least one a year, monitoring results, should be communicated in a report-based way, to the regulation authority. Also, the quantities and properties of CO_2 delivered and injected should be addressed in the report. Finally, proof of putting in place, as well as, financial security of the facility must be included in the report.

Article #16

Measures in case of leakages or irregularities

In case of leakages or important irregularities, the corresponding authority needs to be notified and adequate measures that ensure human health should be adopted. Apart from that, measures to eliminate the potential leakages should be taken immediately.

Article #17

Closure and obligations

A storage site, will be closed, as soon as the relevant conditions of the permit are met, or in the case of the operator request. After the closure process, the operator, remains responsible for monitoring, reporting and correcting measures, that might emerge. Operator has also the responsibility of sealing the storage site and remove the injection facilities.

Chapter #5

Article #21 & #24

Access to transport network and storage sites

EU states, should ensure that the users should be able to obtain access to transport networks and storage sites, for the purpose of geological storage of CO_2 that has been captured. Each state has the right to deny access, if certain environmental and risk associated issues are not clarified. In the case of transboundary cooperation, the operating company, should meet the requirements of both legislations.

Annex I

Criteria for the characterization and assessment of a potential storage complex and surrounding area.

Data collection

Sufficient data should be collected in order to construct a 3D static model for storage site including the caprock and surrounding area, including the hydraulically connected areas. Such data, should cover geology and geophysics, hydrogeology, volumetric calculations of pore volume for CO_2 injection and storage capacity, dissolution rates, permeability, fracture pressure, seismicity, presence and conditions of wells and boreholes that might be a leakage pathway. Also, the following about the proximity areas should be noted, and that include: domains that might be affected by CO_2 storage, population density, proximity to valuable natural resources and adequate transport networks.

Building the 3D static geological earth model.

Using the collected data, a three-dimensional earth model, of the proposed storage site, should be created. This model will provide numerical simulations and should characterize the site in terms of: geological structure of the physical trap, geomechanical and flow properties of the reservoir overburden and its surroundings, pore space volume, area and extend of site and fluid distribution.

Characterization of storage dynamic behavior, sensitivity and risk assessment.

A variety of time step simulations of CO_2 injection, should be performed, while the following factors should be considered: possible injection rates and stream properties, the efficacy of the model, reactive process of CO_2 with other materials and both short- and long-term simulations, to establish the behavior of CO_2 for several years forward. Also, the model should give insights into, pressure and temperature of the storage formation as a function of injection rate, areal and vertical extend of CO_2 vs time, CO_2 trapping mechanisms, storage capacity and pressure gradient, fracturing risk, CO_2 entering the caprock risk, rate of migration, fracture sealing rates, changes in formations fluid chemistry and increased seismicity.

Risk assessment

The risk assessment is expected to comprise the following:

(a) Hazard characterization: potential leakage pathways, potential magnitude of leakage events, critical parameters affecting a potential leakage, any possible displacement of CO_2 and new substances formation and any other factors that could pose a hazard to human health.

(b) Exposure assessment: A study based on the environmental characteristics of the surrounding area and human population above the site.

(c) Risk characterization: A study, that includes an assessment of safety and integrity of the site, in short and long term.

1.2 Available technologies for Carbon Capture and Storage

The process to effectively store carbon dioxide, begins with its capture from the source of production. There are three main types of carbon capture technology (CCT). Pre-combustion capture, which refers to the CO_2 removal from the fossil fuel, prior to combustion, such as the formation of synthesis gas from the gasification process of feedstock (such as coal). Post combustion capture, referring to the CO_2 capture after the combustion of the fossil fuel and oxyfuel combustion, which is the burning of fossil fuel in oxygen instead of air. So, a complete combustion takes place and CO_2 is formed and collected. All the methodologies above include different technologies that are chosen based on the type of power plant, the capacity of CO_2 removal and the cost. Recently, since the implementation of European Union's Emissions Trading System (EU ETS), and the pricing of the emitted CO_2, companies, have a huge financial incentive to employ carbon capture technologies and reduce the carbon footprint of their activities.

1.2.1 Pre-combustion

In the pre-combustion process, a fossil fuel is reformed by the reaction $CH_4 + H_2O = 3H_2 + CO$ or is partially oxidized to form a synthesis gas that consists of hydrogen and carbon monoxide. Next in the reforming reactor, CO shifts to CO_2 under the water gas shift reaction $CO + H_2O = H_2 + CO_2$ [17]. A stripping column with a solvent is used to recover CO_2 (around 90%). In the case of pre-combustion, the carbon capture occurs before combustion, so, there is already high pressure and there is an absence of combustion-based pollutants, including sulfur and nitrogen oxides (SO_x, NO_x). The most power cycle most suited to perform pre-combustion capture is the coal gasification power cycle (Figure 6), while the available technologies include physical absorption, pressure swing adsorption and membrane capture processes [18].

Solvent based capture involves physical or chemical absorption of carbon dioxide from syngas into a liquid carrier forming a CO_2-absorber bond, that latter breaks by increasing temperature. Membrane technologies are utilized to separate CO_2 and H_2 in synthesis gas (formed by coal gasification). Membranes may use physical or chemical mechanisms of separation and are composed of metallic, ceramic or, in some cases, polymeric materials, with high permeability and selectivity. There are also some new concepts of pre-combustion capture methods, involving nanomaterials or temperature-swing and pressure-swing regeneration, that promises lower costs and less energy penalty [19] [20].

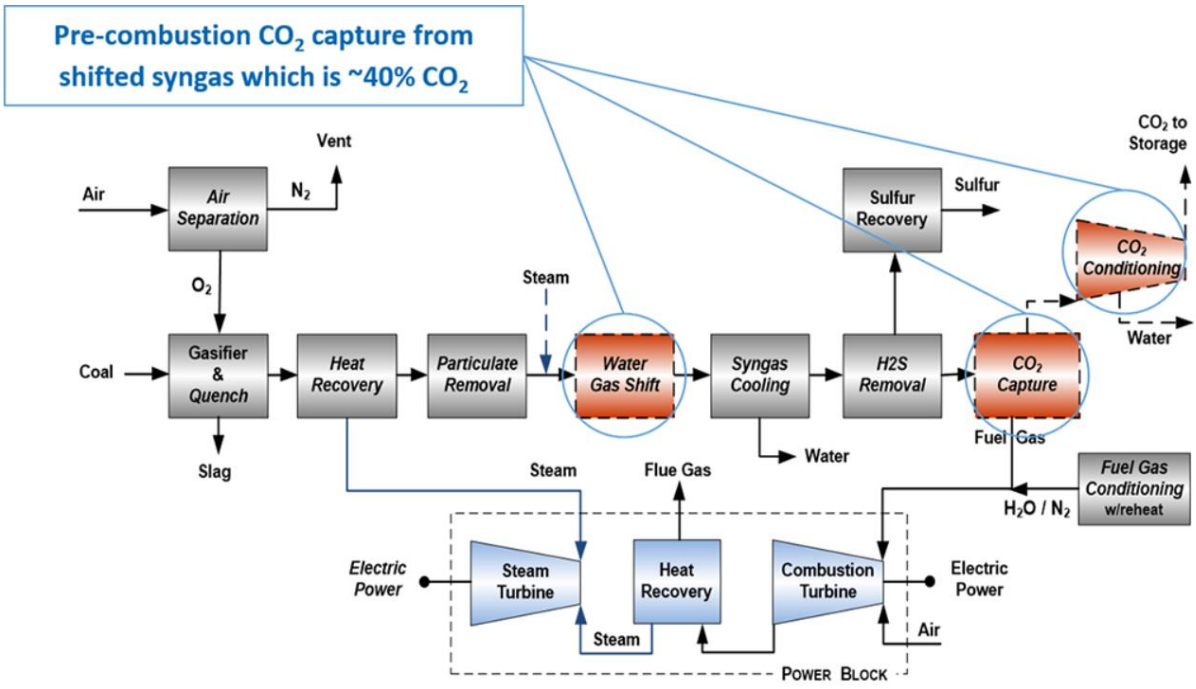

Figure 6. A Process diagram of carbon capture in a coal gasification power plant [20].

1.2.2 Post-combustion

Post-combustion capture deals with the treatment of exhaust gases. CO_2 is removed from the carbon rich flue gas, again, with the use of solvent under chemical absorption. In this case nitrogen and sulfur oxides cause degradation of the solvent and tend to be a major cost. In comparison with pre-combustion, it is more energy intensive and requires greater capital cost. There is a wider range of available technologies, although, some of them are not commercially employed. Those include, Absorption (Chemical/Physical), adsorption, membrane separation but also, cryogenic separation and bio-fixation [21].

1.2.3 Absorption

Absorption (see Figure 7) in post-combustion is a similar process to that in pre-combustion, but at a different location in the power plant. In this case, CO_2 is absorbed from flue gas into a solution under a chemical reaction, leaving the rest of the gas to stream to pass through. The absorbent is regenerated to be reused and CO_2 is collected. Interestingly, there are several drawbacks of this method. The great heat required for solvent regeneration, increases the cost, while the need for corrosion control due to SO_x and NO_x presence, reduces the efficiency of the catalysts and increases the power supply needed [22].

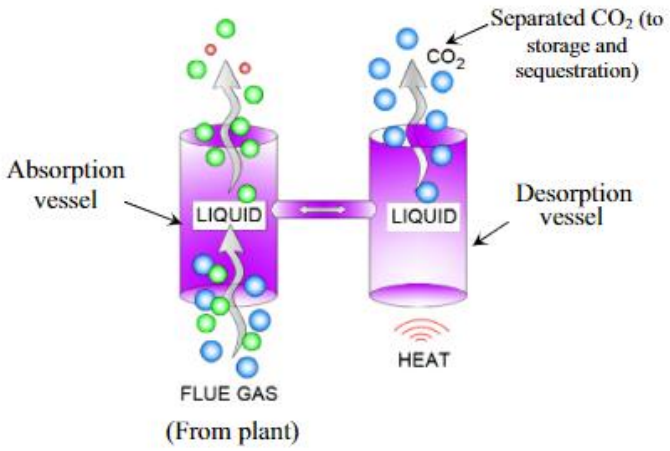

Figure 7. Carbon capture process, using amine solvent for absorption [22].

1.2.4 Membranes

Membranes (see Figure 8) in the post-combustion case, use the same polymer or ceramic material, to separate CO_2 this time from flue gases. The greatest issue with such technique, despite the high selectivity to CO_2, is the degradation of materials at high temperatures and therefore efficiency loss [23].

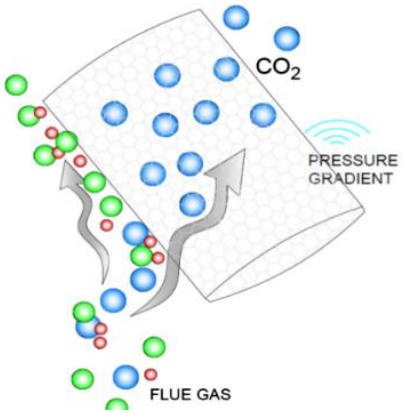

Figure 8. Membrane carbon capture schematic [22].

1.2.5 Cryogenic and Bio-fixation

Cryogenic CO_2 separation (see Figure 9) uses the principle of liquid state temperature and pressure difference in constituent gases of flue gas. In this case, CO_2 is cooled and condensed and therefore removed from the stream of flue gases. Other experimental techniques involve algae bio-fixation. This technique, uses photosynthetic organisms that capture CO_2. Though an expensive technique with low efficiency at large scale so far, it is a purely natural way of carbon removal [24] [25].

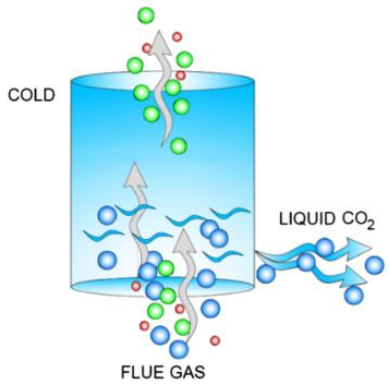

Figure 9. Cryogenic separation of CO_2 [22].

1.2.6 Adsorption

Separation using adsorption (see Figure 10) is a technique that is based on the adsorption/desorption properties of the mixture and actually refers to the adhesion of particles from a liquid or gas state to a surface. These ions form a thin film on the surface of the materials. Comparing to other techniques it has a comparative advantage with regards to the adsorbent regeneration by thermal or pressure modulation, reducing drastically the energy consumption of the post-combustion carbon capture. Some of the key advantages of the technique are, (i) ease of regeneration of adsorbent, (ii) durability, (iii) high selectivity to CO_2, (iv) increased capacity of adsorption and (v) stability of the cycle. On the other hand, improved materials are required, that tend to increase the capital cost, in some cases significantly enough to make the technology less

economic than other methods. The CO_2 capture can be performed both by chemical and physical adsorption that use chemical or physically based solvents, respectively [26] [27].

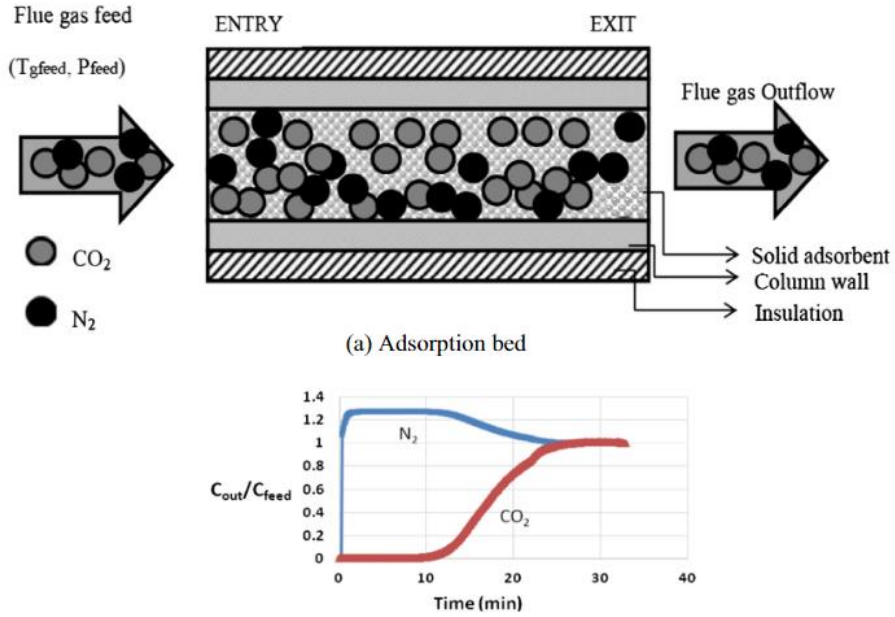

Figure 10. Adsorption technique using N_2 as a solvent [26].

1.2.7 Oxy-fuel combustion

Oxy-fuel combustion involves the burning of fuel in nearly pure oxygen conditions, instead of air. In this way, the production of byproducts other than CO_2 in the flue gas is minimized. Then CO_2 is separated from flue gas by dehydration and cryogenic purification. An oxy-fuel combustion plant is consists of (i) an air separator unit for oxygen production, (ii) boiler or a gas turbine for the power generation, (iii) flue gas processing unit for the control of the quality of flue gases and (iv) a CO_2 processing unit that purifies the CO_2 stream. Usually oxy-fuel combustion is encountered in coal fired power plants and is categorized as oxy-PC and oxy-CFB process [28] [29].

1.2.8 Oxy-PC combustion

Referring to pulverized coal combustion, which is extensively used for electricity generation (see Figure 11). Power plants with oxy-PC CO_2 capture, have capacities of 100-500 MWe the combustion occurs in 95-97% oxygen resulting in CO_2 concentrations around 65-85% dry basis. The main parameter in such method is how oxygen and recycled flue gas are introduced in the boiler. Special attention is paid in the SO_x particles that are recycled in the boiler and are able to cause a number of issues [30].

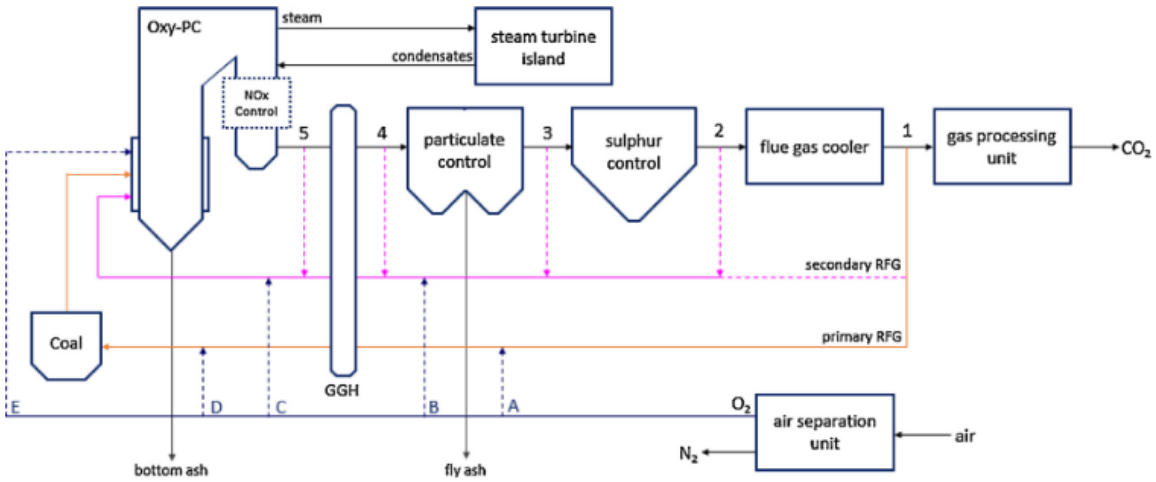

Figure 11. Pulverized coal power plant configuration with oxy-PC carbon capture [30].

1.2.9 Oxy-CFB combustion

Oxy-combustion employs circulating fluidized bed boilers. The main phenomena affecting combustion of solid fuel in a circulating fluidized bed us the solid fuel properties, like evaporation of moisture, devolatilization, gasification of char, gas phase reactions and other. In oxy-CFB, the share of CO_2 and H_2O is higher than in air-fired CFB [31].

1.3 CO_2 TRANSPORT

The transport of CO_2 is a significant stage of carbon capture and storage (CCS) and it has to be delivered in a safe and reliable way. There are three key ways to transport CO_2 and these are through pipelines, trucks and ships, see Figure 12.

The most widely used way of transport is through pipelines. CO_2 is transported as liquid or as high-density gas. Several authors [32] [33] state that the most efficient way to transport CO_2 is in a supercritical phase (P > 7.38 MPa, T > 31.1 ^oC). There are several specifications regarding the properties of CO_2 aimed to be transported through pipeline system, reported in Table. 1. Such specifications need to be met strictly, when CO_2 is driven to enhanced oil recovery (EOR), while some deviations may be accepted to carbon dioxide transportation for geological storage. Dry CO_2 has proven not to cause corrosion issues to metal pipelines, if the relative humidity does not exceed 60%. In the case of water present, corrosion is much more significant with an estimation of around 0.7 mm yr^{-1} for 150 to 300 hours exposure at 40 ^oC and 9.5 MPa. If dry CO_2 cannot be transported, pipes made from stainless steel, that is corrosion resistant, have to be chosen. The physical properties of CO_2 also need to be controlled. Table. 2 provides the details for carbon dioxide properties that need to be satisfied considering CO_2 critical parameters are: T_c = 31.1 ^oC, P_c = 7.38 MPa, ρ_c = 470 kg/m^3 Figure 13 [34].

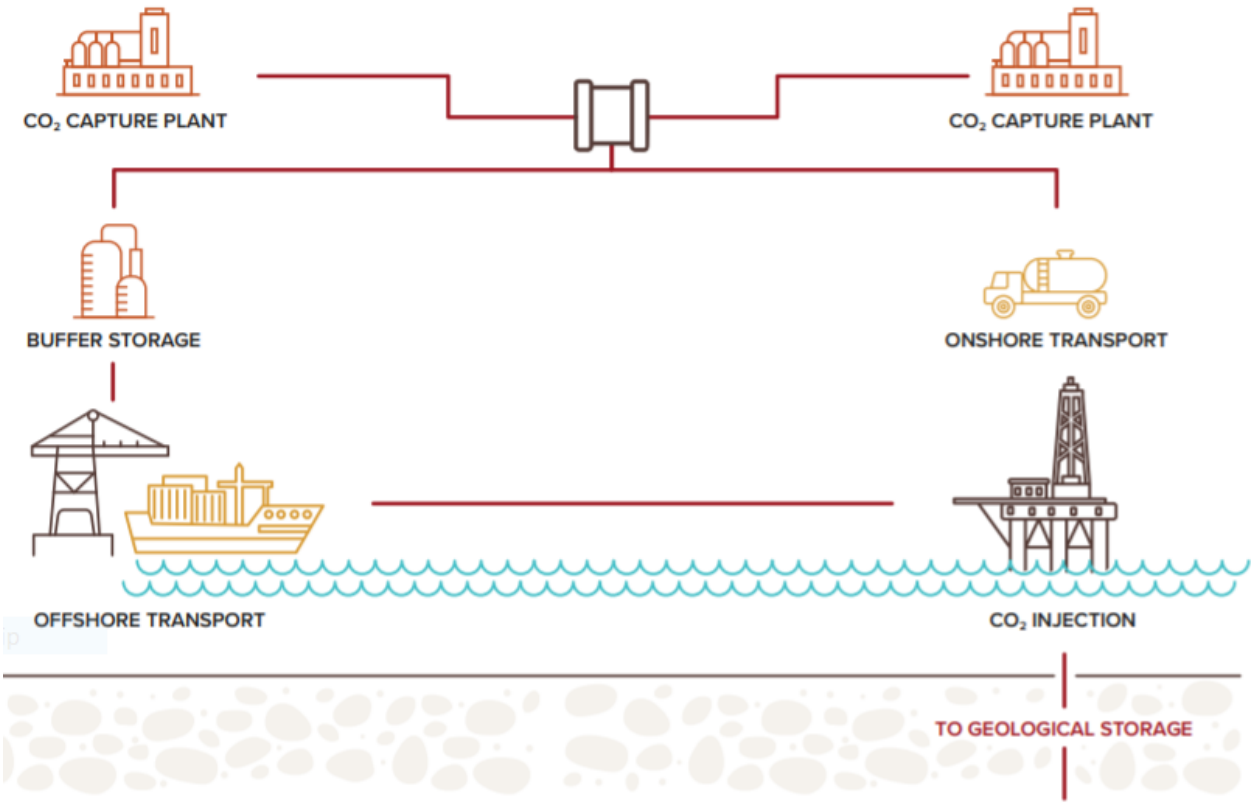

Figure 12. Flow chart of carbon capture and transportation, from source to geological storage [33].

Table 1. Specifications of quality of CO_2 in pipeline transportation.

(a) Carbon dioxide: Concentration at least 95%.
(b) Water: Zero concentration of liquid water and no more than 0.489 m^{-3} in the vapor phase.
(c) Sulphur: Not more than 1450ppm.
(d) Temperature: Less than 48.9 ^{o}C
(e) Nitrogen: Not more than 4%.
(f) Oxygen: Not more than 10 ppm.
(g) Hydrogen Sulphide: Concentration less than 1500 ppm.

Table 2. Properties of carbon dioxide in pipelines [78].

Properties	Gas	Supercritical	Liquid
Density (kg m^{-3})	1	100-200	600-1600
Diffusivity (m^2 s^{-1})	10^{-5}	10^{-7}	10^{-9}
Viscosity (Pa.s)	0.1	1	10

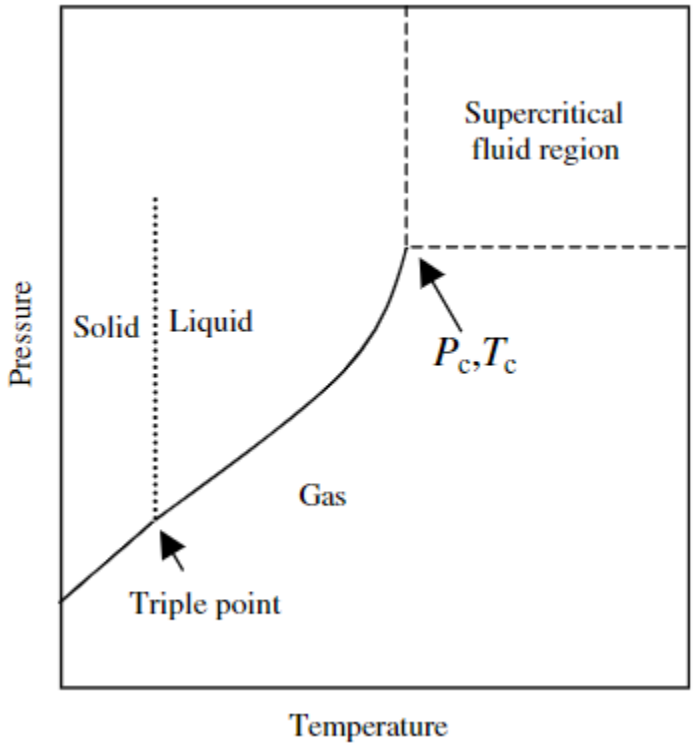

Figure 13. Phase diagram of CO2 [34].

A critical point in the design of pipeline network is the calculation of a suitable diameter. It is possible to calculate different diameters using different hydraulic equations. A demonstration of diameter calculation is provided in this study, derived from hydraulic equations for turbulent flow [35].

$$D^5 = \frac{32 \times f_F \times Q_m^2}{\rho \times \pi^2 \left(\frac{\Delta p}{L}\right)} \ [m] \qquad Eq.(1)$$

where D is the diameter (m), f_F is the Fanning friction factor, Q_m is the mass flowrate in kg s^{-1}, ρ is the density in kg m^{-3}, Δp the pressure drop in Pa and L the length in meters. The formula derived from turbulent flow hydraulic equation for circular pipelines and is based on the Bernoulli equation as stated below, while a schematical representation is presented in Figure 14.

$$z_1 + \frac{p_1}{\rho g} + \frac{v_1^2}{2g} = z_2 + \frac{p_2}{\rho g} + \frac{v_2^2}{2g} + \Delta F \quad Eq.(2)$$

where *z* is the height (m), *p* pressure (Pa), v velocity (m s^{-1}) and *F* refers to frictional and local losses. In the case of no height difference assumed ($z_1 = z_2$) Figure 14. and analyzing the hydrostatic line ($v_1 = v_2 = 0$) the equation becomes:

$$\frac{p_1}{\rho g} = \frac{p_2}{\rho g} + \Delta F \quad Eq.(3)$$

where ΔF is calculated as:

$$\Delta F = \frac{f}{2g} \times \frac{v^2}{R} \times L \quad Eq.(4)$$

where *R* is the hydraulic diameter radius (m) and for a circular pipeline is equal to $\frac{D}{4}$ and *v* is the velocity defined by the volumetric flow rate.

Figure 14. Pipeline connecting two reservoirs considered in equations to calculate the pipe diameter for a desired flow rate.

The Fanning friction factor is calculated from White-Colebrook law, defined as:

$$\frac{1}{\sqrt{f}} = -2\log\left(\frac{e}{14.8R} + \frac{2.51}{Re\sqrt{f}}\right) \quad Eq.(5)$$

With the Darcy-Weisbach friction factor $f = 4f_F$, *e* referring to roughness height (m) and *Re* the Reynolds number for fully developed flow given by the following equation.

$$Re = \frac{\rho v l}{\mu} \quad Eq.(6)$$

where ρ is density (kg m^{-3}), *v* mean velocity (m s^{-1}), *l* is the characteristic length (m) which in the case of a pipeline is equal to the diameter while μ is the dynamic fluid viscosity (Pa s).

Some typical values for such numbers, derived from real projects are reported in Table 3. While they might vary in per case situations, such data can provide a useful tool to estimate the pipeline diameter according to the mass flowrate of CO_2 that needs to be transported for injection purposes. Such a correlation is presented in Figure 15, that combines data from four different studies and determines the pipeline diameter.

Table 3. Overview of parameters and typical values used to calculate pipeline diameters.

Parameters	**Studies [34] [36] [37] [38] values range**
Temperature [^{o}C]	10-40
Pressure [MPa]	7.5-15
CO_2 density [kg/m^3]	800-899
CO_2 viscosity [Pa s]	0.00006-0.00008
Pipeline length [m]	200 000
Height difference [m]	200

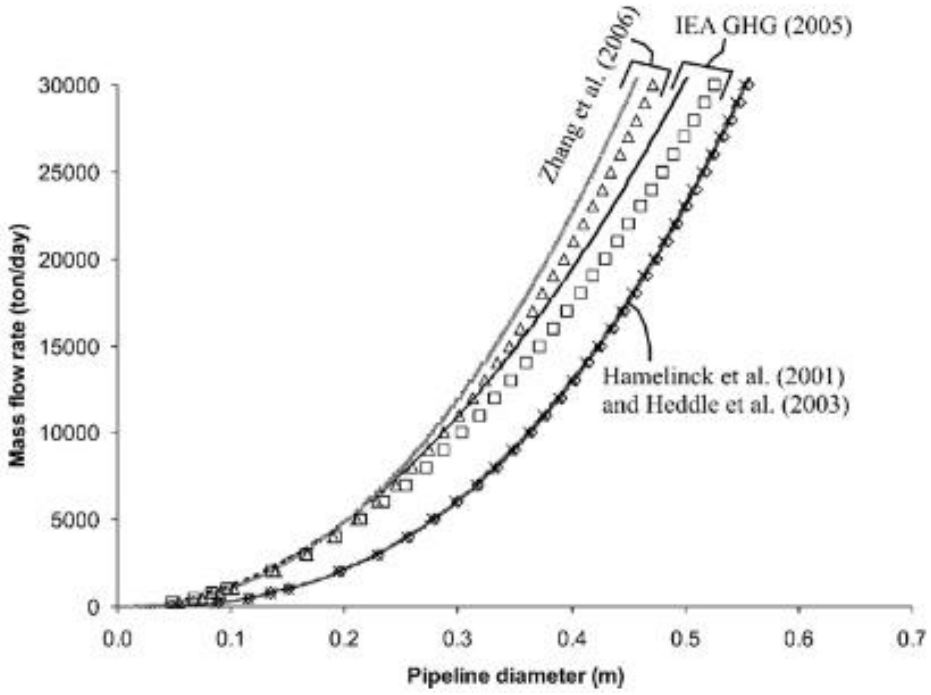

Figure 15. Pipeline diameter as a function of mass flow rate (ton per day).

1.3.2 Ships for CO_2 transport

Carbon dioxide can be transported to the injection site by ships, when larger distances are required. The tankers used for CO_2 transportation are the same used for liquified natural gas, LNG. Such carriers reach more than 200,000 m^3 in capacity. For transportation purposes, the gas has to be compressed at a pressure close to 0.6 MPa and temperature close to -52 ^{o}C. During the transport, the heat transfer from surrounding area to storage tank walls will lead to boiling of the liquid, a situation that would increase the pressure substantially and leads to an inherent the risk of blowouts. Therefore, a refrigeration process should be followed to maintain the low temperatures required. CO_2 can be used as refrigerant; else an external refrigerant fluid can do. Such low temperatures are the product of a liquefaction process shown in Figure 16. [39].

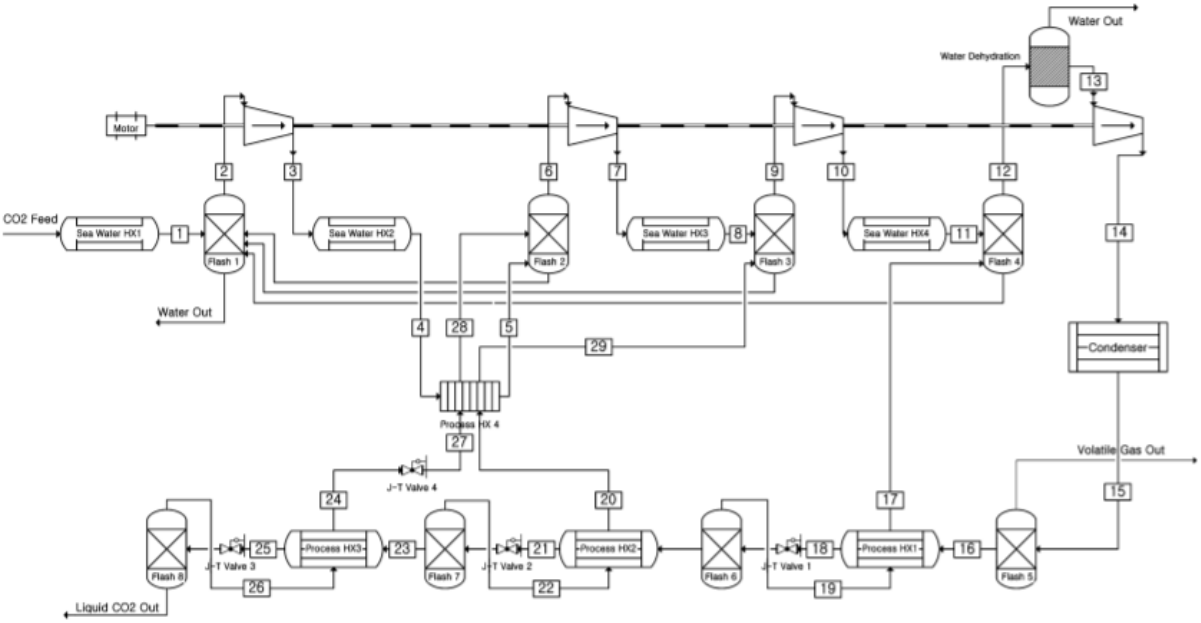

Figure 16. Flow diagram of a liquefaction process to obtain CO2 at 0.6 MPa and -52 oC [40].

1.4 Side effects of CO2 storage

Storage safety is a key aspect of carbon capture and storage. It is of great importance that the CO_2 injected underground remains there, and leakage to the ambient is avoided. According to several studies [41] [42] more than 99% of CO_2 geologically deposited will remain there for the first 1000 years. On the other hand, some side effects of carbon dioxide storage are unavoidable in some cases.

1.4.1 Cap rock fracturing

From a geomechanical point of view, carbon dioxide injection in the subsurface will increase the stresses applied to the cap rock and result to alterations in pore pressure, buoyant pressure and volume of the rock [43]. The decrease of the effective stress, will lead to an increase in volume, which consequently leads to higher porosity of the rock of the reservoir. As a domino effect, the permeability of the porous medium is expected to increase favoring the migration of the fluid [44]. Figure 17 demonstrates the relation between the normal stress and the fracture permeability according to the following equation:

$$k = k_o \exp(-C'\sigma'_n) \qquad Eq.(7)$$

where C' is a fitting parameter, k_o is the permeability of fracture at zero normal stress, σ the normal stress [45].

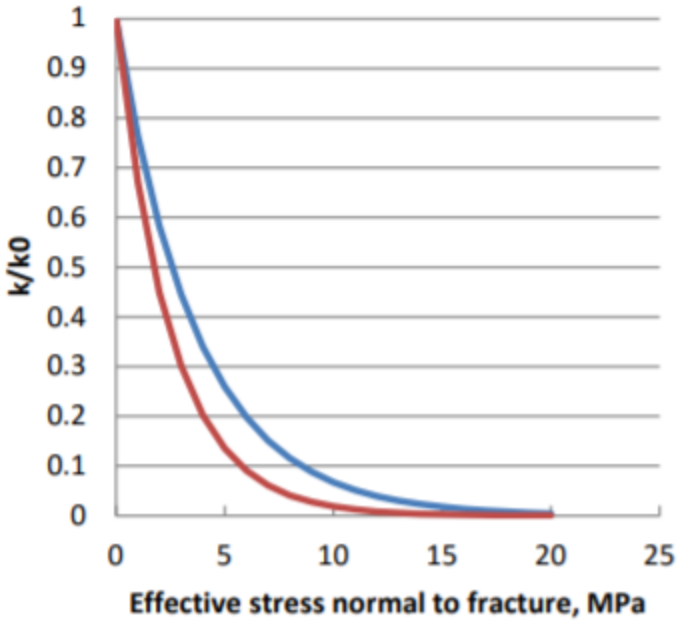

Figure 17. Fracture permeability vs effective normal stress for C'=0.27 blue line and C'=0.4 red line [42].

1.4.2 Earthquakes and storage mechanisms

Earthquakes are unlikely to release large amounts of carbon dioxide into the environment, if the carbon dioxide is properly stored. On the other hand, geological sequestration in high seismic risk areas should be avoided. The trapping mechanisms of the geological formations are sufficiently effective to resist significant CO_2 leakage in most cases [46]. This is true as other mechanisms act and avert leakage. An important amount of injected CO_2 can be trapped by capillary mechanisms within the permeable sections of the reservoir. Homogenous trapping occurs during the post injection phase through imbibition and CO_2 bubbles are trapped by capillary forces [79]. Apart from that, dissolution of CO_2 in saline aquifers is one of the fundamental mechanisms of storing carbon dioxide in subsurface. This might lead to density increase of the fluid and therefore pressure build-up but large aquifers offer pressure dissipation and increased pressure is averted [80].

1.4.3 Geological risks in CO_2 storage reservoirs

Wilkinson, [81] has studied the most common geological risks encountered when exploring for a CO_2 storage reservoir. Since CCS employment is still limited, reliable database for evaluation of such risks is still absent. Therefore, the experience of hydrocarbon exploitation is utilized for the conduction of a statistical analysis of geological risks, derived from 651 relinquishment reports of exploration licenses in UK.

According to the study, the most important risk factors for new borehole drilled for CO_2 storage, are reservoir presence, reservoir quality and trap definition. In the case of an absent or very thin reservoir, could lead in termination of the injection process due to low volumes encountered, comparing to the ones that are expected. According to the study, such risk is of some importance in oil and gas reservoirs as around 85 % of the exploration wells, find the target reservoir. On the other hand, when saline aquifers are considered, the risk of missing the target volume calculated is close to 20%.

The proper estimation of trap is highly associated with the eventual amount of CO_2 that will be injected. A good trap determination, requires its depth, relief and geometry to be described correctly. There is an inherent risk in defining traps has to do with the parameters described before, but also with the quality of seismic data, neighboring units and the geological background of the basin. The probability of correctly identifying the trap in Paleogene reservoirs of North Sea is found to be around 85%, while there is great discrepancy on such result, the important outcome is that there is always significant chance to miss-evaluate the trap of a selected aquifer.

A general remark from the study, states that carbon dioxide storage aquifers, are expected to be larger than many hydrocarbon fields and involve factors that are not considered in the hydrocarbon exploitation. As a consequence, the geological risk of drilling to locate a CO_2 storage site, is higher than the estimated risk for hydrocarbon exploitation.

1.5 CO_2 IN ENHANCED OIL RECOVERY (EOR)

Enhanced oil recovery is a key process enabling the recovery of a greater amount of hydrocarbons from the subsurface. To start from the beginning, oil is recovered through expansion as the reservoir pressure drops. As soon as the pressure drops significantly, the field will stop oil production, since there is no further driving force for production. Also, since oil at high pressures and temperature, is a mix of several chemicals in the gaseous phase, that are preferentially produced as the pressure drops in the reservoir (due to the lower viscosity). This process is called primary production and is designated with a red line in Figure 18.

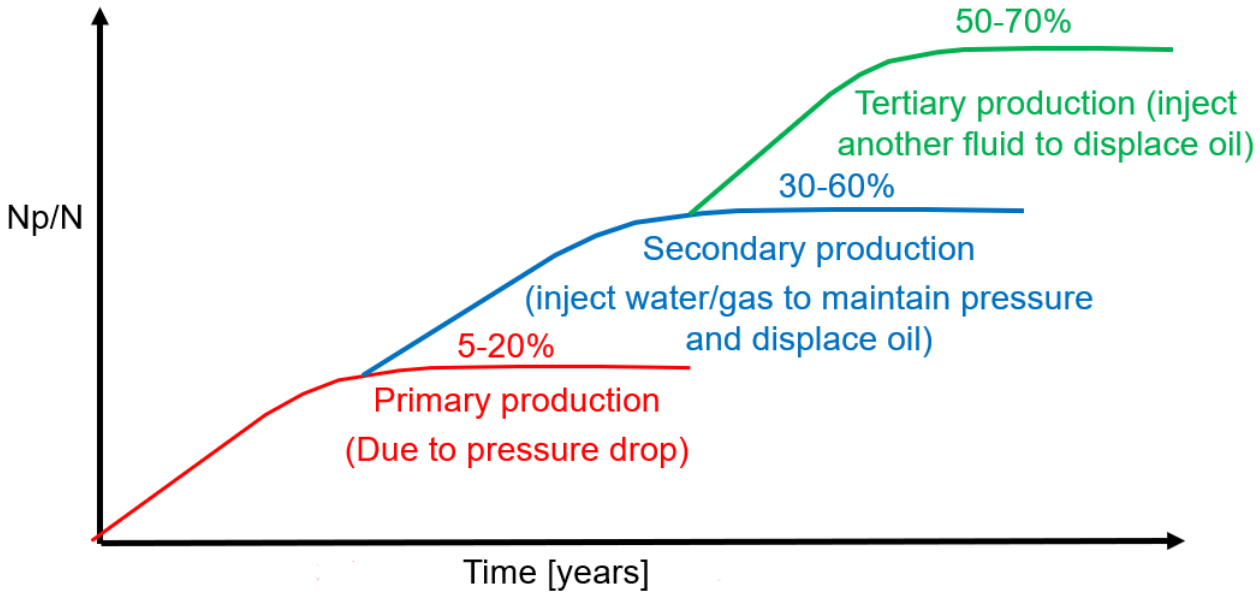

Figure 18. Production of oil for different stages of production.

The next method applied to recover 30-60% of the remaining oil is secondary production, that is the injection of another fluid, which can be gas or water, into the reservoir. This fluid occupies the available pore space while displacing the remaining oil from the rock pores. Under secondary production, the reservoir pressure is maintained above the bubble point, avoiding gas production and high recoveries are observed.

Finally, the way to achieve maximum production, is tertiary recovery which refers to the injection of another fluid, in most cases other than water, to displace the remaining oil from rock pores. The latter is also called enhanced oil recovery and includes injection of gases such as CO_2, foams, polymers or surfactants [47].

Lately, CO_2 injection for enhanced oil recovery in reservoirs with very low permeability and porosity, has been studied thoroughly, indicating that CO_2-EOR is a possible but uneconomical for storage and production [48]. According to the IEA [49], CO_2 driven enhanced oil recovery represents around 20% of the total EOR. From the CO_2 injected, a portion remains underground while a percentage, returns with oil. If the CO_2 is re-separated from oil, in a closed loop process, and re-injected, this will lead to a permanent storage in the subsurface. Ironically, most of the CO_2 used in EOR (70% in US) is obtained from natural underground deposits and only a fraction of it comes from source captured carbon dioxide. Furthermore, the IEA, projects that under the New

Policies Scenario, carbon dioxide for enhanced oil recovery will rise from 0.55 million barrels per day in 2020 to 1.64 million barrels per day Figure 19. Up until October 2020, 85% of all EOR production fields are placed in North America, while in Europe only Croatia uses it in its 'Zutica' field, Brazil also has three fields, China four and from one UAE and Saudi Arabia.

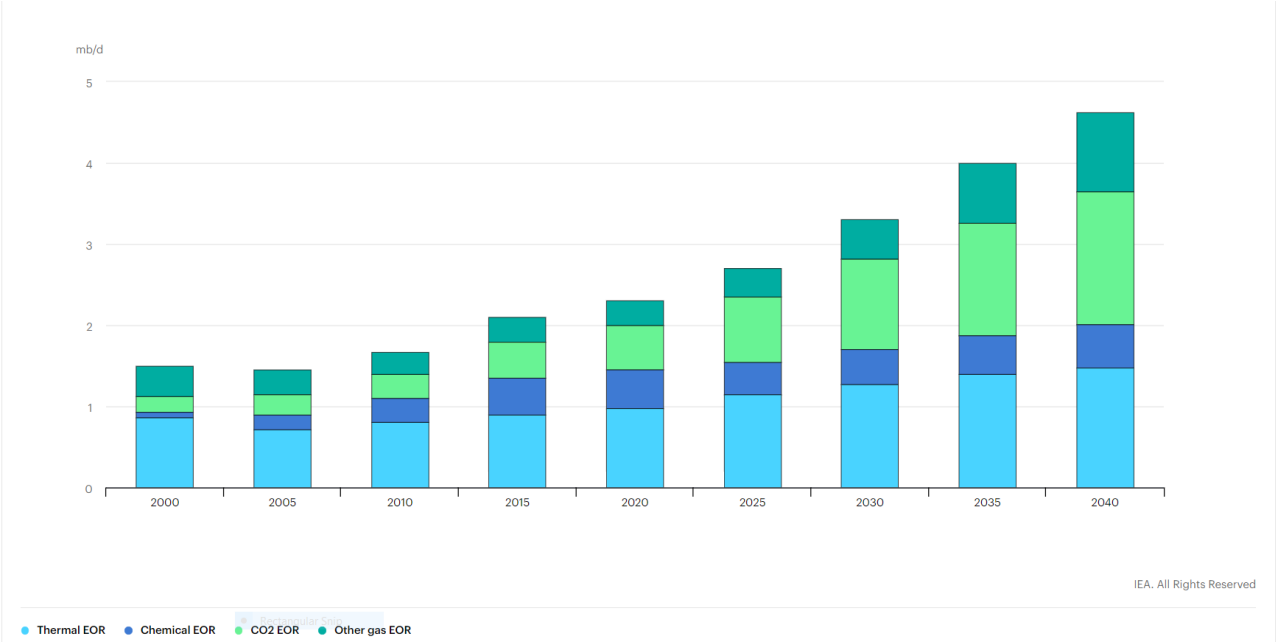

Figure 19. EOR production in the New Policies Scenario, 2000-2040 [50].

1.6 Carbon dioxide migration

After the careful selection of a reservoir, injection wells are placed in order to deposit the captured CO_2 underground. After the injection, plume is expected to migrate to the top of the reservoir due to buoyancy [82] that drives the less denser gas upwards, over the denser brine while afterwards, spreads laterally. The presence of impermeable seals on top of the reservoir and beneath, expect to keep the plume spreading only across the radial direction. On the other hand, several cases of aquifers that are not closed below, exist and are called, open aquifers. They can be either dipping aquifers (represent several aquifers in North Sea and more specifically in UK) or open aquifers with large-scale structural closure. Studies [83], [84] has shown that, the greater the aquifer dip angle, the grater the migration velocity. Permeability is also an important factor in the migration of CO_2. The highest the absolute permeability the greater the migration of carbon dioxide. The overall migration though, is a process that takes several years to complete while in short term is important as it determines the pressure dissipation at the selected aquifer that CO_2 is injected.

1.7 Effect of impure CO_2 injection

As described in previous chapters, the collection of CO_2 to be injected, happens from nearby industrial processes. Such processes, in many cases, involve combustion that results to several exhaust gases, including carbon dioxide. The separation of the latter, is subject to infiltration of several impurities in its stream. Those may shift the properties of the phase diagram of CO_2 and therefore make it more or less active with species existing underground, or extra treatment is required to purify the streams, with subsequent increase in costs. Such impurities are mainly NO_x and SO_x by products of combustion processes that are highly toxic and have sever global warming index [85].

According to Aminu et al. [86], from a geochemical perspective, impurities can influence a storage system by the formation of carbonic acid or bicarbonates by dissolution of CO_2 in water. Presence of SO_2 leads to H_2S production while NO_2 reaction with water leads to production of strong acids like HNO_3.

Such elements formed due to the presence of impurities, affect the pressure dissipation on the reservoir. In a case study, on a Bunter sandstone formation, in a monitoring period of 100 days, and constant injection rate, maximum pressure reached by the 30^{th} day in the case of pure CO_2, while if impurities included, keeping every other parameter constant, maximum pressure is reached between the 50^{th} and 90^{th} day, given the species included. The study resulted that, impurities affect the pressure build up in the reservoir but only for an initial period of time and though toxic for the surrounding environment, the security of stored CO_2 is not inhibited.

To define is to limit.

Oscar Wild

CHAPTER II

2.1 Carbon dioxide storage assessment in the North Sea

In this project, the assessment of CO_2 geological deposition under the North Sea is studied thoroughly. While other studies have been conducted during the past decade, there have been country focused or specified in certain geological formations, such as Anthonsen et al. [64] who studied the Baltic Sea, Bachu et al. [77] and Heinemann et al. [74] who investigated the Bunter formations and Bentham et al. [73] in the Southern North Sea. In this thesis a total of 426 potential fields will be studied and categorized according to their suitability for carbon sequestration. These sites include oil and gas fields, depleted or under production, as well as saline aquifers, belonging to the territorial sea of the United Kingdom, Norway, Denmark, the Netherlands and Germany. In order to apply the methodology below, a set of assumptions were undertaken and will be discussed later. This study will give an added value in the literature of common studies as it will provide a first order assessment of the available CO_2 that could potentially be stored beneath the North Sea. In addition, it should be mentioned that, despite our theoretical knowledge of the physics, underground petrophysical properties may vary and therefore any candidate fields that storage will take place would need a second order study with more experimental results to define the capacity in a more accurate way. In this study the data acquisition is from online databases presented at Table 4 and those derived from log measurements. The full list with the fields considered and their characteristics can be found in the Database at the end of the text.

2.1.1 Data characterization

The essential data to identify the storage capacity come mainly from oil and gas fields in each country, as well as saline aquifers suitable for geological storage in each country. This data comes with information on geophysical characteristics such as permeability, porosity, field thickness, depth and area as well as rock and water compressibility, CO_2 density and viscosity, pore pressure and others that will be discussed in detail in the following paragraphs. These properties are characteristics unique for each field, and are found from down-hole (log) measurements and the analysis of rock samples taken from the reservoir. In most cases, those data are available from independent studies and are reported in literature but in other cases should be estimated under the assumptions discussed below. To that extent, an index on the data was created ranging from A to C (robust to poor data) as shown in Figure 20.

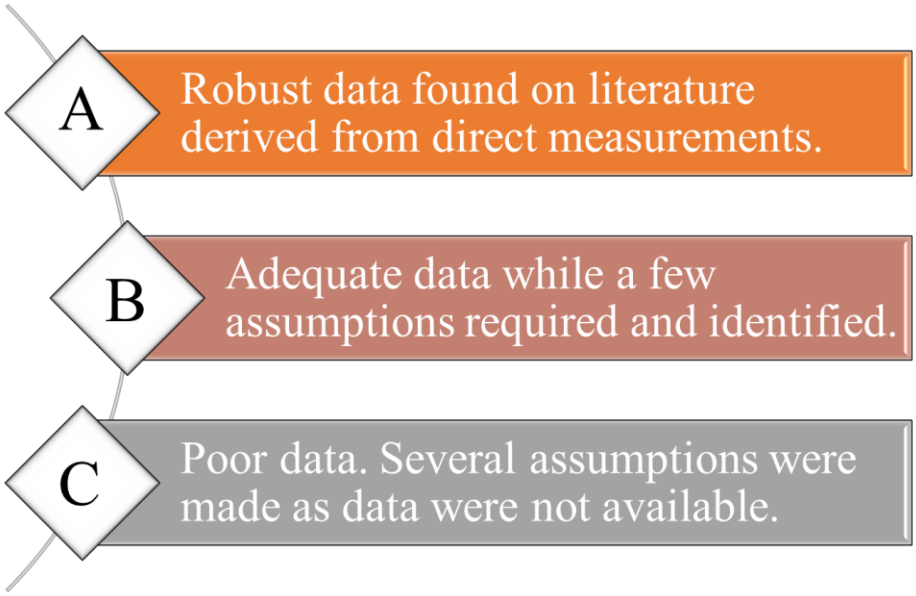

Figure 20. Data classification proposed by the author.

The databases used are available in literature and are reported below in Table 4.

Table 4. Data sources for the analysis in this thesis.

Country	Reference
United Kingdom	▪ CO2 stored [57] ▪ Gluyas et al. [58] ▪ Zimmerman [59]
Netherlands	▪ Geological Survey of the Netherlands [52]
Norway	▪ Norwegian Petroleum Directorate [54] ▪ CO_2 storage atlas [53]
Denmark	▪ Danish Energy Agency [51] ▪ Danish Geological Society [56]
Germany	▪ Grassmann et al. [55] ▪ Anthonsen et al. [64]

2.1.2 Assumptions

It is critical to state the set of assumptions made in order to fill the missing data and produce results. Every parameter in the software (CO2BLOCK) required data that in some cases were not straightforward available and several calculations or assumptions were needed. In more detail:

Depth

Depth can be measured as follows, see Figure 21:

$$Shallowest\ depth = Free\ water\ level\ depth - thickness \quad Eq.(8)$$

$$Average\ depth = Free\ water\ level\ depth - \frac{thickness}{2} \quad Eq.(9)$$

Whenever data for shallowest depth, average depth and thickness were not directly available the following were considered. Shallowest depth was calculated from Eq. (8) as the difference between the free water level and thickness. The average depth is calculated as free water level depth minus half thickness Eq. (9). When free water level depth data were not available, instead oil water contact was used to the calculation as shown in Figure 21.

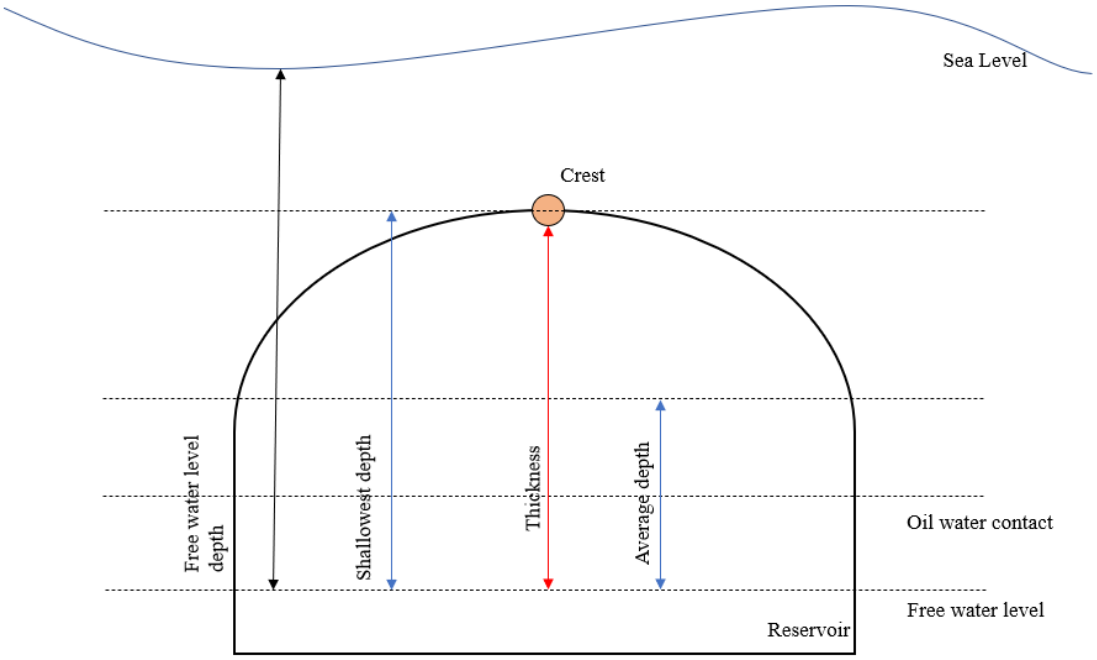

Figure 21. Reservoir depths considered in the assessment of storage capacity.

Area

In the case of area of the field, when adequate data were not available, two paths were followed in this project. Providing that values for gross rock volume exist, the equation used is:

$$A = \frac{v}{t} \quad Eq.(10)$$

where v is the gross rock volume and t is gross thickness (m). While in the case of absent data, gross rock volume is calculated from standard oil in place (STOIIP) with Eq. (10) to calculate area:

$$STOIIP = \frac{v \times \phi \times S_o}{B_o} \quad Eq.(11)$$

where v is the gross rock volume, ϕ is porosity (fraction), S_o is residual oil saturation, B_o is oil formation volume factor (the conversion of reservoir to surface volume), *STOIIP* is the stock tank oil in place. In the case of incapability of calculating *STOIIP*, area is estimated from available GIS photographs. Especially, for the area of the Netherlands oil and gas fields, where data were not available online, we used an approximation. The average area of oil and gas fields in the UK (where data are available) is calculated and the result is used in every field in the Netherlands. Though an error is introduced, this approximation enables a first order estimation of a total capacity of carbon dioxide deposition in the Netherlands.

Porosity and permeability

In a reservoir or a saline aquifer porosity and permeability differ across space and log measurements provide a range of results. Usually, in databases, the most encountered results of permeability or porosity are reported. In other cases, a range of log measurements results are provided. In such cases, the average of the provided data is used in the calculations. When data for porosity and permeability are not available, average values corresponding to the geological formations.

2.2 FLUID FLOW IN POROUS MEDIA

In this section we will review flow in porous media and introduce the equations used to assess carbon dioxide injection in the subsurface and storage capacity.

A porous medium refers to any substance that contains both a solid matrix and void spaces called pores [63]. The latter may contain liquid or gas and are characterized by porosity ϕ which is the fraction of the porous media that is void space.

It is important to state how fluid flows and what equations govern such flow. In general, fluid flow is governed by the Navier-Stokes equation, given for Newtonian incompressible fluid of standard viscosity μ [60]:

$$\mu\nabla^2 v = \rho\left(\frac{\partial v}{\partial t} + v.\nabla v\right) + \nabla P - \rho g \quad Eq.(12)$$

where v is the velocity field vector, P is the fluid pressure and g is the gravitational acceleration. The driving force of flow is gravity and the pressure gradient $+\nabla P - \rho g$ of Eq. (12). Now, let V be a fluid volume bounded by a surface S, then the rate at which mass crosses the surface is:

$$\int \frac{\partial \rho}{\partial t}\, dV = -\int \rho v . dS \qquad Eq.(13)$$

Using Gauss' theorem, surface integral is transformed into one over the same volume.

$$\int \frac{\partial \rho}{\partial t}\, dV = -\int \nabla . (\rho v) dV \qquad Eq.(14)$$

Since the integrals are equal, we have,

$$\frac{\partial p}{\partial t} + \nabla . (\rho v) = 0 \qquad Eq.(15)$$

Eq. (15) can be used to determine the variation of pressure within a storage formation. The density can be written as a function of pressure using compressibility, while the velocity can be written in terms of a pressure gradient for flow in porous media, presented below.

While the pressure drop in absolute values is in the order of magnitude of tens of MPa, at the pore scale it is a few Pa. In such case, density variation is so small, that can be considered constant and the velocity field is divergence free in an incompressible fluid.

$$\nabla . \nu = 0 \qquad Eq.(16)$$

The arrangements of fluid phases that are in contact with each other and a solid surface, is controlled by the energy balance. Displacement occurs as one fluid pushes another from its pore. However, in the pore scale, this energy balance occurs in a pore-by-pore level. The Young-Laplace equation relates the pressure difference between the phases to the curvature of the various interfaces and is derived from an energy balance considering a change in the volume of one of the phases:

$$P_c = \sigma \left(\frac{1}{r_1} + \frac{1}{r_2}\right) = k\sigma \qquad Eq.(17)$$

where k is the total curvature of the interface, σ is the interfacial tension between phases and is measured in force (N m^{-1}) or energy (J m^{-2}) units, r_1, r_2 are the radii described in Figure 22. P_c is the capillary pressure defined as the difference of oil and water pressures ($P_c = P_o - P_w$).

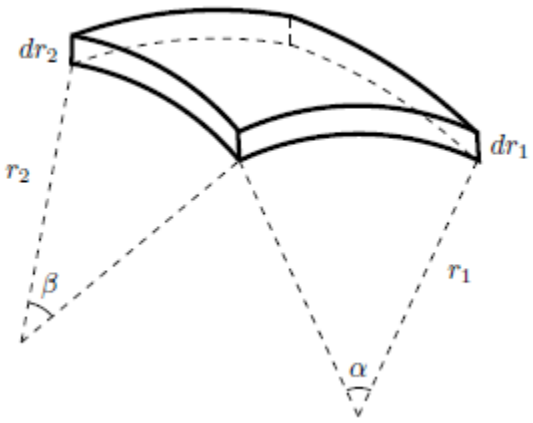

Figure 22. Small expansion of interface between 2 liquids where r_1 and r_2 are the principal radii of curvature [63].

For slow steady state flows of porous media, there is the possibility of simplifying the Navier-Stokes equation introduced before. The Reynolds number describes the ratio of internal forces to viscous ones and is defined as

$$Re = \frac{\rho v l}{\mu} \quad Eq.(18)$$

where v refers to the flow speed, l to the characteristic length, which in the case of porous media, refers to the distance between pores, while ρ is the fluid density and μ the viscosity of the fluid. In media constituting from grains (granular) the characteristic length is associated with the size of the grain $l=d$ where d is the grain diameter, while in carbonates it is more difficult to estimate l and approximations are used. To define the length scale, we can use

$$l = \pi \frac{V}{A} \quad Eq.(19)$$

where V is the volume of system (pores) while A is the surface area of the spheres. To specify Reynolds number though, the average velocity needs to be determined. In general, local velocity may vary significantly, therefore we need to make an approximation based on average flow speeds. In deep saline aquifers used for CO_2 storage, flows range from 1 m/day to as low as 1 m/year obtaining flowrates around 10^{-6} m/s. Therefore, Reynolds number is at the range of 10^{-4} to 10^{-6} meaning that the internal effects are negligible comparing to the viscous dissipation. As a consequence, in porous media, turbulent flow is never observed and consequently the internal term in Navier-Stokes equation can be ignored.

$$\mu \nabla^2 v = \rho \frac{\partial v}{\partial t} + \nabla P - \rho g \quad Eq.(20)$$

Now if also steady state flow is assumed, velocity is only a function of space. Therefore, the previous equation is re written as:

$$\mu \nabla^2 v = \nabla P - \rho g \quad \text{Eq.}(21)$$

This equation applies to both single-phase and multiphase flow with the latter also needing to take into account the pressure changes across fluid interfaces.

An averaging of the above equation leads to Darcy's law, an empirical equation, describing flow in sand and generalized by Wyckoff et al. [62]

$$q = -\frac{K}{\mu}(\nabla P - \rho g) \quad Eq.(22)$$

where q is the Darcy velocity measuring the fluid flow per unit area of the porous medium and not actual velocity. K is the permeability and is an intrinsic property of the porous medium and in SI is measured in m^2, while in reservoir engineering it is most commonly encountered in Darcy or D. Since K relates vectors q and $\nabla P - \rho g$ it is therefore a tensor. Accordingly, Darcy's law can be written as

$$q_i = -\frac{K_{ij}}{\mu}\left(\frac{\partial P}{\partial x_;} - \rho g_j\right) \quad Eq.(23)$$

A porous media can be approximated by a set of capillary tubes of different size, as shown in Figure 23. Larger tubes tend to dominate over the flow. The cross sectional is d^2 and pore space occupies an area equal to πr^2. The total area is

$$A = n \times d^2 \quad Eq.(24)$$

were n is the number of tubes calculated as

$$n = \int_{r\_min}^{r\_max} f(r)\, dr \quad Eq.(25)$$

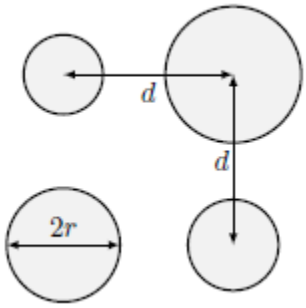

Figure 23. Cross section of tubes with varying radius [63].

Then the porosity can be calculated as the ratio of total cross-sectional area of void space to total area,

$$\phi = \frac{\pi \int_{r\_min}^{r\_max} r^2 f(r)\, dr}{nd^2} \quad Eq.(26)$$

Accordingly, permeability is calculated as

$$K = \frac{\phi r^2}{8} \quad Eq.(27)$$

In the case of multiphase flow in pore space, Darcy's equation is expressed as follows:

$$q_p = -\frac{k_{rp}K}{\mu_p}\left(\frac{\partial P}{\partial x_;} - \rho_p g\right) \quad Eq.(28)$$

where *p* represents the phase, k_{rp} is the relative permeability of phase *p*, representing how much the flow is restricted by other phases present in pore space and is a function of saturation.

Now that Darcy's law is defined, it is important to state the conservation equations of volume. Firstly, we encounter the conservation of mass for a porous medium. The difference is that in a porous medium, an averaging of the available volume. Assuming phase *p*, immiscible flow and considering a volume *V* bounded by surface *S* we have:

$$\int \frac{\partial \rho_p \phi S_p}{\partial t}\, dV = -\int \rho_p q_p\, dS \quad Eq.(29)$$

where $\rho_p \Phi S_p$ indicates the mass per unit volume of phase while the minus means that a net flow out of the volume leads to a decrease in mass. Using the Gauss theorem, the surface integral is transformed to a volume one.

$$\int \frac{\partial \rho_p \phi S_p}{\partial t}\, dV = -\int \nabla.\left(\rho_p q_p\right) dV \quad Eq.(30)$$

Now, since we considered an arbitrary volume, the above equation holds true and therefore the integrals must be equal and therefore

$$\frac{\partial \rho_p \phi S_p}{\partial t} = -\nabla.\left(\rho_p q_p\right) \quad Eq.(31)$$

Now in pore scale, considering that density is thought of being constant, porosity is also constant, and flow is very close to incompressible even for gas injection, Eq. (31) is transformed as:

$$\phi \frac{\partial S_p}{\partial t} + \nabla.q_p = 0 \quad Eq.(32)$$

Here *p* designates the phases. Saturation of all phases sums to unity and therefore the time derivative tends to zero. Therefore,

$$\nabla.q_t = 0 \quad Eq.(33)$$

were q_t is the total Darcy velocity (flow per unit area).

Now we can derive the relations for saturation and pressure for a two-phase flow. Then the total Darcy velocity will be calculated defining mobility. In the oil & gas industry, such study, assists in the determination of how pore-scale configuration of phases affects reservoir recovery.

It also assists us in the optimal design of injection and storage of CO_2. Multiphase flow is described by an extension of the Darcy law, Eq. (28):

$$q_w = -\frac{k_{rw}K}{\mu_w}(\nabla P_w - \rho_w g) \quad Eq.(34)$$

$$q_o = -\frac{k_{ro}K}{\mu_o}(\nabla P_o - \rho_o g) = -\frac{k_{ro}K}{\mu_o}(\nabla P_w + \nabla P_c - \rho_o g) \quad Eq.(35)$$

where the capillary pressure is $P_c = P_o - P_w$. Summing the equations above we have:

$$q_t = K(-\lambda_t \nabla P_w - \lambda_o \nabla P_c + \lambda_w \rho_w g + \lambda_o \rho_o g) \quad Eq.(36)$$

where $\lambda = \frac{k_r}{\mu}$ describing the mobility, with $\lambda_t = \lambda_o + \lambda_w$ the total mobility. Rearranging the previous equation, we define the Darcy velocity,

$$q_w = \frac{\lambda_w}{\lambda_t} q_t + K\frac{\lambda_w \lambda_o}{\lambda_t}(\rho_w - \rho_o)g + K\frac{\lambda_w \lambda_o}{\lambda_t}\nabla P_c \quad Eq.(37)$$

The Darcy velocity is composed of three components.

- $\frac{\lambda_w}{\lambda_t} q_t$ *(Advection term)* Defines the contribution to flow driven by the total movement of both liquid and gas phase.
- $K\frac{\lambda_w \lambda_o}{\lambda_t}(\rho_w - \rho_o)g$ *(Gravitational term)* Describes the tendency of water to move downwards under gravity in the presence of oil. Oil as more buoyant will move upwards. This term is highly affected by the density difference of the phases and is dependent of the mobilities of both phases.
- $K\frac{\lambda_w \lambda_o}{\lambda_t}\nabla P_c$ *(Capillary term)* This term describes the contribution of capillary forces. $\nabla P_c = \frac{dP_c}{dS_w}\nabla S_w$ is positive term and is the one affecting water imbibition into the pore space.

Considering the fractional flow f_w defined as:

$$f_w = \frac{\lambda_w}{\lambda_t} + \frac{K}{q_t}\frac{\lambda_w \lambda_o}{\lambda_t}(\rho_w - \rho_o)g_x + \frac{K}{q_t}\frac{\lambda_w \lambda_o}{\lambda_t}\frac{dP_c}{dS_w}\frac{\partial S_w}{\partial x} \quad Eq.(38)$$

The conservation equation for water becomes in one dimension:

$$\phi\frac{\partial S_w}{\partial t} + \frac{\partial q_w}{\partial x} = 0 \quad Eq.(39)$$

and for a finite total velocity with $q_w = f_w q_t$:

$$\phi\frac{\partial S_w}{\partial t} + q_t\frac{\partial f_w}{\partial x} = 0 \quad Eq.(40)$$

In this section the fluid flow in porous media was discussed, presenting the multiphase flow described by Darcy's law. The pore scale saturation described by Buckley-Leveret does not apply in great saline aquifers as the gross rock volume is extremely high and pressure effects cannot be ignored. In our case we use a pressure-based approach that correlates the pressure build up from each well with brine displacement.

2.4 METHOD OF STORAGE ESTIMATION

The tool to calculate the storage is the CO2STORED software (available here) developed to receive as input the geophysical characteristics of specific fields and from this to predict the capacity as a function of the number of injection wells. There are several ways in the literature that can estimate the storage capacity in a rock volume. The novelty with this model, is the calculation of the pressure response to CO_2 injection. This parameter is essential to consider, since it is this that constraints the injectivity.

Pressure response to CO_2 injection

According to [65] the pressure buildup to CO_2 injection into a single well in a reservoir with open boundaries and under the assumption of no fractures and traps, is calculated as:

$$\Delta p(r,t) = \frac{Q\mu_w}{2\pi kH} \times \begin{cases} \frac{\mu_c}{\mu_w}\ln\left(\frac{\psi}{r}\right) + \ln\left(\frac{R}{\psi}\right), & r < \psi \\ \ln\left(\frac{R}{r}\right), & \psi < r < R \\ 0 & r > R \end{cases} \quad Eq.(41)$$

Eq. (43) presents the solution of Eq. (15) introducing the sizing parameters of the reservoir where $\Delta p(r,t)$ is the pressure variation at time t and distance r from the injection well, Q is the volumetric flow rate, k is the absolute permeability, H the reservoir thickness, μ_w and μ_c are brine and CO_2 viscosities respectively, α is the reservoir compressibility, while, ψ represents the radius of a fictious equivalent vertical interface such that $\psi = \exp(\omega)\,\xi$ and $\omega = \frac{\mu_c+\mu_w}{(\mu_c-\mu_w)}\ln\left(\sqrt{\frac{\mu_c}{\mu_w}}\right) - 1$, $\xi = \sqrt{\frac{Qt}{\pi\phi H}}$, ϕ is the porosity, R refers to the radius of pressure propagation and is determined as:

$$R = \sqrt{\frac{2.25kt}{\mu_w a}} \quad Eq.(42)$$

and expands proportionally with $\sqrt{t}$.

In the case of a closed reservoir, under the assumption that the CO_2 plume radial extension ψ is smaller than reservoir radius R_c, the above equation is modified as:

$$\Delta p(r,t) = \frac{Q\mu_w}{2\pi kH} \times \begin{cases} \frac{\mu_c}{\mu_w}\ln\left(\frac{\psi}{r}\right) + \ln\left(\frac{R_c}{\psi}\right) + \frac{2R^2}{2.25R_c^2} - \frac{3}{4}, & r < \psi \\ \ln\left(\frac{R}{r}\right) + \frac{2R^2}{2.25R_c^2} - \frac{3}{4}, & \psi < r < R \\ 0 & r > R \end{cases} \quad Eq.(43)$$

In case of multi-well injection, the pressure response at location x_i can be approximated as the superposition of single well pressure responses

$$\Delta p_{sup}(x_i, t) = \sum_{j=1}^{n} \Delta p(d_{ij}, t) \qquad Eq.(44)$$

where n is the number of wells, $\Delta p(r, t)$ is the pressure response to a single well injection at distance r from the injection well, while d_{ij} is the distance between location x_i and x_j. Assuming an open boundary and that the same flowrate is injected at each well the superposed pressure response at x_i is estimated as

$$\Delta p_{sup}(x_i, t) = \frac{Q\mu_w}{2\pi kH}\left[\frac{\mu_c}{\mu_w}\ln\left(\frac{\psi}{r_0}\right) + ln\left(\frac{R_c}{\psi}\right) + \sum_{j=2}^{n}\ln\left(\frac{R}{d_{ij}}\right)\right] \qquad Eq.(45)$$

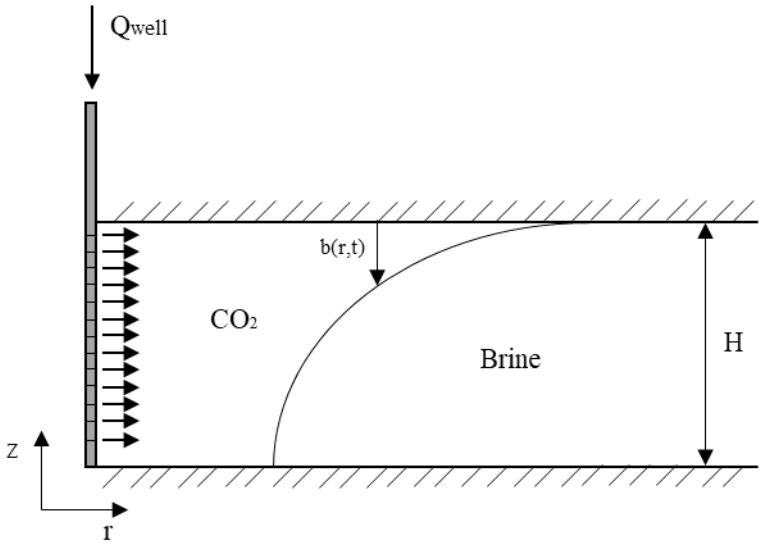

Figure 24. Typical profile of the region into which CO_2 is injected.

Nonlinear Δp/Q relationship

The extension of the CO_2 plume is affected by the flowrate. This implies that Δp does not depend on Q for $r < \psi$ (Figure 24). For both open and closed reservoirs, the difference between the overpressure associated with two different flowrates is calculated as:

$$\Delta p_D(r,t,Q_2) - \Delta p_D(r,t,Q_1) = -\delta \ln\left(\frac{\psi_2}{\psi_1}\right) = -\frac{\delta}{2}\ln\left(\frac{Q_2}{Q_1}\right) \qquad Eq.(46)$$

and

$$\delta = \frac{\mu_w - \mu_c}{\mu_w} \qquad Eq.(47)$$

rearranging the previous equation,

$$\Delta p(r,t,Q_2) = Q_2\left[\frac{\Delta p(r,t,Q_1)}{Q_1} - b \times ln\left(\frac{Q_2}{Q_1}\right)\right] \qquad Eq.(48)$$

and

$$b = \frac{\mu_w - \mu_c}{4\pi kH} \qquad Eq.(49)$$

Solving the above equation for Q_2 results in the calculation of flowrate after having estimated the overpressure for the first case Q_1. The relation can be observed in Figure 25.

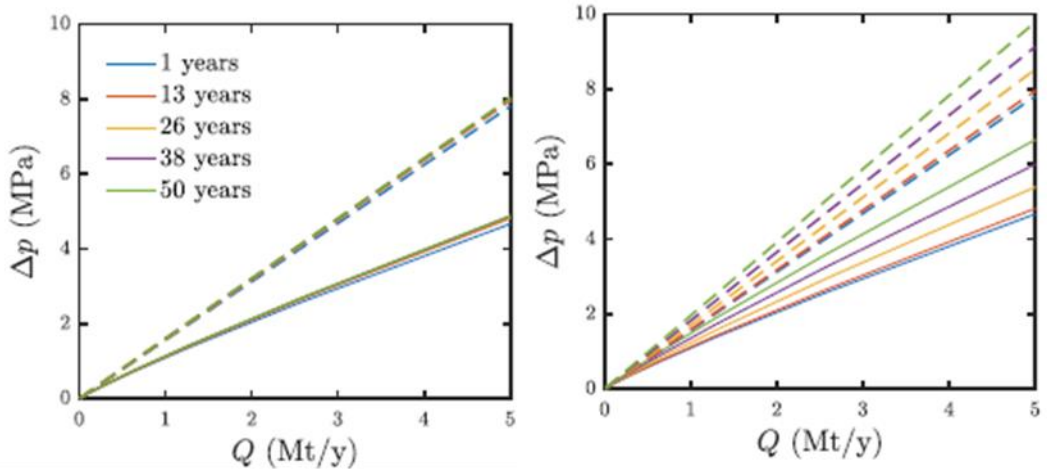

Figure 25. Absolute pressure build-up at the central well of a 16 well grid under different CO_2 flowrate scenarios for year 1 (left) and year 50 (right).

2.5 THE MODEL

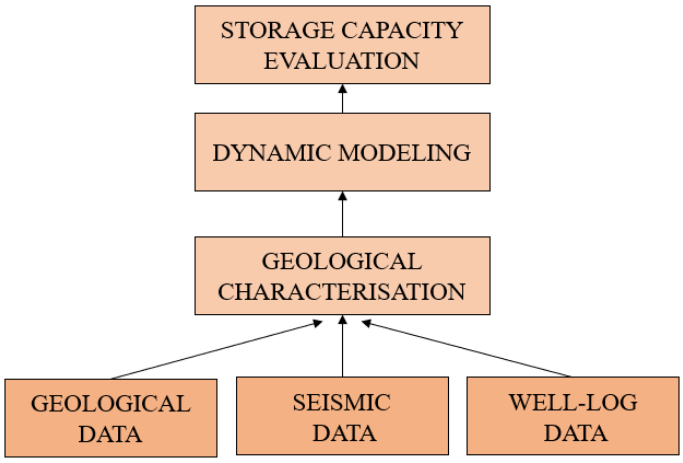

Figure 26. Overview of workflow to determine storage capacity.

The model combines geological data including rock compressibility, permeability and porosity, as well as spatial data such as area of field and gross rock volume, but it also requires water/brine properties provided as input (Figure 26). The model produces an estimation of the maximum injection rate and ultimately the storage capacity of a reservoir, utilizing the pressure build up in every injection well. CO_2 is injected in a number of *n* wells on a geological grid with spacing *d*. First, the maximum overpressure sustained by the reservoir is estimated according to the mechanical conditions for failure. Next, the pressure increase is estimated according to a reference injection flowrate given the pressure constraint. Then, the maximum allowable injection rate is calculated, respecting the fact that the overpressure should not be exceeded. Finally, constraints of aquifer type, wells spacing and rock compressibility, are taken into consideration in order to eliminate unfeasible scenarios.

2.5.1 Limits to pressure build-up

One of the greatest uncertainties in carbon geological sequestration is the reservoir response to a pressure increase. Extensive leakage of CO_2 back to the atmosphere due to fractures that may pre-exist or caused due to seismic activity is a major concern that should be taken into account while assessing storage capacity. Rock failure may happen in either tensile or shear mode. Tensile failure is more likely to occur along planes when the pore pressure exceeds the sum of min principal stresses σ_3 and rock tensile strength, S_0. According to Zoback et al. [66] the limiting pressure build-up for tensile failure is given by

$$\Delta p_M^t = \sigma_3 - p_0 + S_0 \qquad Eq.(50)$$

where p_0 is the initial pressure, assumed equal to hydrostatic one. In our case, we assume $S_0 = 0$ meaning that fracture pressure corresponds to the minimum principal stress.

Shear failure occurs along a given orientation when the shear stress τ exceeds the frictional forces according to Mohr-Coulomb criterion:

$$\tau - [C + (\sigma_n - p)\tan\varphi] \geq 0 \qquad Eq.(51)$$

where σ_n is the stress that acts normal to the orientation, φ is the friction angle, and C is the rock cohesion. The latter, according to Jaeger et al. [67] is assumed to be equal to $2S_0$. The limiting pressure for shear failure is calculated as

$$\Delta p_M^S = \frac{k_0 - \theta}{1 - \theta}(\sigma_1 - p_0) + C\cot\varphi \qquad Eq.(52)$$

where $k_0 \leq 1$ refers to the ratio of the minimum and maximum principal stress. The assumption of $C = 0$ refers to the likelihood of shear stress failure to happen along planes of weakness like faults.

The difference of shear (Δp_M^S) and tensile (Δp_M^t) stresses, indicates which one of the two overpressure limits will be exceeded first.

$$\beta = \Delta p_M^t - \Delta p_M^S = \left(k_0 - \frac{k_0 - \theta}{1 - \theta}\right)(\sigma_1 - p_0) + S_0 - C\cot\varphi \qquad Eq.(53)$$

Positive values of β indicate that shear failure is more likely to happen than tensile and vice-versa. In the case of rocks with zero cohesion $C = 0$, failure mostly occurs in shear mode ($\beta > 0$), since the first term in Eq. (62) is positive, as shown in Figure 27.

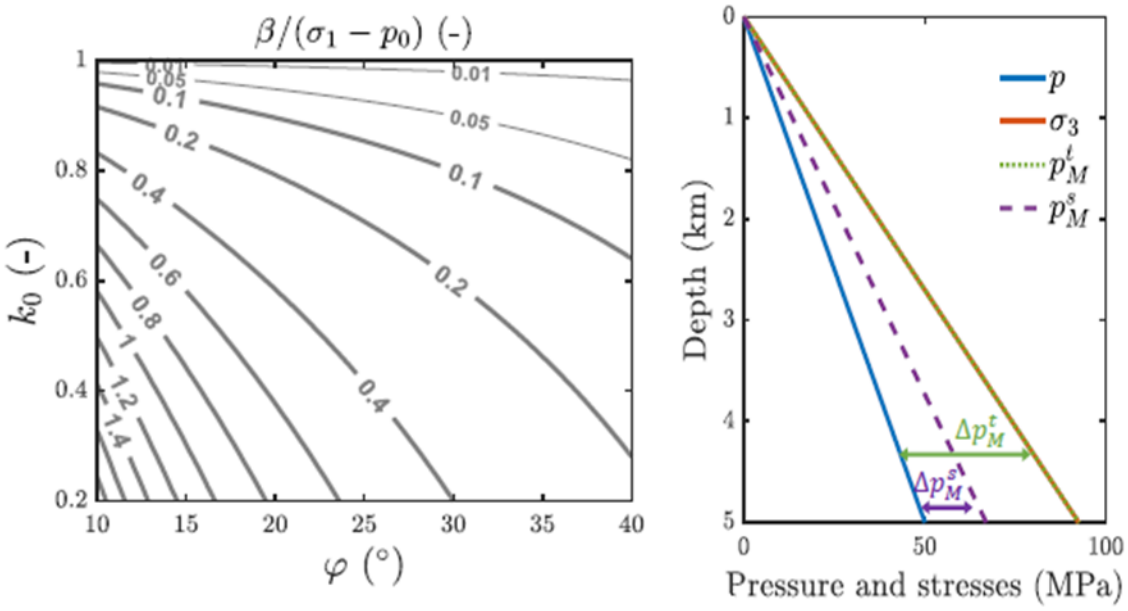

Figure 27. Potential for tensile and shear failure in cohesionless rocks.

In the left graph, the factor $\frac{\beta}{\sigma_1 - p_0}$ of Eq. (62) changes with the stress ratio k_0 and with the internal friction angle, but remains always positive indicating likelihood of shear failure rather than tensile one. The right graph indicates the variation of pressure and pressure limits with depth. It is created by assuming $k_0 = 0.5$ and $\varphi = 27^o$.

In cohesive rocks, in contrast, tensile failure is more likely to occur ($\beta < 0$) at shallow depths, where the effective stresses are smaller, even for small values of rock tensile stress S_0 as shown in Figure 28. In the software, the maximum sustainable overpressure is evaluated (Δp_M) as

the lower value of tensile and shear failure pressures Δp_M^t, Δp_M^S. On the other hand, such values are characterized by great uncertainty in their quantification and are affected by reservoir heterogeneity. Having reliable data of the magnitude of principal stresses, we are able to define the planes that are more likely to fail and define, eventually, the critical overpressure. However, such data are not present for all the fields and aquifers examined, and therefore an uncertainty is introduced in the overpressure estimation results.

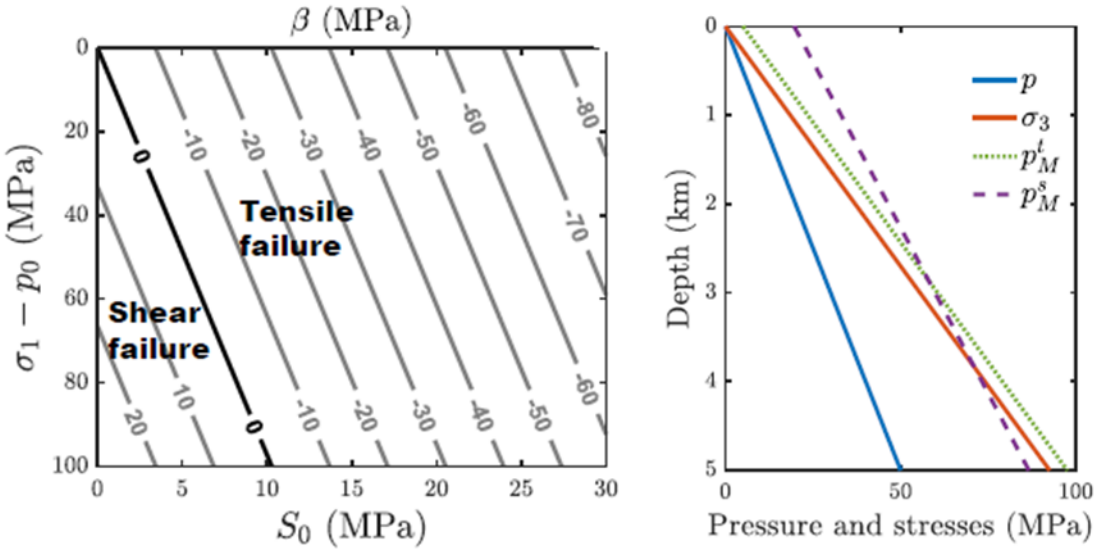

Figure 28. Example of potential for tensile and shear failure in cohesive rocks (β < 0).

In this case the value of β indicates that failure is function of confining stress (σ_1-p_o) (left). In the right graph the variation of pressure is plotted with depth. In cohesive rocks, the potential for tensile failure is greater than for shear failure at shallow depths.

2.5.2 Pressure build-up for reference injection rate

The next step in the model is the calculation of the pressure build-up with respect to the CO_2 injection rate, in a closed time interval. This calculation is important in the estimation of the maximum possible injection rate that will be subjected to certain constraints. This approach leads to the evaluation of various scenarios of well numbers and inter-well spacing for a given injection rate ratios in the reservoir. Figure 29 demonstrates the response of pressure build-up to a reference injection rate of 10 Mt y^{-1} for a 40 year period. As the number of wells and their spacing increases, pressure build-up decreases in a non-linear way. This provides us with potential designs for CO_2 injectivity on a reservoir, respecting the critical pressure limit Δp_M.

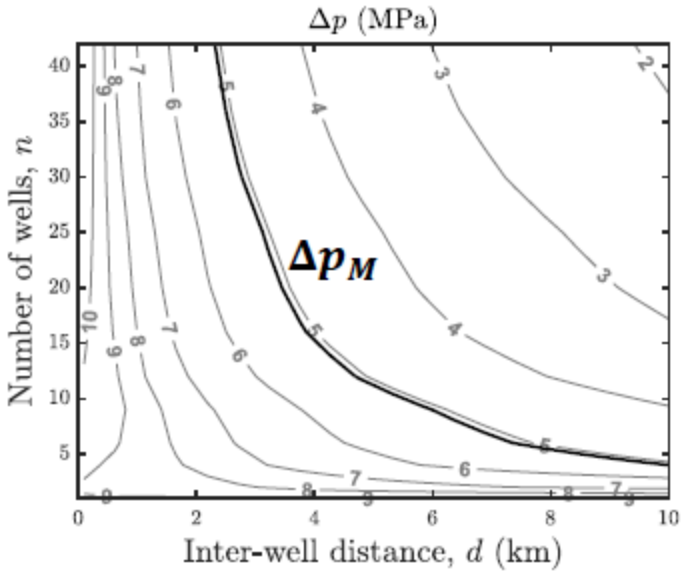

Figure 29. Pressure build-up at the reservoir under 40-year CO2 injection with different spacing scenarios, while the black line represents the critical pressure limit.

2.5.3 Maximum flowrate

Now that the maximum allowable pressure has been estimated, we can use it to determine the maximum sustainable flowrate Q_M. This rate leads to the estimation of the maximum amount of CO_2 that can be stored in a closed time interval *t*, without exceeding the suggested pressure limit. In single phase flow, pressure build-up and injection flowrate increase linearly, while in multiphase flow, according to Szulczewski et al. [68] the same relationship can be assumed for small variations of flowrate. This allows the estimation of the maximum allowable injection flowrate as

$$Q_M(t) = \frac{Q_r \Delta p_M}{\Delta p_r(t)} \qquad Eq.(54)$$

where Δp_r is the pressure response to the reference flowrate Q_r. In the case of larger variations in flowrate, the overpressure is non-linear leading to significant errors in storage capacity calculation. The relation between overpressure and flowrate is given by Eq. (48). From that, the direct calculation of maximum flowrate is derived as

$$Q_M(t) = -\frac{Q_r \widetilde{\Delta p_M}}{W\left(-\widetilde{\Delta p_M}\, e^{-\widetilde{\Delta p_r}(t)}\right)} \qquad Eq.(55)$$

Here the maximum and the reference flowrate, refer to the injection into each well, $W(x)$ refers to the Lambert's function for $x < 0$ and $\widetilde{\Delta p_M}$ and $\widetilde{\Delta p_r}$ defined as follows

$$\widetilde{\Delta p_M} = \frac{\Delta p_M}{b Q_r} \qquad Eq.(56)$$

$$\widetilde{\Delta p_r} = \frac{\Delta p_r}{bQ_r} \qquad Eq.(57)$$

where b is defined by Eq. (49) The direct estimation provides an assessment of the maximum flowrate for a number of scenarios, illustrated in Figure 30.

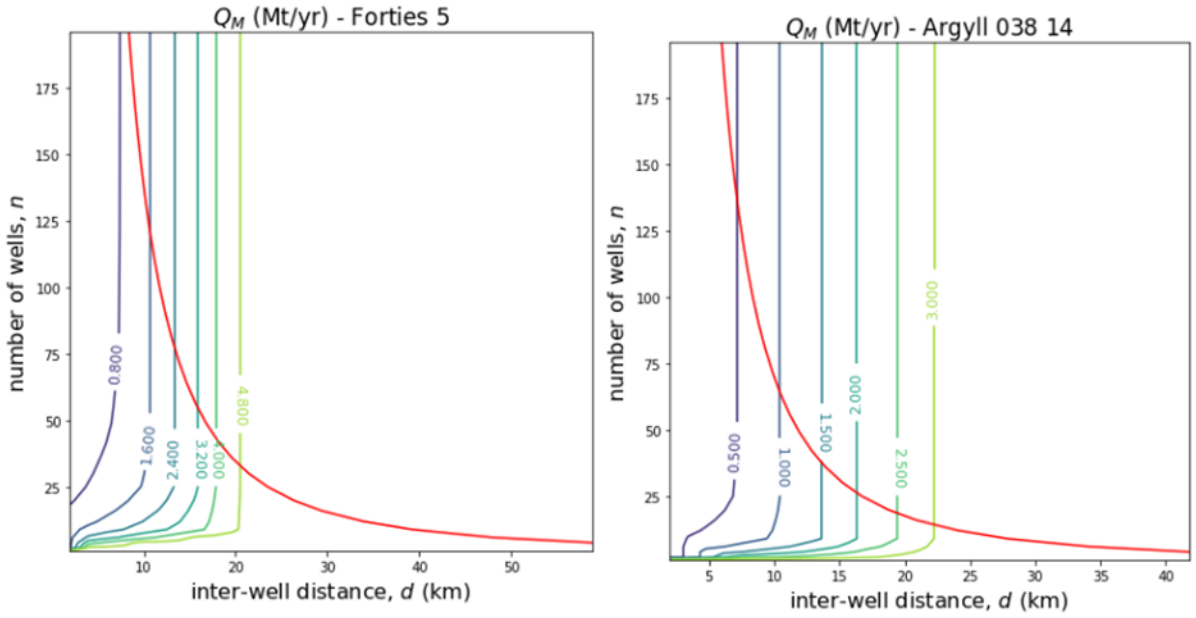

Figure 30. Plausible flowrate for a number of scenarios for Forties and Argyll fields under different scenarios of well number and spacing under 40 years of injection.

2.5.4 Constraints of the model

The first constraint has to do with the need to avoid CO_2 plume interference. In this constraint, the half of the inter-well distance is smaller than the plume average propagation distance resulting in

$$d > 2\sqrt{\frac{Q_M t}{n\pi\varphi H}} \qquad Eq.(58)$$

Another constraint limits the number of wells at a given area (referring to the area of the reservoir A). Assuming that the well distribution is a Cartesian grid (Figure 31), the constraints imposed by the area size of the reservoir is given by

$$d \leq \sqrt{\frac{A}{n}} \qquad Eq.(59)$$

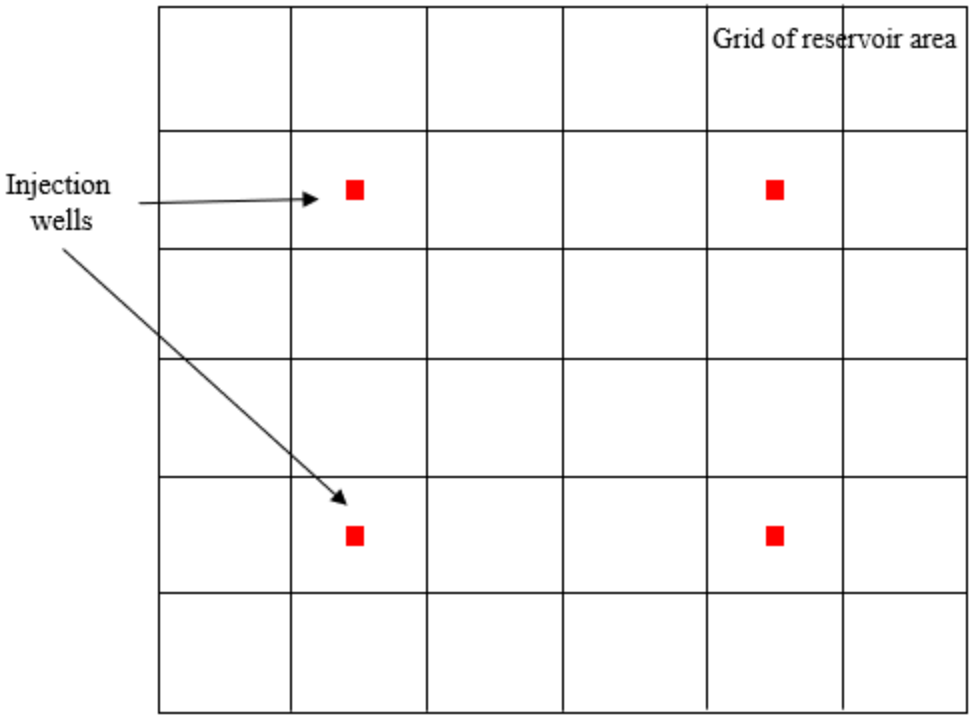

Figure 31. Grid of the reservoir area and placement of injection wells.

In the case of a "closed" aquifer, the available recovery area is reduced according to the following equation in order to approximate the reduced capacity.

$$r_c = \sqrt{\frac{A}{\pi}} \qquad Eq.(60)$$

Apart from these, there are technical limitations on the maximum injectable flowrate per well given by current technological advancement. Such value is noted as Q_s such that

$$n \geq \frac{Q_M^{tot}}{Q_s} \qquad Eq.(61)$$

where Q_M^{tot} is the total injection rate referring to the sum of the injection of the n wells. Results of the storage capacity are reported as shown in Figure 32.

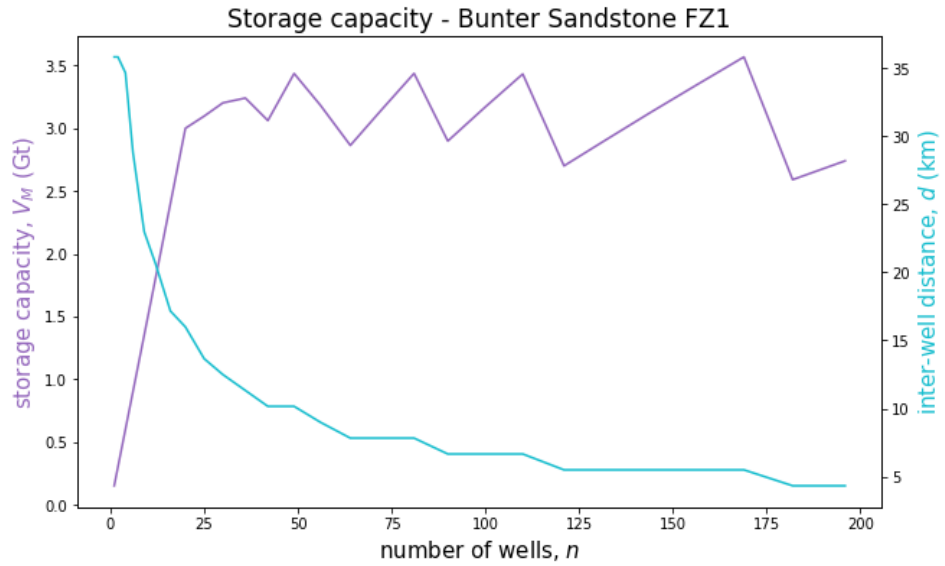

Figure 32. Storage capacity for 30 years of Bunter Sandstone zone 1, as a function of well number, for the plausible scenario of injection rate discussed before.

In the case some parameters are not provided, the further calculations are made to determine them.

(i) Pressure at the top of the reservoir

$$P_0 = Hydrostatic\ gradient\ \times mean\ depth \qquad \text{Eq. (62)}$$

(ii) Temperature at the center of the reservoir

$$T_0 = Temperature\ gradient\ \times depth \qquad \text{Eq. (63)}$$

(iii) Rock compressibility

$$c_{rock} = c_{default} \qquad \text{Eq. (64)}$$

While several default parameters are used in case they are not provided and are reported in Table 5.

Table 5. Default parameters that are used if they are not provided.

Parameter	**Value**
Lithostatic gradient	23 MPa km^{-1}
Hydrostatic gradient	10 MPa km^{-1}
Temperature gradient	33 ^oC km^{-1}
Default stress ratio (s3/s1)	0.7
Rock cohesion	0 MPa
Rock compressibility	5 $\times 10^{-4}$ MPa^{-1}
Water compressibility	3 $\times 10^{-4}$ MPa^{-1}
Salinity	180000 ppm

2.5.5 Sensitivity analysis

At this point it is essential to run a sensitivity analysis on the software described before, to assess its robustness as well as its potential flaws. The initial inputs on the software are reported in Table 6. where the subsequent result of storage capacity in 30 years is calculated at 13.8 Gt CO_2.

Table 6. Parameters and values considered as a baseline for the sensitivity analysis.

Parameter	**Value**
Permeability (mD)	100
Area (km^2)	100
Pore pressure (MPa^{-1})	16.6
CO_2 density (tonne m^{-3})	0.662
Reservoir thickness (m)	100
Salinity (ppm)	89000

Figure 33 presents a sensitivity analysis on how the software responds to different values of certain parameters and if the results produced, correspond with physical explanations. It is important to mention that when one parameter was changed, all the others remained unchanged, in order to single out the effect of one sole parameter on capacity. Beginning from the top left chart of porosity, values varied from 0.01 to 0.45 that include the spectrum of this study. Results seem to reach a peak at 0.1 porosity while for larger porosities a plateau seemed to be reached, with a small deviation of around 5% in the capacity. In the top middle graph permeability was plotted against capacity. The range was from 1 mD to 5 D, while the capacity increases with permeability until a plateau is reached where permeability no longer affects the storage potential of the aquifer. From a physical point of view, permeability represents the resistance to fluid flow though the rock and low values mean that flow is restricted. As permeability increases, pressure dissipates easier in the reservoir volume as CO_2 is injected. In the case of an "open" aquifer, CO_2 propagates and occupies the pore spaces while displaces brine in the process. In the case of high permeability rocks, this process happens much easier as CO_2 dissipates quicker enabling high capacities. In the event of a "closed" aquifer, there is no easy way for the pressure to dissipate and therefore it will build-up, drastically reducing escape ways for brine. As of the chart, from a point and after increasing permeability (making flow easier) capacity doesn't increase further.

At the top right graph, pore pressure as a function of capacity is plotted. The range is from 15 to 25 MPa^{-1} and as pressure increases, capacity is reduced as pressure diffusion process becomes more difficult. In the middle row first chart, the area vs capacity is presented. It is clear that the greater the reservoir area, the greater the storge capacity, given the fact that all other parameters are constant. The same behavior is observed for CO_2 density, though a 50% increase in density leads to a 30% increase in capacity. It is true that CO_2 density reduces with depth and values ranged from 0.5 to 0.75 tonne m^{-3}. Salinity as is plotted at a range from 50000ppm to 250000ppm, while seems that no affection is noted on storage capacity. In the bottom line of the figure, stress ratio $\frac{s_3}{s_1}$ is reported on the left, while capacity increases linearly with it. The variation is from 0.5 to 1.3 while the default value is 0.7.

Also, rock and water compressibility is plotted with the increase of both causing an increase

in the capacity. Apart from these graphs, a sensitivity analysis showed poor results for fields with thicknesses less than 40 m and/or area less than 15 km^2. Such results lead to the exclusion from the study, fields with thicknesses less than 40 m and group some of the fields with proximal geophysical characteristics and areas less than 15 km^2. An analytic table with the fields considered will be provided in the next chapter.

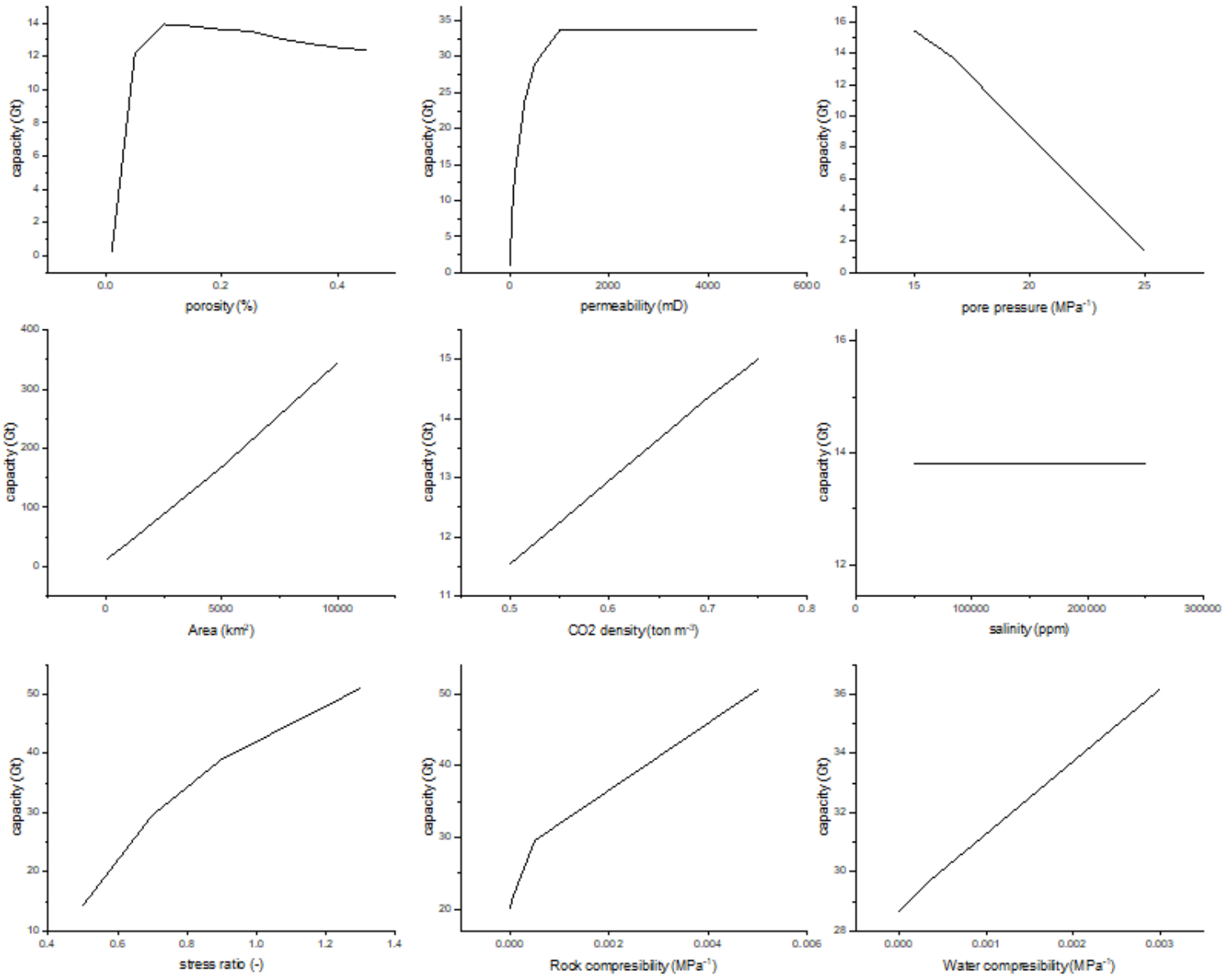

Figure 33. Sensitivity analysis on major parameters considered in the software.

You have the brushes, you have the colors, paint the heaven and enter.

Nikos Kazantzakis

CHAPTER III

RESULTS

Capacity results

In this section, the North Sea CO_2 storage capacity potential is reported for territories belonging to the United Kingdom (UK), Denmark, Norway, the Netherlands and Germany. In more detail, several offshore oil and gas fields were considered as well as saline aquifers. In more detail, the fields studied in every country, picked according to geophysical data availability. For the United Kingdom, 82 oil & gas fields considered (some of them depleted or close to depletion, while others are fully operating) and 88 saline aquifers (12 Brent formations, 48 Bunter Sandstone formations, 13 Cormorant fields, 4 Statfjord formations, 4 Nansen, 3 Spilsby Sandstone formations, 2 Chalk Group formations ech.). For Denmark, adequate data were retrieved for 14 oil and gas fields, while for Norway 10 deep saline aquifers were considered. In Germany, a large oil field (Mittelplate) was studied along with two Bunter formation aquifers. For the Netherlands 247 oil and gas fields (depleted or not) were considered due to huge databases available online. Before providing the capacity results, the data classification grade is reported for the studied countries. This characterization was explained previously (Figure 20, Section 2.1.1) and has to do with the quality of the data as well as the assumptions made and the outcome is reported in Table 7.

Table 7. Data characterization for the fields considered in the study.

Country	Data score
United Kingdom	**A** (Some assumptions only in Cormorant, Nansen, Bunter and Statfjord saline aquifers regarding the depth)
Denmark	**A** (Some assumptions in 3 oil fields regarding their area)
Norway	**B** (Assumptions regarding the volume of the saline aquifers)
Germany	**A** (No extra assumptions)
Netherlands	**C** (Assumptions regarding the area (km^2) of the oil and gas fields, while all other geophysical and geospatial characteristics were provided in literature. Therefore, an area of 76 km^2 per field was assumed as an average of the oil and gas fields of the other great database available, the one for the UK)

United Kingdom

Below the results of the study are reported. Figure 34 presents the storage capacity in UK's oil and gas fields. The total calculated CO_2 that can be potentially stored in the fields studied, are 18.2 Gt using around 195 wells. Greatest capacity is observed for the Forties oil field (Figure 38), a massive field of 93 km^2 characterized by high permeability and porosity that can potentially store 3 Gt of CO_2 over the next 30 years. Apart from that, Statfjord oil field, Brent oil field and Leman gas field are among the fields that can potentially store more than 1 Gt of CO_2. Figure 35 presents the storage capacity in UK's Brent formations saline aquifers. The total amount of CO_2 that can be potentially stored over 30 years is 26 Gt using 328 wells. The greatest saline aquifer is Rannoch_211_23, a high permeable aquifer with a potential of storing 6.3 Gt. While Ness_003_02 and Tabaret_211 are among the aquifers that can potentially store more than 3 Gt of CO_2.

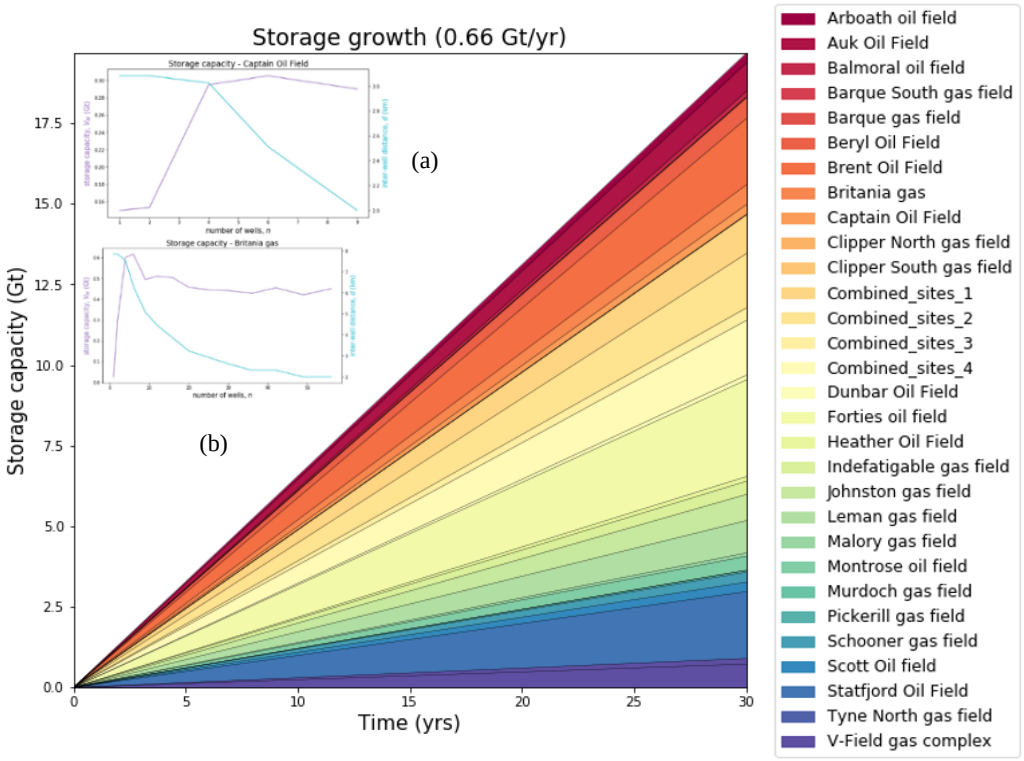

Figure 34. Storage capacity in UK's oil and gas fields studied. Also shown is the capacity as a function of the number of wells for two key fields (a) Captain oil field and (b) Britannia gas field.

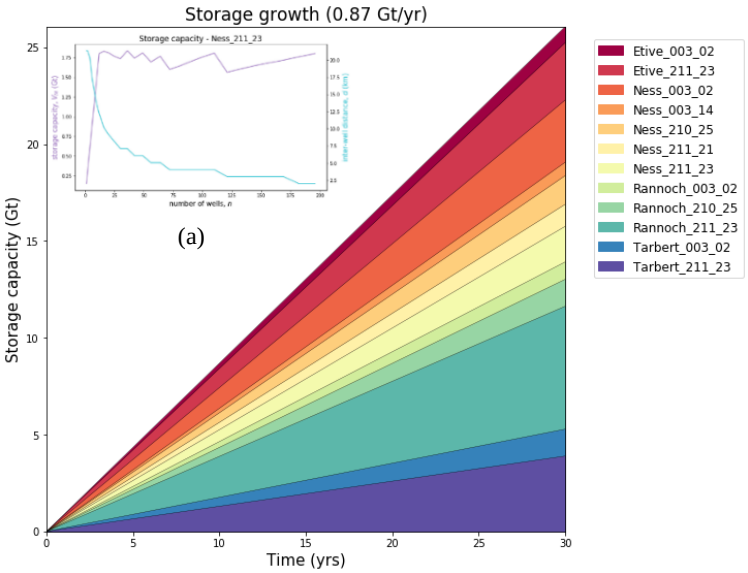

Figure 35. Storage capacity in UK's Brent Formations. Also shown is the capacity as a function of the number of wells for Ness_23 field (a).

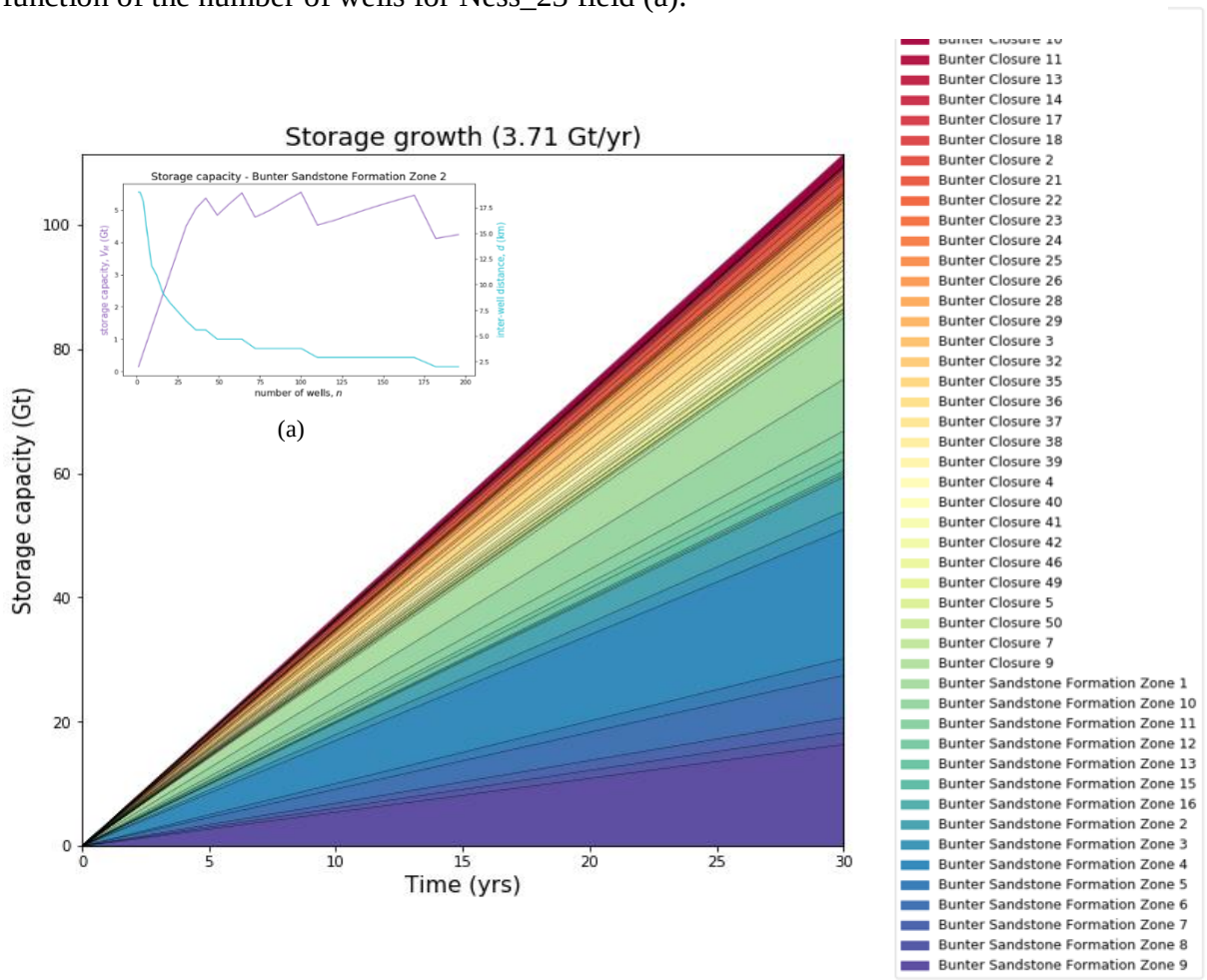

Figure 36. Storage capacity in UK's Bunter Sandstone formations. Also shown is the capacity as a function of number of wells for Bunter Zone 2 field (a).

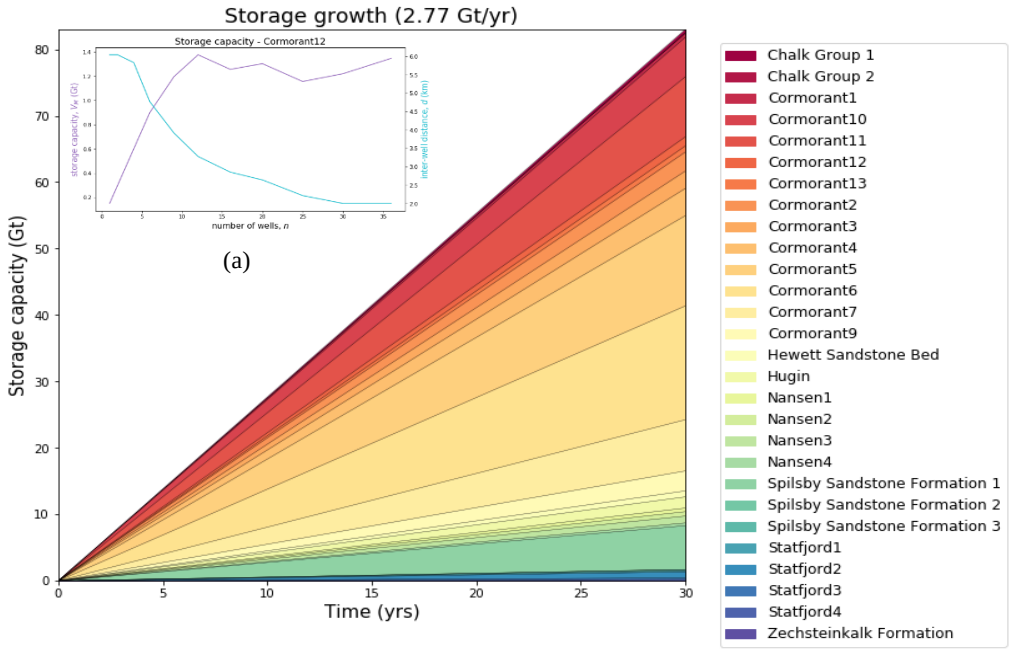

Figure 37. Storage capacity in rest UK's formations. Also shown is the capacity as a function of number of wells for Cormorant 12 field (a).

Figure 36 presents the storage capacity in the UK's Bunter formation saline aquifers. Bunter sandstone formations are characterized by permeabilities close to 100mD and low porosities around 12%. On the other hand, they are massive in volume resulting in large capacities. The 48 fields considered are able to store 110 Gt of CO_2 using in total 1340 wells over 30 years . Bunter sandstone formation zone 4 has a potential of 20 Gt alone that can provide a safe way to deposit carbon dioxide for the proximal industrial plans in UK.

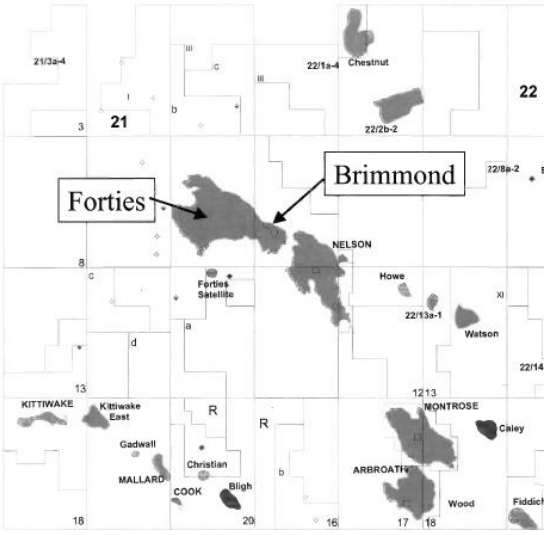

Figure 38. Forties oil field GIS photo [52].

Apart from the Bunter and Brent formations, a small number of other formations were studied as well. According to Figure 37, two Chalk formations, 13 Cormorant fields, 4 Nansen Group formations, 4 Statfjord, 3 Spilsby Sandstones, 1 Hugin, 1 Hewett Sandstone bed and one Zechteinkaik Formation provide an additional 82 Gt of CO_2 storage potential. Characterized by closed aquifers with low permeability high porosity, most those deep storage sites are massive in area and provide great capacities under 1053 wells.

It is important to mention here that the storage capacity is a function of the number of wells through which CO_2 is injected. As can be seen from the embedded charts in the main Figures, capacity is increased at first with the number of wells, until a point where a plateau is reached and from that increasing the number of wells doesn't increase capacity. Indeed, since the approach to storage is pressure based, a great number of wells may also penalize storage due to excessive pressure increases.

Denmark

Figure 39 presents the storage capacity of Denmark's oil and gas fields. Under 30-years of injection the storage capacity is estimated at 3.8 Gt or 130 Mt of CO_2 per year. As from 2017 Denmark emitted 31 Mt of CO_2 per year, an amount that can be offset through injection in only Harald gas field and Kraka oil field. In general, such oil and gas fields present low permeability and high porosity with average volume, but adequate to cover the excess emissions locally.

Norway

Figure 40 examines the storage capacity in deep saline aquifers of Norway. The results demonstrate that an amount close to 50 Gt of CO_2 can be stored in the ten designated aquifers in a rate of 1.6 Gt per year that is able to offset four times the current emissions of the country. Those ten aquifers are Stord Basin (NOR_106) with a capacity of 300 Mtn, Utsira and Skade aquifer (NOR_107) that has the greatest capacity reaching 15.7 Gt of CO_2, the Bryne and Sanders formation (NOR_108) with a capacity of 13.8 Gt, Sognefjord Delta aquifer (NOR_109) able to store 4.35 Gt, Johansen and Cook formations (NOR_110) with a potential of 2.66 Gt, Statfjord (NOR_111) with 3.71 Gt potential, Gassum formation (NOR_112) with 2.3 Gt, Paleogene Mounds (NOR_113) enabling 2.75 Gt of CO_2 deposition, Hugin East formation (NOR_114) for 79 Mt and Fiskebank formation aquifer (NOR_115) with 1.66 Gt over 30 years.

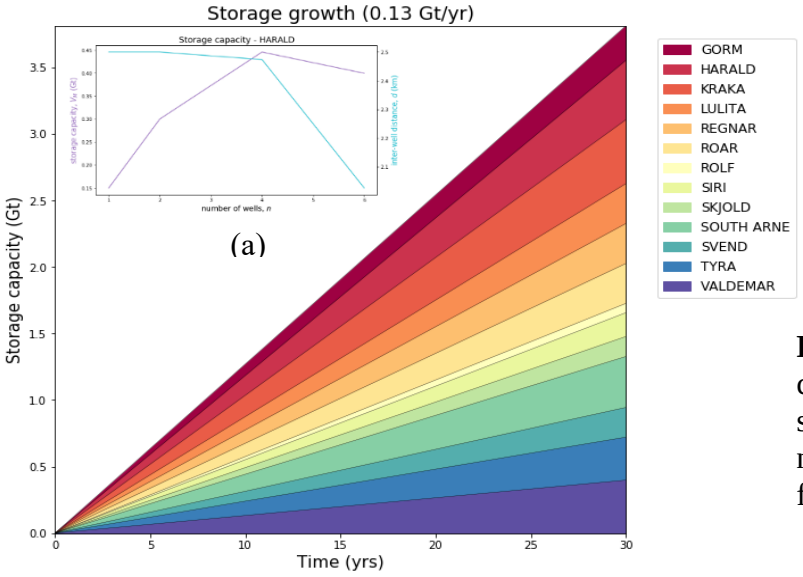

Figure 39. Denmark's storage capacity in its oil and gas fields. Also shown is the capacity as a function of number of wells for the Harald oil field (a).

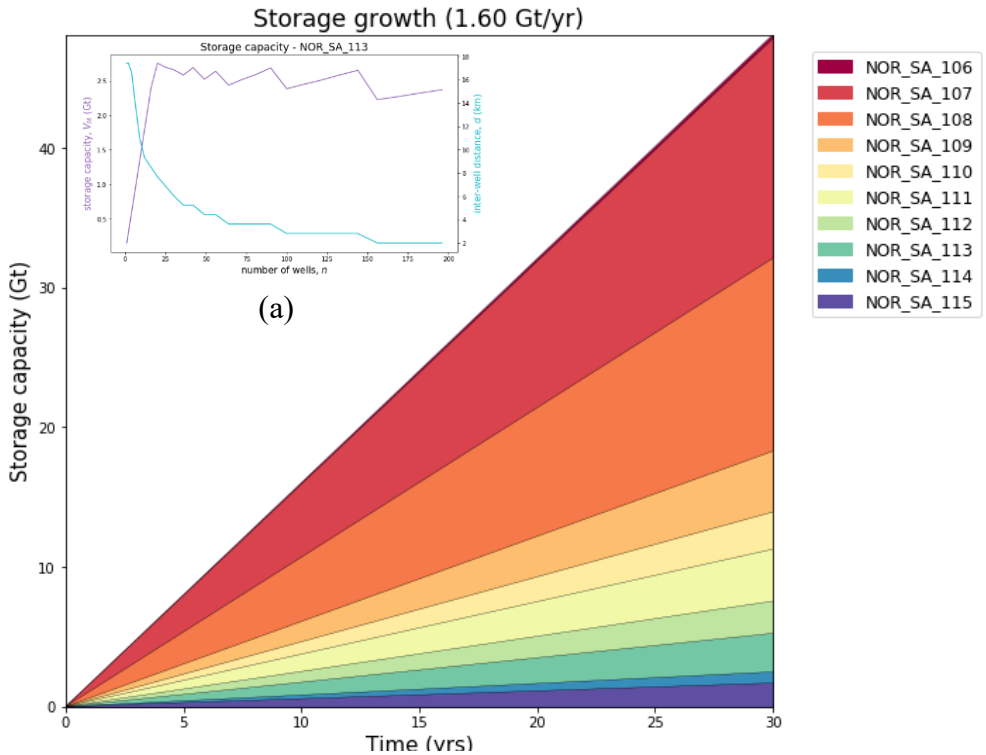

Figure 40. Norway's storage capacity in deep saline aquifers. Also shown is the capacity as a function of number of wells for the NOR_113 field (a).

Netherlands

In the Netherlands, from the 247 oil and gas fields studied, the thirty with the greatest capacity are shown in Figure 41. In total 1439 wells are able to inject 147.7 Gt of CO_2 during a 30-year span providing a vast storage potential that not only covers national emissions but European as well. Among the fields with the greatest capacity are NETH_317 or SCH-586 which is its code name with 2.4 Gt potential and NETH_291 or RTD-01 with same storage capacity potential. The geophysical characteristics comprise, on average, from low porosity ($\bar{\phi} = 0{,}13$) and high permeability close to 500 mD.

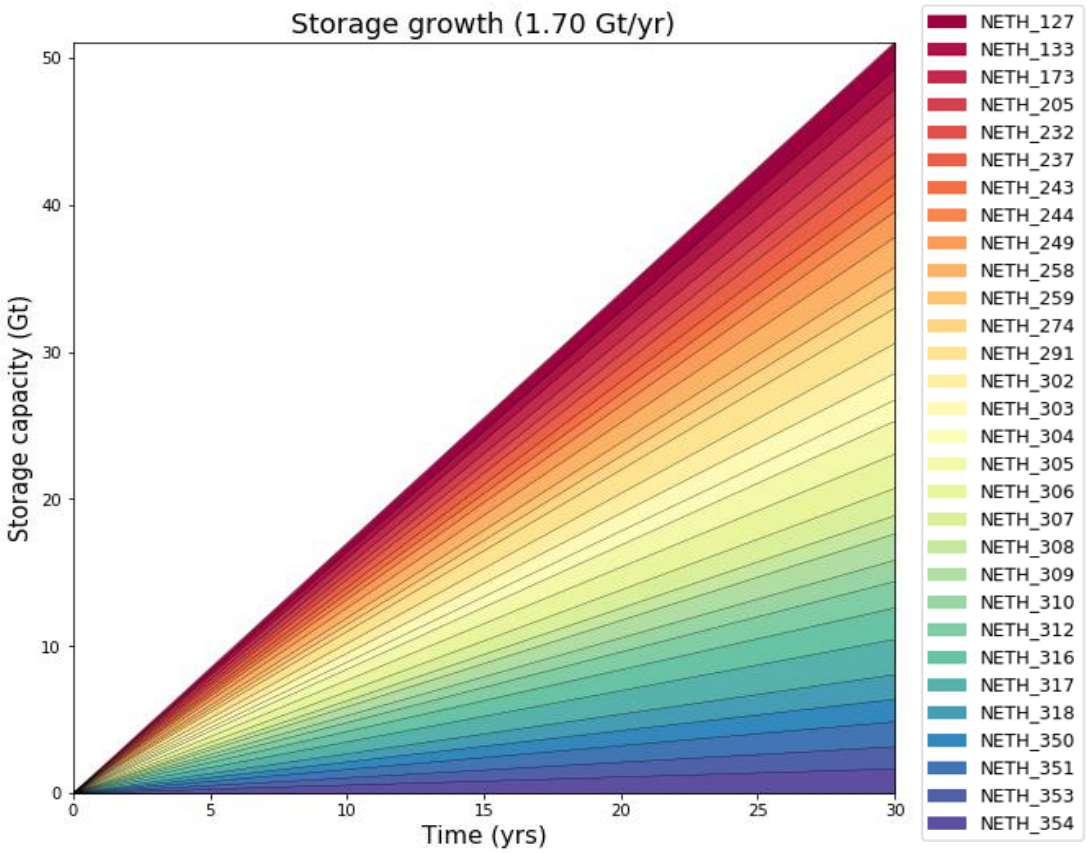

Figure 41. Netherlands CO2 storage capacity in oil and gas fields.

Germany

Germany is a country characterized by few offshore oil and gas fields, with Mittelplate oil field being the greatest in size and storage potential. As can be observed in Figure 42 (a) Mittelplate alone can store 630Mt of CO_2 using 6 wells. Adding to those, the two suggested Bunter formations, the total capacity reaches 1.64 Gt after 30 years of injection with a proximal rate of 0.03 Gt per year.

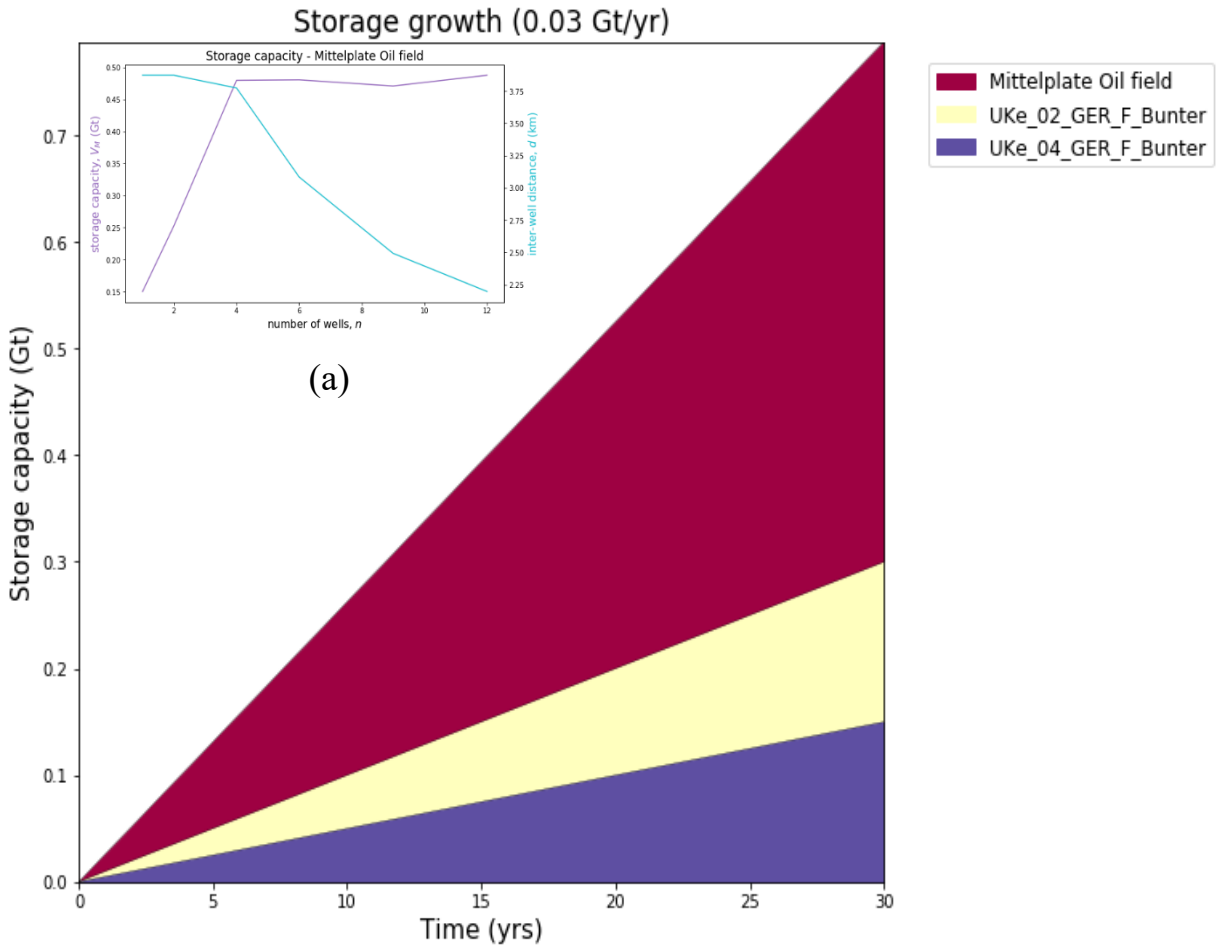

Figure 42. Storage capacity in the fields studied for Germany. Also shown is the capacity as a function of the number of wells for the Mittelplate oil field (a).

Comparison of capacity and demand for CCS

One of the most important outcomes of the study is reported in Figure 43, that compares the amount of CO_2 emitted in a yearly basis to the amount that can be stored in the aquifers studied. The United Kingdom has the potential to store almost 8 Gt per year while its current emissions are 20 times lower [69]. The Netherlands has the potential to store almost 30 times the current emitted amount reaching a potential of 5 Gt [70] per year while Norway has the potential of 1.6 Gt per year, 36 times their rate of emissions. Denmark has a potential of 127 Mt per year or 4 times their current emissions while Germany emits more than it can store in the three designated storage sites. Such very encouraging results, though, shouldn't distract the global efforts to combat dangerous climate change and its side effects that are proven catastrophic for all living habitats on the planet. Extensive carbon capture and storage can be used to provide policy makers, much needed, time in order to fully implement other important mitigation strategies. As international community is still dependent on fossil fuels and is projected to be for the next 30 years, the available carbon budget in order to avert global warming further than 1.5 ^{o}C is expected to be consumed long before 2050 [71], whereas this

period can be prolonged further in the case of CCS employment.

Complementary to the previous comments, it is important to mention that there is great uncertainty in the geophysical characteristics of deep-underground porous rocks and this study itself, has applied several assumptions, both in the software and data part, that may cause errors in the estimates of available storage capacity. It is our intention to keep the errors in the part of the geophysical uncertainties while minimizing the ones associated with the capacity calculation from a physical point of view. To determine whether our calculations associate with reality, as a first step, a comparison study was conducted with other studies available in literature, while results are presented in Table 8.

Table 8 provides a benchmark between the estimated results of storage capacity that we calculated using the pressure-based method, and other studies available in literature: most of them used the volume-based method. In UK's territory, De Simone et al. estimated a total of 140 Gt CO_2 capacity examining only 25 fields both oil & gas as well as the aquifer Bunter and Brent formations. Bentham [76] conducted a same study that included several oil & gas fields in UK and resulted to 5.6 Gt capacity but only in half of the storage sites comparing to our study. Heinenmann [74] conducted a volume-based analysis on several Bunter formations in UK territory, resulting in 7.8 Gt capacity over 30 years. This capacity is subject to 1 Mt per year injection rate, while if we calibrate this in our study's data (5 Mt/y injection rate) the previous result is 39 Gt of CO_2. In most cases, deviations in the results are the outcome of different calculation approaches or, most commonly, the different assumptions that authors consider to estimate missing data. Antonsen et al. [64] made a study on exactly the same oil and gas fields in Denmark as the ones in this study. The results presented few deviations as the total capacity estimated by the authors was 2.2 Gt. Halland et al. [76] conducted a study on Norwegian saline aquifers and resulted at 44.8 Gt at only a 10% deviation.

Table 8. Benchmark of results with other studies in the literature.

Country		**Calculated**	**De Simone et al. [72]**	**M. Bentham [73]**	**N. Heinenmann et al. [74]**	**K.L. Anthonsen et al. [75]**	**E. K. Halland et al. [76]**
				Gt (CO_2)			
United Kingdom	Oil & Gas	18.2	60-140	5.6	x	X	X
	Bunter	111.3		14.3*	39**	X	X
	Brent	26.08		x	x	X	X
	Rest	82.9	X	x	x	X	X
Denmark		3.81	x	x	x	2.2	X
Norway		48.1	X	x	x	X	44.8
Netherlands		147.7	X	x	x	X	X
Germany		1.64	x	x	x	X	X

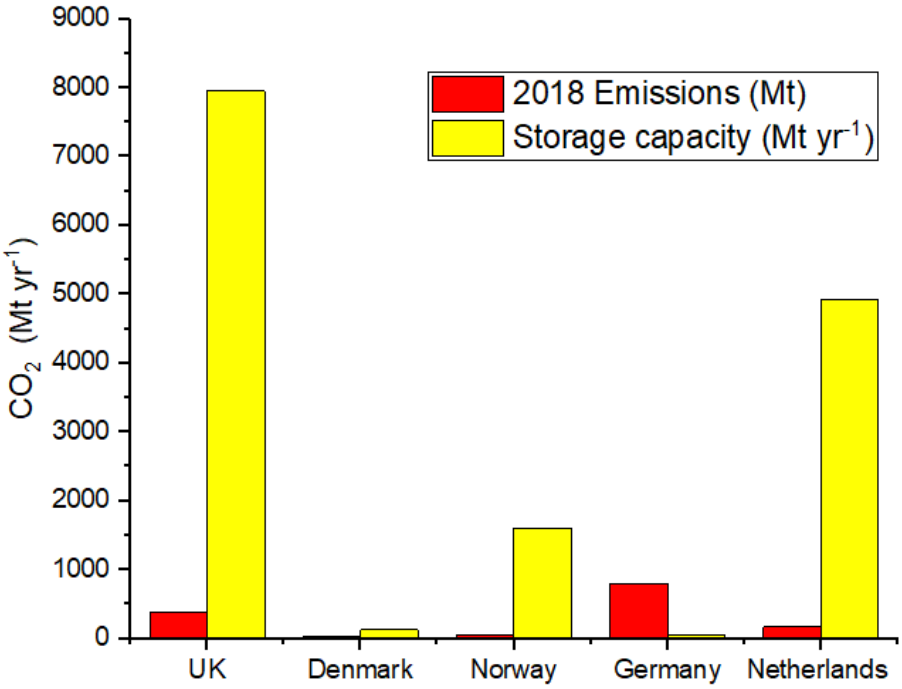

Figure 43. Carbon dioxide emissions per year and storage potential in aquifers studied.

Cumulative results for North Sea capacity

Figure 44 is a graphical representation of the results analyzed previously. It demonstrates the capacity of each country separately and from that but also from the previous charts, we can draw the conclusion that North Sea can act as a massive carbon dioxide storage site, that covers the needs in storage not only of the countries it bounds but for a great part of Europe as well. While the costs of carbon capture and storage are not considered in this study, they can play an important role in the adoption of extended CCS, but with carbon pricing and governmental grants, placing CO_2 underground is all the more possible and all the closer to implementation. And it should be if we intend to combat climate change seriously. However, the overall conclusion is that there is plenty of storage capacity to meet the likely needs of CCS this century.

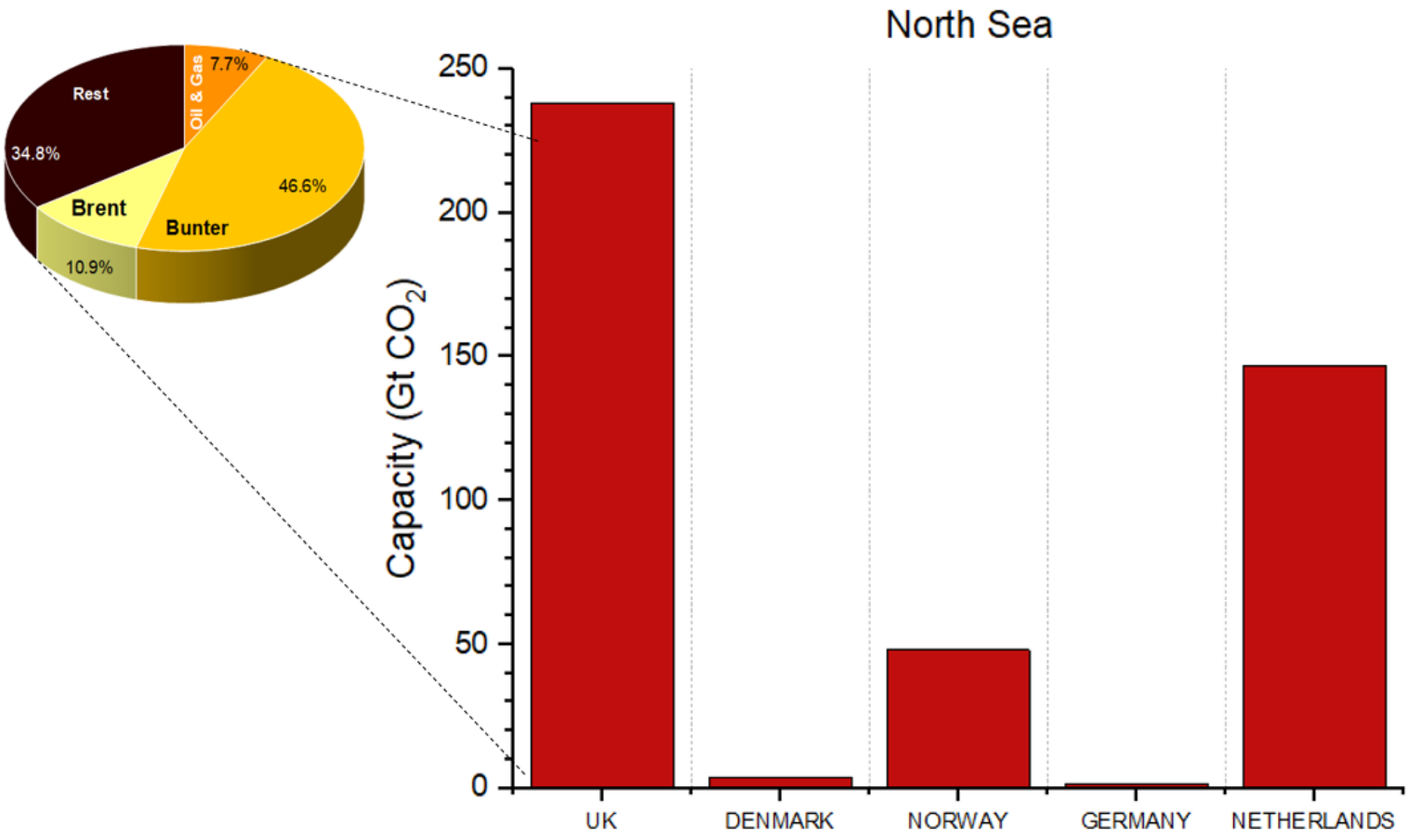

Figure 44. Cumulative results on carbon dioxide storage in North Sea territories as calculated in this study.

STORAGE EFFICIENCY

CO_2 storage efficiency in a reservoir indicates how much void space is occupied by carbon dioxide with respect to the available pore volume of the rock.

$$E = \frac{V_{CO_2}}{V_\Phi} \qquad Eq.(65)$$

where V_{CO_2} refers to the volume carbon dioxide occupies in the aquifer in the 30-year period, V_Φ is the gross rock volume in pore scale. It is true, that CO_2 in the aquifer conditions and its volume, depends on its density ρ_{CO2}, which is a function of temperature and pressure [77].

$$V_{CO_2} = \frac{M_{CO_2}}{\rho_{CO_2}} \qquad Eq.(66)$$

$$V_\Phi = A \times H \times \phi \qquad Eq.(67)$$

where M_{CO_2} is the carbon dioxide mass stored in the aquifer which has been calculated previously, A is the reservoir area, H refers to the reservoir thickness and ϕ is the porosity of the rock. According to the above equations, apart from the stored mass of CO_2 that is a function of a set of parameters analyzed in the previous chapter, storage efficiency is affected negatively by the designated area of injection (A) and the porosity of the rock (ϕ). For the density of the injected carbon dioxide, a fixed value was chosen at 0.662 tonne m^{-3}.

To put it in simple numbers in order to get the order of magnitude of expected efficiency, we use the compressibility equation below

$$c = \frac{1}{v}\frac{dP}{dv} => \frac{dv}{v} = cdP \qquad Eq.(68)$$

where the ratio $\frac{dv}{v}$ is the designated efficiency (volume of CO_2 injected divided by rock volume) c is the compressibility and is defined as $c = c_{rock} - c_{water}$. Water compressibility is around 4×10^{-10} (Pa), while in North Sea, according to Zimmerman [59] sandstone formations compressibility can be scaled at around $10^{-9}\ Pa^{-1}$. According to the previous equation, for pressure drops at the scale of 1MPa, efficiencies at the order of magnitude of few percent are expected. It is expected that rock properties and other parameters such as pressure depletion affect the final efficiency of carbon dioxide storage in saline aquifers.

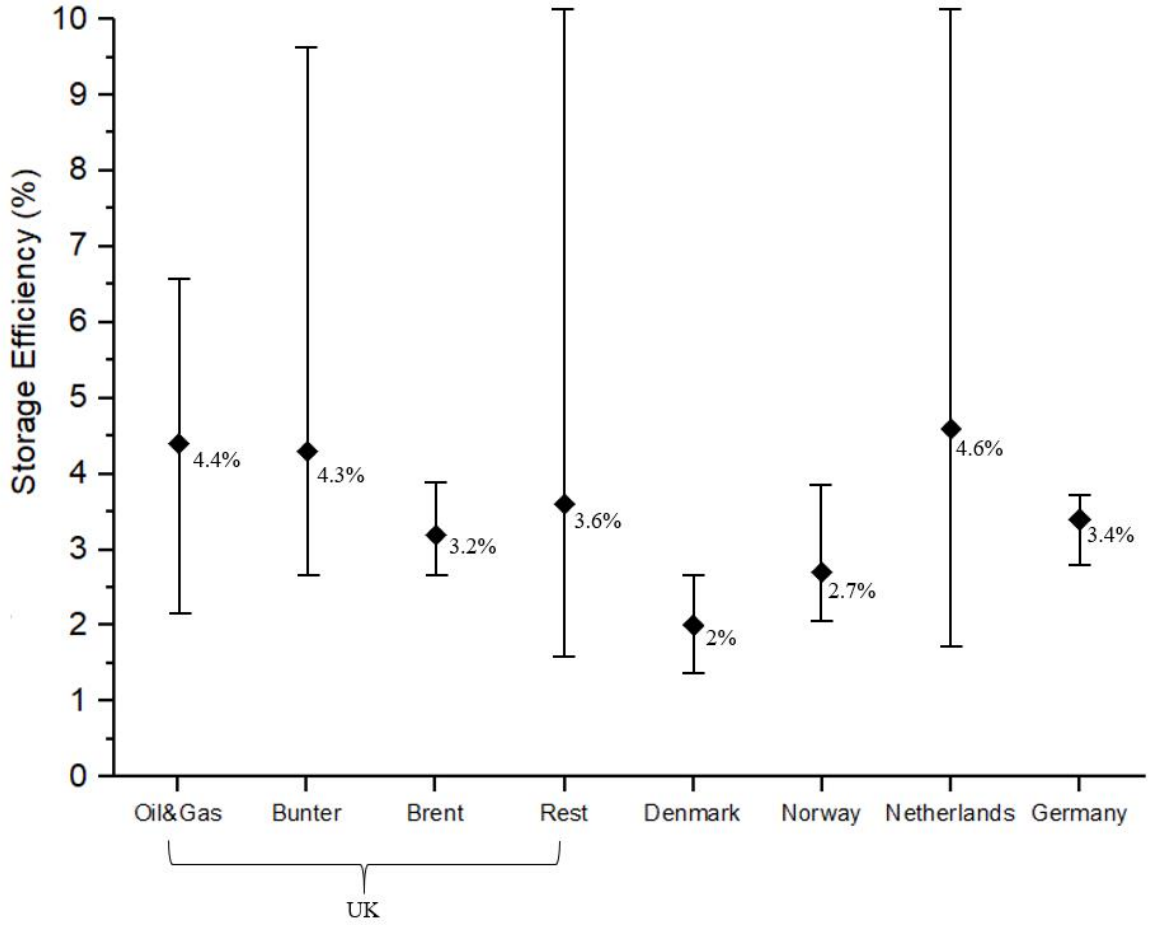

Figure 45. Average storage efficiency in the selected fields and saline aquifers.

Figure 45 represents an average of the storage efficiency of the selected oil and gas fields as well as saine aquifers. In more detail, the average efficiency for UK's Oil & Gas fields, according to this study, is 4.4% (2.1%-6.6%), for the Bunter geological formations in UK, is 4.3% (2.2%-9.5%), while Brent formations present much lower efficiencies, mainly due to the higher porosities of the rocks, and due to the great area they occupy, values that are denominators in the ratio. Those classified as 'Rest' are fields are of various formations that is the reason for the wide range in storage efficiency. Spilsby and Nansen formations present higher efficiencies comparing to Cormorant and Chalk fields. Oil & Gas fields in Denmark present an average efficiency of 2% with a range from 1.7% to 2.5%. Comparing to UK's Oil & Gas fields, high permeability reservoirs are present in Denmark but also, UK fields tend to be greater in size. In Norway's saline aquifers the average storage efficiency is 2.7% (2.2%-3.7%) due to their grate volumes of the rock (Sanders Formations 6 km^2 area, Ustria formation 2.8 km^2). Netherlands Oil & Gas fields present an average efficiency of 4.6% (1.9%-10%) while Germany's fields present medium size gross rock volumes with an average efficiency 3.4% (3.3% -3.7%). These numbers appear small, but the volumes of the storage aquifers are huge, and so still provide more than adequate capacity as discussed previously.

CONCLUSIONS & DISCUSSION

Carbon capture and storage has been proved to be one of the important mitigation strategies to avoid the uncharted waters of climate change. Extensive CO_2 capture and injection into the subsurface prevents its release into the atmosphere and stores it permanently for several thousands of years. This process, theoretically, can be done in many formations around the world, ether inland or offshore while it is of great importance that the selected storage sites to be in close proximity to the emission sources. In Europe, the greatest part of the carbon dioxide emissions is concentrated in the boundary areas/regions of the North Sea and are a product of increased industrial activity of the countries of northern Europe. Therefore, the North Sea – or, more precisely, the porous rock formations under the North Sea, presents an ideal place from geospatial point of view, to apply such techniques. As in most cases though, it is better said than done, and therefore several issues arise when it is high time to implement injection in the subsurface.

This study is a comprehensive analysis of 441 potential locations in the North Sea territory categorized based on the country of origin that can be used as carbon storage fields. These are oil and gas fields, depleted or not and several other saline aquifers, with the most common belonging to the Bunter and Brent formations. It has been found that, over 30 years, a total amount of 440 Gt of CO_2 can be stored in the fields examined, with 238 of them belonging to the UK (18.2 Gt in oil and gas fields, 111 Gt in Bunter formations, 26 in Brent formations and 82 Gt in the other formations studied), 3.8 Gt can be stored in Denmark's oil and gas fields, with a rate of 127 Mt yr^{-1}, 48 Gt can be stored in Norway's saline aquifers, 1.64 Gt in Germany's 3 potential sites identified and a total of 147 Gt in the Netherlands oil and gas fields, as can be seen in Table 9.

Table 9. Results of storage capacity in the examined countries of North Sea territory.

Country	Total CO_2 storage capacity (Gt)	CO_2 injection rate (Mt yr^{-1})
United Kingdom	238	7954
Oil & Gas fields	18.2	608
Brent formations	26	869
Bunter formations	111	3710
Rest formations	82	2765
Denmark	3.8	127
Norway	48	1603
Netherlands	147	4925
Germany	1.64	55
Total	**440**	**22620**

Considering the average CO_2 emissions of those countries, in the aquifers studied, the UK and the Netherlands can cover 20 times its current carbon footprint, Denmark more than twice, while Norway more than 12 times. Last but not least, the storage efficiency was estimated in the selected fields providing an average of 3.9% in UK, 2% and 2.7% in Denmark and Norway respectively, 3.4% in Germany and 4% in the Netherlands. These numbers are subjected to a number of assumptions both on the storage model and the available data. The later are difficult to acquire as they are a product of down-hole measurements of the rocks and are accompanied with

great uncertainties.

As for the storage model, the storage capacity estimation is calculated on a pressure-based basis, meaning, the pressure build-up on every injection well is calculated based on the CO_2 flowrate. In this way, storage capacity is a function of the plume pressure of CO_2 and not only of the geophysical characteristics of the rocks. This is a development from previous studies that calculate the available capacity based on the gross rock volume available in the formation, neglecting the pressure response of each injection well. It is vital that pressure is considered, since excessive pressures may lead to problems with injection and – more seriously – induce fracturing and earthquakes, allowing possible some of the stored gas to escape to the atmosphere or ocean.

These numbers, provide us with a clear outcome, considering even the potential uncertainties and errors, which is that extensive application of carbon capture and storage, can be effective in putting CO_2 underground and in this way, not only the concentration of CO_2 in the atmosphere is reduced but we provide ourselves with essential time to implement other more time demanding, mitigation strategies in order to avoid global warming greater than 1.5 ^{o}C by the end of the century.

FURTHER DEVELOPMENT

The current study can be further developed by enhancing the available geophysical data and/or retrieving some new databases, reducing the uncertainties associated with this aspect of the work. In addition, more and more fields can be included and a final categorization of the fields based on the results retrieved here and, on a scale, on how good they are in storing CO_2. On top of that, it would be of much interest to go on with a specific site assessment regarding the injection placement, well design and an update on the retrieved data of geophysical and rock characteristics. Something like that would be easier for depleted or nearly depleted oil and gas fields where the technological equipment already exists, compared to saline aquifer sandstone formations that are drilled for the first time.

The triptych, geophysical data – storage assessment - specific field design, should always be taken into consideration in a further comprehensive study that aims to initiate underground storage. Such a concept is already taking place in Norway's territory as a partnership of three big oil & gas companies. The Northern Lights project is a full-scale CCS project that collects CO_2 from the nearby cement and waste-to-energy plants and deposits it in the North Sea location with an injection rate of 3.5 Mt of CO_2 per year. This project is considered a state of the art and is expected to provide essential information to scale up and extensively adopt CCS technologies.

DATABASE

Code	Unit Name	Domain type	Depth Shallowest (m)	Depth Mean (m)	Thickness (m)	Area (km^2)	Permeability (mD)	Porosity (%)	Capacity (Gt)
UK_01	Combined Sites_01	Open	2743	2830	174	70.5	228	0.2	0.669
UK_02	Combined Sites_02	Open	3142	3234	202	119	418	0.14	1.285
UK_03	Combined Sites_03	Open	1636	1817	83	40	3528	0.23	0.387
UK_04	Combined Sites_04	Open	2687	2638	142	162	319	0.168	0.846
UK_05	Arboath oil field	Open	2414	2464	100	31.2	80	0.24	0.312
UK_06	Auk Oil Field	Open	2296	2448	304	93	5	0.19	0.878
UK_07	Balmoral oil field	Open	2330	2415	170	15	1000	0.25	0.177
UK_08	Barque gas field	Open	2399	2505.5	213	36	1	0.11	0.011
UK_09	Barque South gas field	Open	2399	2505.5	213	36	1	0.11	0.011
UK_10	Beryl Oil Field	Open	3292	3368	152	48	350	0.17	0.644
UK_11	Brent Oil Field	Open	2495	2625	260	77	650	0.21	2.052
UK_12	Britannia gas	Open	3813	3851	76	246	60	0.15	0.616
UK_13	Captain Oil Field	Open	861	886	50	38	7000	0.31	0.305
UK_14	Clipper North gas field	Open	2401	2500	198	22	1	0.11	0.007
UK_15	Clipper South gas field	Open	2401	2500	198	26	1	0.11	0.010
UK_16	Dunbar Oil Field	Open	1054	1096.5	85	48	40	0.13	0.145
UK_17	Forties oil field	Open	1864	2040.5	353	93	700	0.27	3.000
UK_18	Heather Oil Field	Open	2832	2866	68	56	20	0.145	0.144
UK_19	Indefatigable gas field	Open	2806	2851.5	91	155	30	0.15	0.409
UK_20	Johnston gas field	Open	3159	3201.5	85	192	10	0.17	0.813
UK_21	Leman gas field	Open	1799	1920.5	243	253	6	0.12	1.000
UK_22	Malory gas field	Open	2756	2793.5	75	19	24	0.14	0.103
UK_23	Murdoch gas field	Closed	3805	3822.5	35	20.2	73	0.106	0.071
UK_24	Montrose oil field	Open	2380	2447	134	40	80	0.24	0.438
UK_25	Pickerill gas field	Open	2718	2745	54	33	10	0.12	0.058
UK_26	Schooner gas field	Closed	3597	3791	388	55	30	0.1	0.308
UK_27	Scott Oil field	Open	3516	3570.5	109	35	1000	0.15	0.295
UK_28	Statfjord Oil Field	Open	2670	2800	260	77	500	0.23	2.247
UK_29	Tyne North gas field	Closed	3518	3578.5	121	15.8	35.1	0.11	0.123
UK_30	V-Field gas complex	Open	2197	2332.5	271	126.9	5.4	0.135	0.900
UK_31	Bunter Sandstone Formation Zone 5	Open	2000	2200	113.2	1465	15	0.14	2.713
UK_32	Bunter Closure 10	Open	2000	2200	179	11.8	15	0.26	0.150
UK_33	Bunter Closure 11	Open	3000	3300	86	12.7	15	0.14	0.050
UK_34	Bunter Closure 13	Open	2000	2200	107	60	15	0.16	0.134
UK_35	Bunter Closure 14	Open	3000	3300	144	59	15	0.07	0.294
UK_36	Bunter Sandstone Formation Zone 4	Open	2000	2200	198	11640	100	0.14	20.771
UK_37	Bunter Closure 1	Open	4000	4400	269	105	100	0.29	1.835
UK_38	Bunter Closure 4	Open	4500	4950	174	79	100	0.21	1.241
UK_39	Bunter Closure 5	Open	3000	3300	147	83.7	100	0.2	0.778
UK_40	Bunter Closure 7	Open	4500	4950	320	19	100	0.14	0.439
UK_41	Bunter Closure 35	Open	5500	6050	245	158	100	0.26	2.535
UK_42	Bunter Closure 36	Open	7500	8250	221	71	100	0.17	1.294
UK_43	Bunter Closure 37	Open	4000	4400	212	86	50	0.15	0.900
UK_44	Bunter Closure 38	Open	3500	3850	195	32	100	0.22	0.711
UK_45	Bunter Closure 39	Open	4000	4400	250	73	100	0.14	1.318
UK_46	Bunter Closure 40	Open	4000	4400	226	46	100	0.14	0.737
UK_47	Bunter Closure 41	Open	4000	4400	181	41	100	0.19	0.728
UK_48	Bunter Closure 42	Open	5000	5500	142	32	100	0.16	0.377

UK_49	Bunter Closure 46	Open	6000	6600	334	36	100	0.15	0.900
UK_50	Bunter Closure 49	Open	2000	2200	100	18	100	0.14	0.150
UK_51	Bunter Closure 50	Open	2000	2200	73	10	100	0.14	0.150
UK_52	Bunter Sandstone Formation Zone 1	Open	3000	3300	145	5125	350	0.14	9.858
UK_53	Bunter Sandstone Formation Zone 2	Open	2000	2200	295	1443	350	0.16	5.552
UK_54	Bunter Closure 32	Open	4000	4400	65	349	350	0.22	1.504
UK_55	Bunter Sandstone Formation Zone 3	Open	1000	1100	185	3200	100	0.09	2.877
UK_56	Bunter Closure 29	Open	5000	5500	269	82	100	0.22	2.101
UK_57	Bunter Sandstone Formation Zone 6	Open	1000	1100	269	5541	100	0.12	6.806
UK_58	Bunter Closure 18	Open	1000	1100	354	24	100	0.17	0.489
UK_59	Bunter Closure 2	Open	2000	2200	292	202	100	0.16	1.209
UK_60	Bunter Closure 21	Open	2000	2200	279	271	100	0.11	1.301
UK_61	Bunter Closure 22	Open	1500	1650	275	27	100	0.12	0.452
UK_62	Bunter Closure 23	Open	2000	2200	236	13	100	0.12	0.150
UK_63	Bunter Closure 24	Open	1500	1650	190	30	100	0.12	0.355
UK_64	Bunter Closure 25	Open	2000	2200	169	17	100	0.12	0.179
UK_65	Bunter Closure 26	Open	3000	3300	283	37	100	0.12	0.635
UK_66	Bunter Closure 9	Open	1000	1100	333	390	100	0.16	0.909
UK_67	Bunter Sandstone Formation Zone 7	Open	1000	1100	218	2482	100	0.16	2.392
UK_68	Bunter Closure 17	Open	2000	2200	172	32	100	0.2	0.526
UK_69	Bunter Closure 28	Open	2000	2200	232	231	100	0.15	1.030
UK_70	Bunter Closure 3	Open	2000	2200	239	81	100	0.19	0.819
UK_71	Bunter Sandstone Formation Zone 8	Open	1000	1100	138	3016	100	0.16	8.327
UK_72	Bunter Sandstone Formation Zone 9	Open	3000	3300	165	6404	50	0.22	3.262
UK_73	Bunter Sandstone Formation Zone 10	Open	3000	3300	125	2856	15	0.19	1.292
UK_74	Bunter Sandstone Formation Zone 11	Open	1000	1100	145	4868	100	0.2	1.918
UK_75	Bunter Sandstone Formation Zone 12	Open	1000	1100	145	1587	250	0.17	0.468
UK_76	Bunter Sandstone Formation Zone 13	Open	1000	1100	203	2096	100	0.14	0.457
UK_77	Bunter Sandstone Formation Zone 15	Open	1000	1100	56	661	350	0.16	1.915
UK_78	Bunter Sandstone Formation Zone 16	Open	1000	1100	56	1065	250	0.3	16.334
UK_79	Rannoch_210_25	Open	1510	1661	125	784	350	0.22	1.391
UK_80	Rannoch_211_23	Open	1010	1111	235	2192	1500	0.24	6.346
UK_81	Rannoch_003_02	Open	1330	1463	75	1299	250	0.19	0.899
UK_82	Etive_211_23	Open	1010	1111	110	2129	1500	0.24	2.960
UK_83	Etive_003_02	Open	1330	1463	70	1307	250	0.19	0.842
UK_84	Ness_210_25	Open	1380	1518	120	1187	350	0.22	1.481
UK_85	Ness_211_23	Open	1010	1111	71	1825	1500	0.24	1.837
UK_86	Ness_211_21	Open	1500	1650	160	580	200	0.2	1.138
UK_87	Ness_003_02	Open	1330	1463	180	1307	700	0.2	3.213
UK_88	Ness_003_14	Open	1250	1375	85	650	280	0.17	0.691
UK_89	Tarbert_211_23	Open	1010	1111	145	2113	1500	0.24	3.894
UK_90	Tarbert_003_02	Open	1330	1463	75	1305	700	0.2	1.389
UK_91	Spilsby Sandstone Formation 1	Open	1467	1617	78.6	11619.8	100	0.16	6.592
UK_92	Spilsby Sandstone Formation 2	Closed	1228.04	1378.04	14	285.7	100	0.23	0.021
UK_93	Spilsby Sandstone Formation 3	Open	808.68	958.68	33	1222	100	0.23	0.178
UK_94	Hewett Sandstone Bed	Open	1039	1189	25.53	6677	500	0.17	0.900

UK_95	Chalk Group 1	Open	1718	1868	689	105	0.55	0.36	0.547
UK_96	Chalk Group 2	Closed	1259.43	1409.43	820.36	19	0.5	0.36	0.050
UK_97	Zechsteinkalk Formation	Open	1371.53	1521.53	31	8180	1	0.06	0.028
UK_98	Cormorant1	Closed	4297	4447	645.78	63	40	0.2	0.600
UK_99	Cormorant2	Closed	4297	4447	645.78	292	40	0.2	2.864
UK_100	Cormorant3	Closed	4297	4447	645.78	265	40	0.2	2.611
UK_101	Cormorant4	Closed	4297	4447	645.78	389	40	0.2	4.099
UK_102	Cormorant5	Closed	4297	4447	645.78	1080	40	0.2	13.576
UK_103	Cormorant6	Closed	4297	4447	645.78	1300	40	0.2	17.120
UK_104	Cormorant7	Closed	4297	4447	645.78	580	40	0.2	7.703
UK_105	Cormorant9	Closed	4297	4447	645.78	309	40	0.2	3.000
UK_106	Cormorant10	Closed	4297	4447	645.78	457	40	0.2	5.950
UK_107	Cormorant11	Closed	4297	4447	645.78	709	40	0.2	9.029
UK_108	Cormorant12	Closed	4297	4447	645.78	146	40	0.2	1.376
UK_109	Cormorant13	Closed	4297	4447	645.78	89	40	0.2	0.908
UK_110	Hugin	Closed	4242	4392	215	470	75	0.2	1.689
UK_111	Statfjord1	Closed	3150	3300	62	216	470	0.22	0.172
UK_112	Statfjord2	Closed	3150	3300	62	1144	470	0.22	0.900
UK_113	Statfjord3	Closed	3150	3300	62	316	470	0.22	0.226
UK_114	Statfjord4	Closed	3150	3300	62	245	470	0.22	0.195
UK_115	Nansen1	Closed	3020	3170	43	980	330	0.14	0.536
UK_116	Nansen2	Closed	3020	3170	43	1182	330	0.14	0.659
UK_117	Nansen3	Closed	3020	3170	43	2115	330	0.14	1.041
UK_118	Nansen4	Closed	3020	3170	43	822	330	0.14	0.405
DEN_01	GORM	Open	1975	2100	250	12	30	0.38	0.261
DEN_02	HARALD	Open	2600	2700	200	25	50	0.36	0.446
DEN_03	KRAKA	Open	1610	1800	380	20	50	0.31	0.480
DEN_04	LULITA	Open	3360	3500	280	3	50	0.26	0.300
DEN_05	REGNAR	Open	1600	1700	200	8	100	0.39	0.300
DEN_06	ROAR	Open	1850	2025	350	14	100	0.33	0.300
DEN_07	ROLF	Open	1650	1800	300	8	5	0.39	0.070
DEN_08	SIRI	Open	1910	2010	200	30	20	0.29	0.179
DEN_09	SKJOLD	Open	1520	1600	160	10	20	0.31	0.150
DEN_10	SVEND	Open	2400	2500	200	25	20	0.3	0.383
DEN_11	SOUTH ARNE	Open	2710	2800	180	17	50	0.36	0.223
DEN_12	TYRA	Open	1890	2000	220	90	20	0.36	0.323
DEN_13	VALDEMAR	Open	2430	2600	340	30	20	0.3	0.399
NOR_106	Stord basin	open	1387.5	1450	125	50	120	0.21	0.300
NOR_107	The Utsira and Skade aquifer	open	1725	2000	550	2800	1000	0.18	15.718
NOR_108	The Bryne and Sandnes Formations	open	1510	1700	380	6000	150	0.2	13.801
NOR_109	The Sognefjord Delta aquifer	open	1600	1750	300	2000	300	0.29	4.351
NOR_110	The Johansen and Cook Formation aquifer	open	1604	1700	192	1600	400	0.26	2.661
NOR_111	The Statfjord Formation aquifer	open	2250	2400	300	1800	200	0.28	3.718
NOR_112	The Gassum and Skagerrak Formation	open	2110	2200	180	1100	450	0.22	2.307
NOR_113	The Paleogene Mounds Formation aquifer	open	1837.5	1900	125	1215	1000	0.28	2.758
NOR_114	Hugin East Formation aquifer	open	1652.5	1700	95	160	500	0.28	0.797
NOR_115	The Fiskebank Formation aquifer	open	1935	2000	130	120	1000	0.3	1.689
GER_01	Mittelplate Oil field	open	2250	2700	90	60	368	0.18	0.637
GER_02	UKe_02_GER_F_Bunter	open	1750	1900	100	11	500	0.2	0.452
GER_03	UKe_04_GER_F_Bunter	open	1600	1850	150	11	500	0.2	0.559
NETH_117	AKM-09	open	3947	4001.5	109	76	127	0.17	0.371
NETH_118	AKM-11	open	3285	3344	118	76	60.1	0.143	0.237

NETH_119	AME-104	open	2928.5	2980	103	76	102	0.126	0.161
NETH_120	ANJ-01	open	2911.3	2966.45	110.3	76	372	0.145	0.303
NETH_121	ANL-01	open	3038.5	3068.25	59.5	76	38.4	0.112	0.206
NETH_122	ANN-01	open	2666.7	2711.35	89.3	76	246	0.167	0.256
NETH_123	ANN-06	open	1514	1594	160	76	171	0.146	0.607
NETH_124	ANV-01	open	2080	2188.5	217	76	1210	0.225	0.081
NETH_125	APS-01	open	2823	2908.5	171	76	182	0.187	0.409
NETH_126	BGM-01	open	3853	3909.5	113	76	180	0.181	0.558
NETH_127	BGM-01	open	1944.5	1998.75	108.5	76	71.3	0.23	1.832
NETH_128	BIR-01	open	2281	2316	70	76	211	0.136	0.600
NETH_129	BIR-13-S2	open	984	1035.5	103	76	50.1	0.21	0.406
NETH_130	BKLM-04	open	1242	1302.5	121	76	1730	0.284	0.198
NETH_131	BKZ-01	open	1259	1312.5	107	76	482	0.241	0.287
NETH_132	BRK-01	open	1204	1254.5	101	76	2090	0.259	0.150
NETH_133	BRK-09	open	2678	2778	200	76	100	0.127	1.336
NETH_134	BRK-13	open	1995	2021.5	53	76	82.7	0.246	0.756
NETH_135	BRK-23	open	2590	2651.25	122.5	76	148	0.174	1.017
NETH_136	BRTZ-01	open	2762	2811	98	76	130	0.156	0.474
NETH_137	BTL-01	open	3546	3756.5	421	76	91.6	0.132	0.150
NETH_138	BTL-01	open	3588	3802.5	429	76	132	0.129	0.380
NETH_139	BTL-01	open	3686	3719.5	67	76	948	0.12	0.300
NETH_140	D12-03-S1	open	1587	1617	60	76	42.8	0.142	0.832
NETH_141	D15-03	open	315	354	78	76	385	0.225	1.018
NETH_142	D15-04	open	2881	2958.5	155	76	277	0.199	0.313
NETH_143	DEL-03	open	4302	4359.5	115	76	101	0.1	0.108
NETH_144	DEN-02	open	2897	2986.5	179	76	52.4	0.171	0.504
NETH_145	DZL-01	open	2632	2685.5	107	76	126	0.157	0.703
NETH_146	E18-06	open	3181.5	3239.5	116	76	169	0.125	0.279
NETH_147	EKL-12	open	3880	3939.5	119	76	43.5	0.189	0.273
NETH_148	EKR-101	open	2688	2768	160	76	452	0.216	0.300
NETH_149	ETV-01	open	4127.3	4197.3	140	76	32.5	0.129	0.404
NETH_150	EWM-01	open	1883	1925.65	85.3	76	35.5	0.139	0.159
NETH_151	F10-01	open	3848	3918.5	141	76	119	0.189	0.998
NETH_152	F16-03	open	2772	2834.5	125	76	1040	0.17	0.165
NETH_153	FLN-01	open	2932	3015.5	167	76	646	0.187	0.124
NETH_154	FRM-01-S3	open	2195	2300	210	76	368	0.163	0.372
NETH_155	G17-A-01	open	3060	3178.5	237	76	61.5	0.153	0.826
NETH_156	G17-A-02	open	3653	3684	62	76	304	0.157	1.214
NETH_157	GAG-01	open	2956	2989.005	66.01	76	45.4	0.191	1.107
NETH_158	GAG-02-S1	open	3314.5	3419	209	76	64	0.175	0.398
NETH_159	GAG-03	open	3272	3324.25	104.5	76	42.1	0.173	0.336
NETH_160	GGT-01	open	3354	3403.25	98.5	76	86.4	0.18	0.150
NETH_161	GRK-01-S1	open	3366	3409.5	87	76	57.3	0.173	0.358
NETH_162	GRK-11	open	2454	2581	254	76	102	0.205	0.150
NETH_163	GRK-13	open	2237	2269	64	76	240	0.175	0.216
NETH_164	GRK-47	open	1994	2087	186	76	96	0.164	0.150
NETH_165	GRT-03	open	1420	1497.5	155	76	464	0.223	0.597
NETH_166	GWD-01-S1	open	1772.5	1846	147	76	78	0.149	0.287
NETH_167	HEW-01-S1	open	2940	2984	88	76	67.4	0.158	0.423
NETH_168	HLE-01	open	3135	3225.5	181	76	62.2	0.17	0.988
NETH_169	HLO-02	open	2496	2616	240	76	50.7	0.137	0.300
NETH_170	HND-01	open	881	1021.5	281	76	438	0.285	0.164
NETH_171	HRS-01	open	959	989.5	61	76	1040	0.301	0.305
NETH_172	HSW-01	open	660.5	686	51	76	55.7	0.278	0.359
NETH_173	IJS-01	open	955	1010	110	76	691	0.264	1.719
NETH_174	IJS-02	open	3447	3559.5	225	76	121	0.128	0.714
NETH_175	IJS-57	open	3616	3642.5	53	76	68.7	0.117	0.104
NETH_176	IJS-57	open	3755	3825	140	76	303	0.176	0.974
NETH_177	J06-01-S1	open	3973	4087	228	76	74.4	0.074	0.600

NETH_178	J06-A-01	open	3936.5	3980.75	88.5	76	57.4	0.1	0.118
NETH_179	JIP-01	open	3360.5	3390.75	60.5	76	36.6	0.116	0.682
NETH_180	K02-02	open	3327.5	3417.5	180	76	44	0.051	0.458
NETH_181	K03-01	open	3323	3352	58	76	66.4	0.125	0.163
NETH_182	K06-02	open	3241	3301	120	76	462	0.183	0.079
NETH_183	K07-03	open	3405	3440.5	71	76	45.8	0.131	0.272
NETH_184	K07-FA-101	open	3719	3746.5	55	76	36.3	0.094	0.137
NETH_185	K07-FB-101	open	3506.5	3538.25	63.5	76	81.9	0.162	0.820
NETH_186	K08-01-S2	open	3771.5	3815.75	88.5	76	40.1	0.155	0.123
NETH_187	K08-12-S1	open	4079	4122	86	76	66.3	0.16	0.077
NETH_188	K09-02	open	2775	2872.5	195	76	113	0.166	0.150
NETH_189	K09AB-A-02	open	3187	3218.25	62.5	76	336	0.195	0.150
NETH_190	K09AB-A-03	open	2929.5	3033	207	76	241	0.182	0.158
NETH_191	K10-01-S1	open	3364	3442	156	76	57.9	0.147	0.498
NETH_192	K10-03	open	3141	3206.75	131.5	76	33.2	0.157	0.364
NETH_193	K10-B-04	open	3306	3335.5	59	76	369	0.207	0.842
NETH_194	K11-01	open	1387	1431	88	76	319	0.22	0.263
NETH_195	K11-02	open	2583.5	2665.25	163.5	76	201	0.203	0.151
NETH_196	K11-02	open	1440	1474	68	76	54.2	0.163	0.369
NETH_197	K13-02	open	1508	1553.5	91	76	221	0.186	0.490
NETH_198	K13-05	open	2469.5	2550.25	161.5	76	185	0.192	0.600
NETH_199	K13-A-01	open	2914	3049.5	271	76	31.2	0.149	0.150
NETH_200	K13-A-01	open	3072.4	3101.7	58.6	76	76	0.162	0.382
NETH_201	K13-DE-03	open	4202	4243.5	83	76	179	0.178	0.591
NETH_202	K14-02	open	1743	1824.2	162.4	76	780	0.219	0.303
NETH_203	K14-11	open	1983	2047.5	129	76	293	0.138	0.150
NETH_204	K15-15-S1	open	1962	2067	210	76	61.1	0.149	0.297
NETH_205	K18-02-A	open	3249	3339	180	76	57.1	0.124	1.383
NETH_206	K18-KOTTER-07-S1	open	2823.5	2905	163	76	157	0.177	0.614
NETH_207	KDK-01	open	4071	4183.5	225	76	344	0.143	0.352
NETH_208	KDZ-02-S1	open	3784	3822.75	77.5	76	109	0.116	0.300
NETH_209	KPD-12	open	4384	4420	72	76	37.1	0.096	0.529
NETH_210	L04-05	open	4086.5	4111.75	50.5	76	44.8	0.143	1.123
NETH_211	L04-A-01	open	2463	2555.5	185	76	327	0.145	0.196
NETH_212	L04-A-02-S1	open	3796	3833.25	74.5	76	30.2	0.097	0.101
NETH_213	L05-05-S1	open	3599.5	3647	95	76	64.8	0.127	0.096
NETH_214	L06-02	open	2439	2464	50	76	142	0.191	0.900
NETH_215	L07-01	open	3879	3917	76	76	111	0.14	0.092
NETH_216	L07-05	open	4139.99	4176.495	73.01	76	52.1	0.09	0.180
NETH_217	L07-10	open	3358	3405	94	76	263	0.213	0.160
NETH_218	L07-B-01	open	3509	3543	68	76	63.4	0.127	0.210
NETH_219	L08-01-S1	open	3130.5	3193.5	126	76	85	0.177	0.129
NETH_220	L09-08	open	3640.5	3723	165	76	155	0.18	0.450
NETH_221	L09-08	open	3095	3186	182	76	180	0.182	0.150
NETH_222	L09-11	open	3787.5	3855.5	136	76	50.6	0.145	0.273
NETH_223	L09-13	open	3994	4033.5	79	76	200	0.159	0.530
NETH_224	L09-FF-101-S1	open	3548	3649	202	76	39	0.106	0.600
NETH_225	L10-06	open	3664	3703.5	79	76	36.4	0.135	0.209
NETH_226	L10-A-01	open	3472	3524	104	76	53.9	0.145	0.309
NETH_227	L11-05	open	2131	2214	166	76	295	0.196	0.283
NETH_228	L13-FC-101-S1	open	2237.5	2322.5	170	76	369	0.153	0.113
NETH_229	L13-FH-101	open	2473.6	2550.1	153	76	653	0.21	0.167
NETH_230	L16-LOGGER-01	open	1205	1290	170	76	487	0.212	0.792
NETH_231	L16-LOGGER-02	open	2020.5	2052.25	63.5	76	37.7	0.153	0.900
NETH_232	L16-LOGGER-08-S1	open	3790	3855	130	76	55.3	0.12	1.249
NETH_233	LED-01	open	1709.7	1815.2	211	76	67.3	0.146	1.126
NETH_234	LIR-45	open	2568	2682	228	76	504	0.199	0.111
NETH_235	M04-03	open	860	885	50	76	875	0.269	0.222
NETH_236	MDZ-01	open	3756	3794	76	76	437	0.158	0.378

NETH_237	MID-103-S1	open	2812	2863	102	76	264	0.172	1.552
NETH_238	MKP-11	open	2756	2813.3	114.6	76	280	0.184	0.523
NETH_239	MSG-01	open	3267	3366.5	199	76	307	0.168	0.460
NETH_240	MWD-01	open	3043	3123.5	161	76	659	0.197	0.493
NETH_241	NBR-01	open	2765	2846.5	163	76	690	0.193	0.578
NETH_242	NOR-04	open	2873	2900	54	76	87.3	0.137	0.908
NETH_243	NOR-05	open	2927	3013.5	173	76	375	0.218	1.233
NETH_244	NOR-23	open	1102	1194.5	185	76	170	0.146	1.223
NETH_245	NRD-01	open	2702	2755.5	107	76	116	0.15	0.150
NETH_246	NRD-01	open	2287	2394.5	215	76	944	0.207	0.929
NETH_247	NWK-02	open	3029	3084.5	111	76	207	0.214	0.600
NETH_248	NWS-01	open	2051	2083.75	65.5	76	34.6	0.154	0.300
NETH_249	OBLZ-01	open	2785.7	2853.1	134.8	76	188	0.193	1.730
NETH_250	ODP-01	open	2790	2880	180	76	181	0.182	0.441
NETH_251	OPH-01	open	1140	1198.5	117	76	641	0.215	0.106
NETH_252	OWG-01	open	2746	2851	210	76	40.1	0.072	0.499
NETH_253	OWG-08	open	2706.5	2762.5	112	76	77	0.096	0.600
NETH_254	P05-03	open	2781.5	2850	137	76	42.8	0.117	0.970
NETH_255	P06-B-01	open	1599.21	1718.21	238	76	1180	0.228	0.299
NETH_256	P06-D-01	open	1648.5	1719.5	142	76	1480	0.25	0.226
NETH_257	P06-D-01	open	2592	2654.5	125	76	45.4	0.105	0.198
NETH_258	P11-04	open	2452	2481	58	76	198	0.137	2.036
NETH_259	P11-04	open	2510	2577.5	135	76	91.6	0.118	1.380
NETH_260	P12-11	open	2529.5	2558.25	57.5	76	157	0.141	0.194
NETH_261	P14-A-01	open	2673	2700	54	76	240	0.149	0.227
NETH_262	P14-A-01	open	3275.5	3309	67	76	97.8	0.122	0.302
NETH_263	P15-F-01	open	1757	1783	52	76	514	0.16	0.188
NETH_264	P15-G-01-S1	open	3007	3099.5	185	76	294	0.183	0.244
NETH_265	P18-02	open	3044	3099	110	76	84.7	0.166	0.161
NETH_266	PNA-02	open	3072	3101	58	76	34.2	0.146	0.323
NETH_267	PRW-01	open	3130	3164.25	68.5	76	34.2	0.112	0.880
NETH_268	PRW-01	open	3286	3388.55	205.1	76	43.1	0.181	0.241
NETH_269	PRW-01	open	1476	1504	56	76	1330	0.219	0.086
NETH_270	PRW-01	open	1217.2	1265.6	96.8	76	3030	0.232	0.087
NETH_271	PSP-01	open	1476	1576	200	76	520	0.247	0.272
NETH_272	Q01-09	open	3406.3	3438.2	63.8	76	31.8	0.134	0.477
NETH_273	Q01-HELM-A-01	open	3610	3680	140	76	600	0.176	0.873
NETH_274	Q01-HOORN-A-01	open	3688	3720.5	65	76	493	0.196	1.401
NETH_275	Q04-B-01	open	2414.58	2464.29	99.42	76	34.3	0.154	0.079
NETH_276	Q04-C-02	open	1734.5	1842	215	76	42.9	0.138	0.958
NETH_277	Q04-C-02	open	991.5	1080.75	178.5	76	274	0.144	0.475
NETH_278	Q08-05-S3	open	1983.5	2104.5	242	76	296	0.164	0.150
NETH_279	Q08-A-01	open	3876	3963.5	175	76	124	0.109	0.299
NETH_280	Q11-02	open	2811.5	2900	177	76	52.5	0.125	0.805
NETH_281	Q13-02	open	2629.5	2720.5	182	76	33.3	0.088	1.073
NETH_282	Q16-08	open	2666	2719.5	107	76	208	0.171	0.488
NETH_283	RDK-01	open	2164	2269	210	76	37.8	0.013	0.289
NETH_284	ROT-01-S1	open	2107	2175.5	137	76	648	0.174	0.247
NETH_285	ROT-01-S1	open	2230	2285	110	76	561	0.186	0.430
NETH_286	RST-01	open	1701	1740.5	79	76	52.6	0.196	0.106
NETH_287	RSW-01	open	1793	1855.75	125.5	76	1580	0.24	0.927
NETH_288	RSW-01	open	1935	2199	528	76	1470	0.125	0.795
NETH_289	RTD-01	open	1720	1749	58	76	64.6	0.262	0.150
NETH_290	RTD-01	open	1884	1914	60	76	46	0.241	1.171
NETH_291	RTD-01	open	1682	1800.5	237	76	48.5	0.257	2.400
NETH_292	RTD-02	open	1544	1612.5	137	76	369	0.17	0.145
NETH_293	RTD-03-S2	open	1650	1707.5	115	76	289	0.2	0.119
NETH_294	RTD-13	open	1521	1581	120	76	1040	0.156	0.333
NETH_295	RWK-01	open	1528	1603	150	76	545	0.156	0.781

NETH_296	RWK-01	open	2988	3014	52	76	142	0.14	0.594
NETH_297	RWK-03	open	2776	2837.5	123	76	67.5	0.148	0.728
NETH_298	RWK-05	open	2837.5	2910.75	146.5	76	191	0.194	0.910
NETH_299	RZB-01	open	852	947	190	76	1740	0.284	0.158
NETH_300	SAP-01	open	765	837.5	145	76	8660	0.333	0.232
NETH_301	SCB-01	open	800	867.5	135	76	2080	0.273	0.549
NETH_302	SCH-124	open	802	896	188	76	8780	0.318	2.025
NETH_303	SCH-167	open	829	921.5	185	76	6920	0.335	1.812
NETH_304	SCH-169	open	920	993.5	147	76	6160	0.335	1.433
NETH_305	SCH-186	open	863	915.5	105	76	7600	0.305	2.243
NETH_306	SCH-188	open	915	990	150	76	3910	0.306	2.326
NETH_307	SCH-203	open	776	833.5	115	76	5010	0.322	1.848
NETH_308	SCH-209	open	862	887.5	51	76	1300	0.274	1.245
NETH_309	SCH-211	open	836	911	150	76	6440	0.308	1.785
NETH_310	SCH-213	open	780	847.5	135	76	523	0.25	1.440
NETH_311	SCH-217	open	898	978	160	76	275	0.276	0.543
NETH_312	SCH-229	open	973	1085.5	225	76	183	0.21	1.796
NETH_313	SCH-381	open	980	1078.5	197	76	894	0.295	0.950
NETH_314	SCH-461	open	934	1039	210	76	2630	0.343	0.722
NETH_315	SCH-462	open	741	808.5	135	76	1780	0.318	0.739
NETH_316	SCH-495-S1	open	2858	2895.5	75	76	131	0.176	2.134
NETH_317	SCH-586	open	2864	2968.5	209	76	96	0.196	2.400
NETH_318	SCH-590	open	2959	3005	92	76	70.3	0.175	1.669
NETH_319	SDB-10	open	2651	2743.5	185	76	182	0.144	0.228
NETH_320	SDM-01	open	2688	2741.5	107	76	452	0.203	0.471
NETH_321	SEB-01	open	2647.9	2757.9	220	76	48.6	0.136	0.173
NETH_322	SLO-01	open	2692	2765.05	146.1	76	517	0.206	0.608
NETH_323	SLO-01	open	2666	2773.5	215	76	61.3	0.125	0.718
NETH_324	SLO-02	open	2709	2782.5	147	76	381	0.194	0.321
NETH_325	SLO-02	open	2701	2774	146	76	483	0.214	1.016
NETH_326	SLO-04	open	2776	2857.25	162.5	76	311	0.191	0.365
NETH_327	SLO-04	open	1875	1900	50	76	746	0.241	0.859
NETH_328	SLO-09	open	2672.3	2729.55	114.5	76	157	0.153	0.961
NETH_329	SMR-01	open	2650	2757.5	215	76	93.1	0.177	0.808
NETH_330	SOW-01	open	2718	2800.5	165	76	382	0.18	0.468
NETH_331	SPI-110	open	2759	2851.5	185	76	85.5	0.141	0.374
NETH_332	SPKO-01-S1	open	2815	2907.5	185	76	208	0.166	0.476
NETH_333	SPKO-01-S1	open	2553	2620.5	135	76	384	0.225	0.900
NETH_334	SPKW-01	open	2846.8	2954.8	216	76	64.4	0.162	0.391
NETH_335	SPKW-01	open	2843	2919	152	76	70.6	0.18	0.672
NETH_336	STW-01	open	2995	3102.5	215	76	70.6	0.174	0.794
NETH_337	TBR-01	open	2437	2510.75	147.5	76	30.1	0.196	0.373
NETH_338	TBR-04	open	1878	1930.5	105	76	43.6	0.161	0.286
NETH_339	TBR-04	open	2675	2735	120	76	265	0.123	0.394
NETH_340	TID-101	open	2699	2756.5	115	76	172	0.171	0.159
NETH_341	TID-901	open	2949	2995	92	76	60.5	0.198	0.150
NETH_342	TUS-01	open	3058	3112.5	109	76	44.5	0.18	0.550
NETH_343	TUS-01	open	2970	3020.5	101	76	67.1	0.2	0.400
NETH_344	UHM-01-S1	open	3084	3147	126	76	45.3	0.18	0.151
NETH_345	UHM-01-S1	open	3128	3183.5	111	76	226	0.165	0.150
NETH_346	USQ-01	open	2391.5	2496.5	210	76	161	0.164	0.179
NETH_347	USQ-01	open	1234	1314	160	76	1810	0.246	0.173
NETH_348	UTB-10-S1	open	1275	1381	212	76	718	0.206	0.476
NETH_349	VLR-01	open	1458	1558	200	76	55.5	0.237	0.627
NETH_350	WAS-01	open	1495	1575	160	76	931	0.241	1.530
NETH_351	WAS-23	open	1142	1229.5	175	76	751	0.292	1.698
NETH_352	WAV-01	open	1735.5	1762.75	54.5	76	439	0.192	0.308
NETH_353	WAV-03	open	1617	1718	202	76	133	0.171	1.499
NETH_354	WES-01	open	1975	2015	80	76	50.7	0.096	1.662

NETH_355	WGD-01	open	1713	1740	54	76	104	0.144	0.390
NETH_356	WIM-01	open	297	336	78	76	352	0.355	0.580
NETH_357	WLK-01	open	1241	1293.25	104.5	76	59.1	0.191	0.137
NETH_358	WYH-01	open	1284	1345.5	123	76	47.3	0.191	0.150
NETH_359	WYK-12	open	2640	2694	108	76	298	0.182	0.466
NETH_360	WYK-22	open	3725	3797	144	76	109	0.138	0.170
NETH_361	WYK-32	open	2792.5	2841.5	98	76	115	0.197	0.172
NETH_362	ZBR-01	open	2899	2954	110	76	44.1	0.196	0.573
NETH_363	ZLV-06	open	2855	2903.75	97.5	76	109	0.216	0.361
NETH_364	ZND-01	open	2829.5	2880	101	76	200	0.202	0.264
NETH_365	ZND-01	open	2938.5	2994.25	111.5	76	59.8	0.179	0.150
NETH_366	ZND-09-S1	open	958	1014	112	76	7940	0.256	0.249
NETH_367	ZND-12	open	1198	1305.5	215	76	57.5	0.203	0.392
NETH_368	ZND-12	open	1011	1063.5	105	76	2930	0.278	0.185
NETH_369	ZOM-13	open	2819	2872.5	107	76	108	0.161	1.115
NETH_370	ZOM-16	open	2898.5	2952.75	108.5	76	99	0.157	0.341
NETH_371	ZOM-26	open	2373	2483	220	76	60.7	0.127	1.135
NETH_372	ZPD-10	open	2398	2447	98	76	98.3	0.181	0.283
NETH_373	ZPD-12-S1	open	3754	3825	142	76	32.6	0.174	0.270

APPENDIX I

DENMARK-OIL &GAS FIELDS CONSIDERED IN THE STUDY

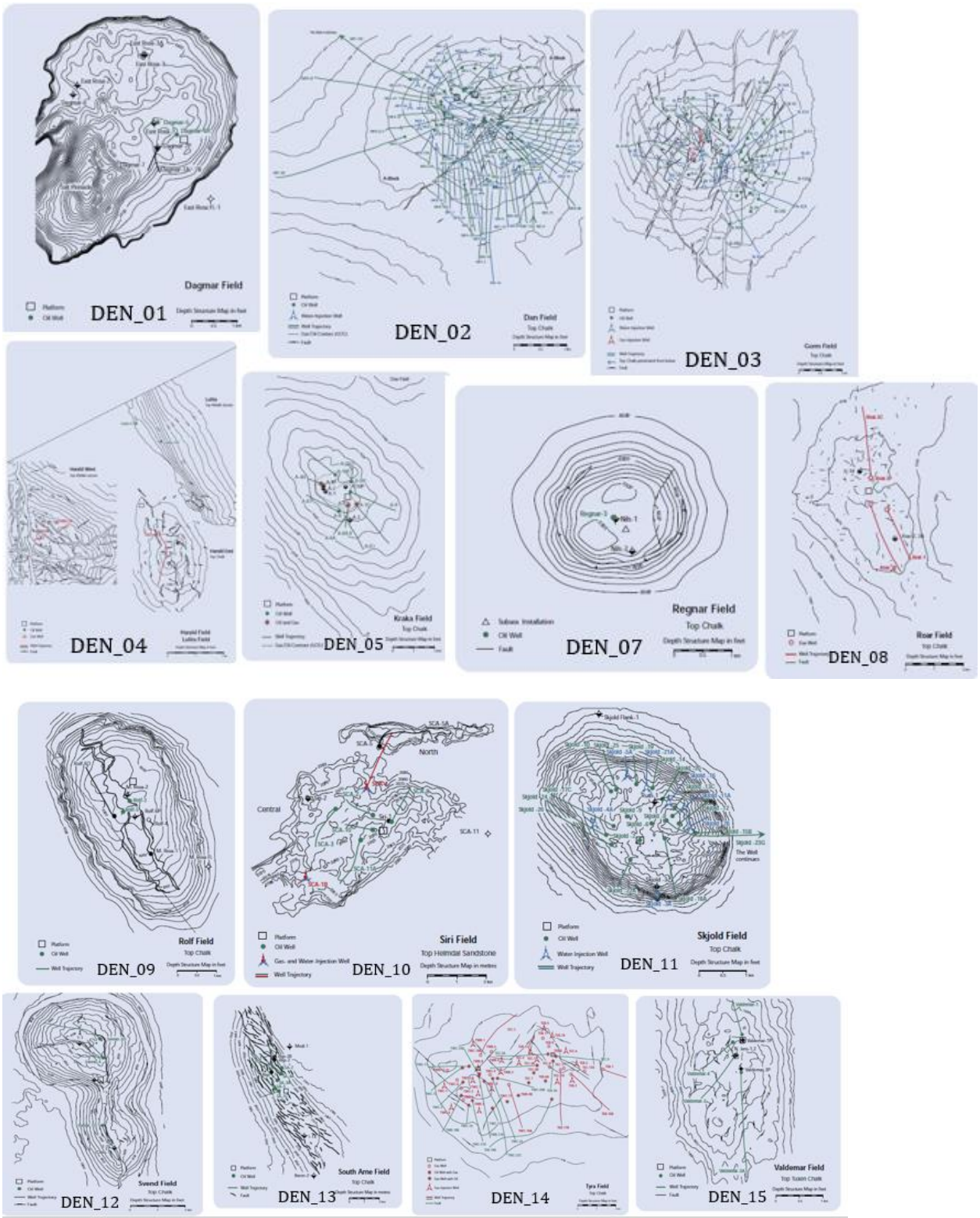

NETHERLANDS-OIL &GAS FIELDS CONSIDERED IN THE STUDY

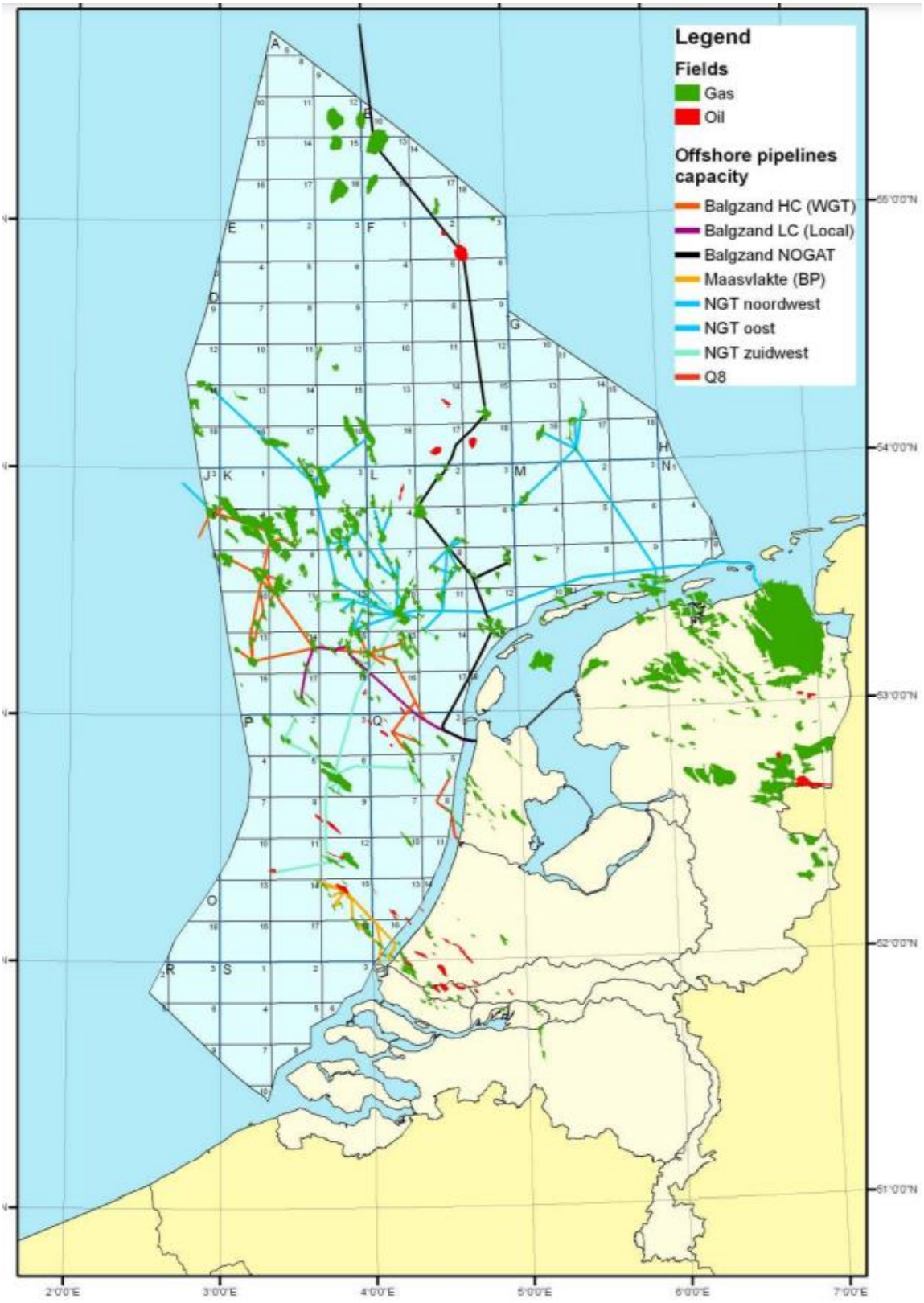

NORWAY SALINE AQUIFERS CONSIDERED

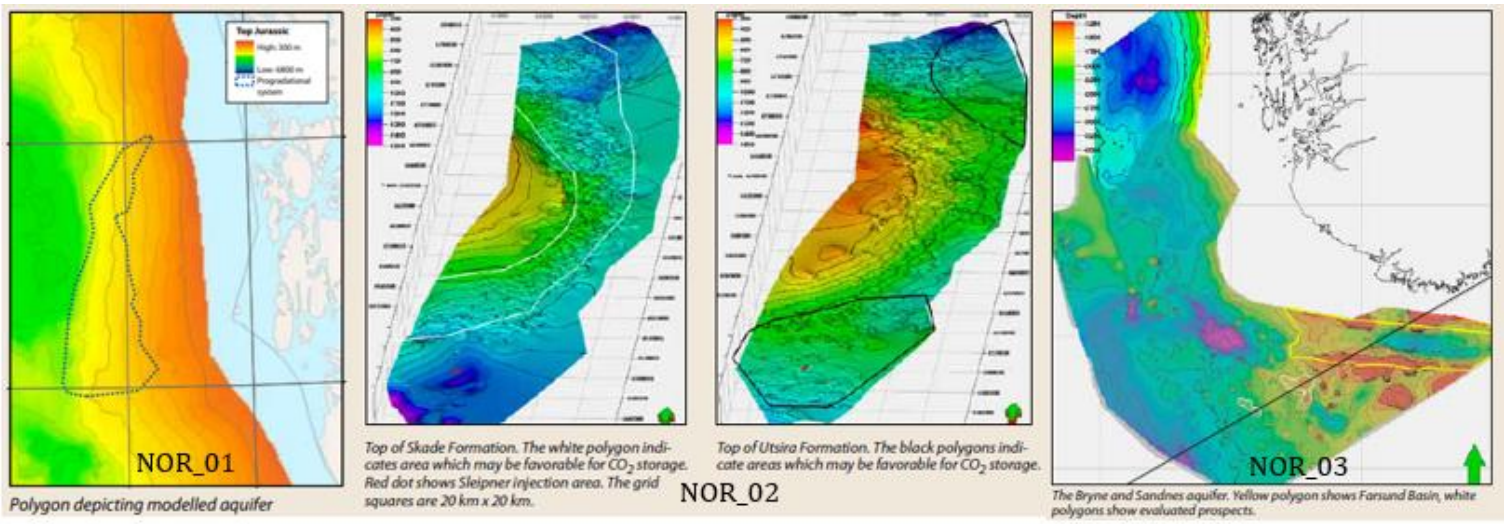

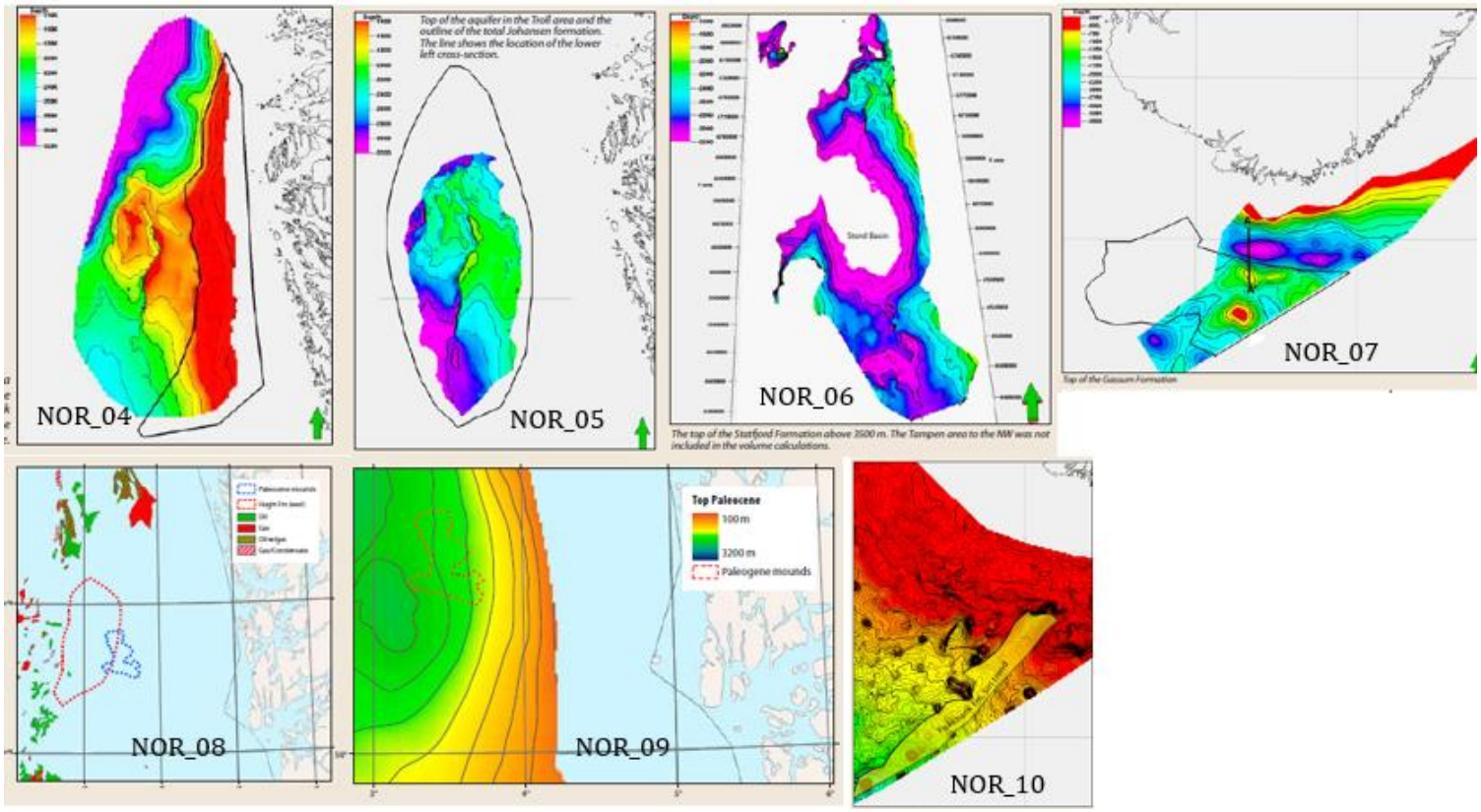

UK Saline aquifers, oil and gas fields

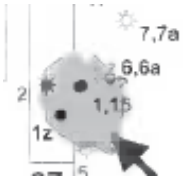

Andrew

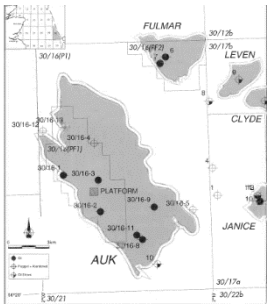

Auk

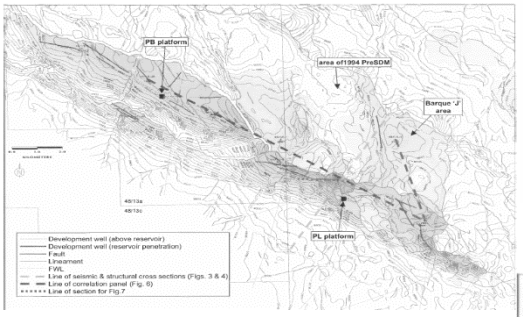

Barque

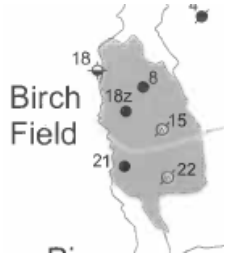

Brich

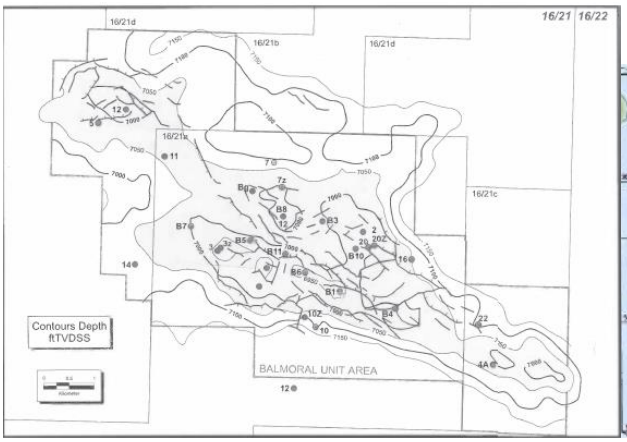

Balmoral

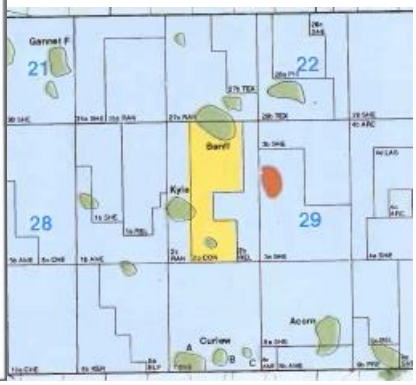

Banf

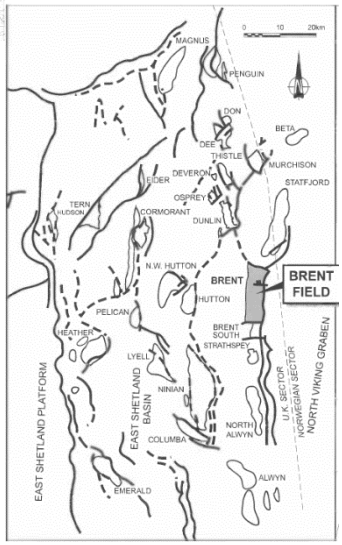

Brent

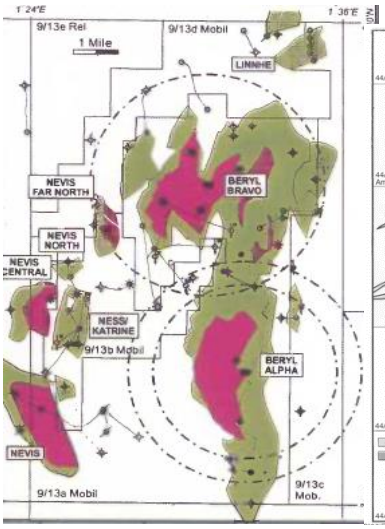

Beryl

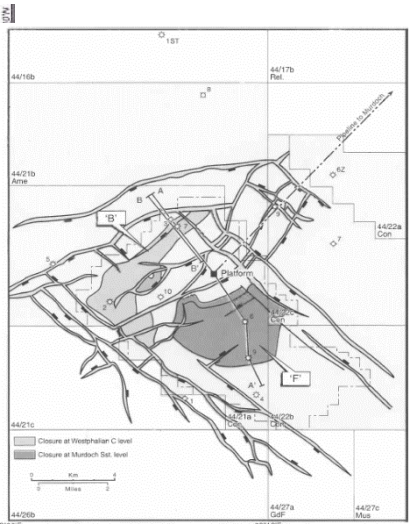

Boulton

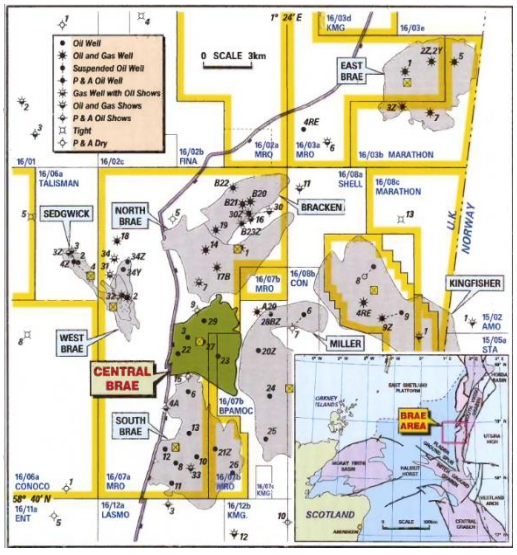

Brae fields

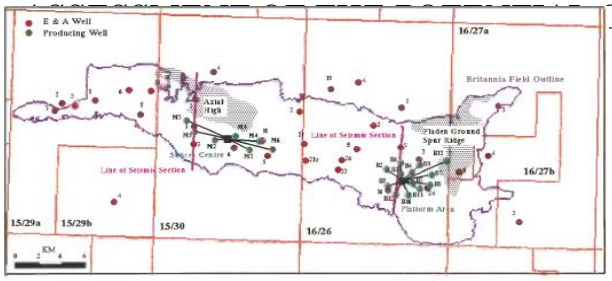

Britannia

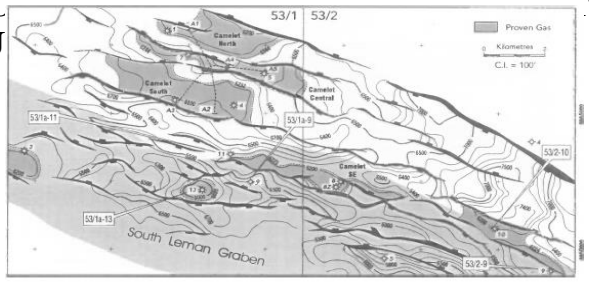

Camelot

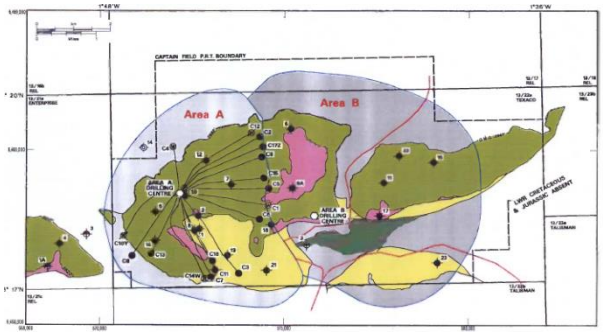

Captain

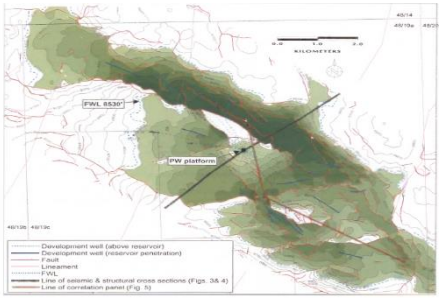

Clipper

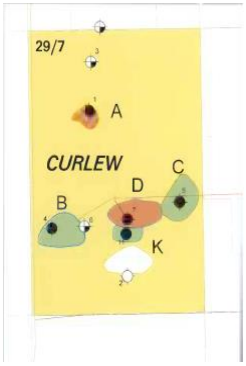

Curlew

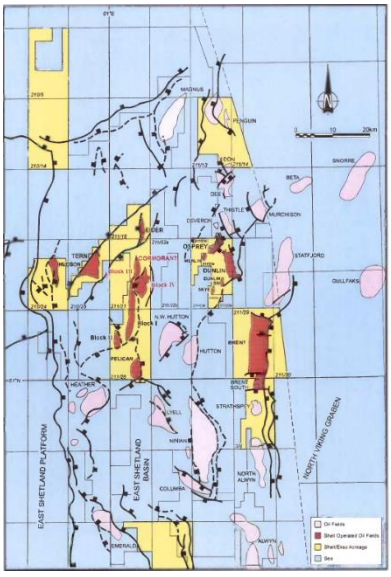

Cormoran

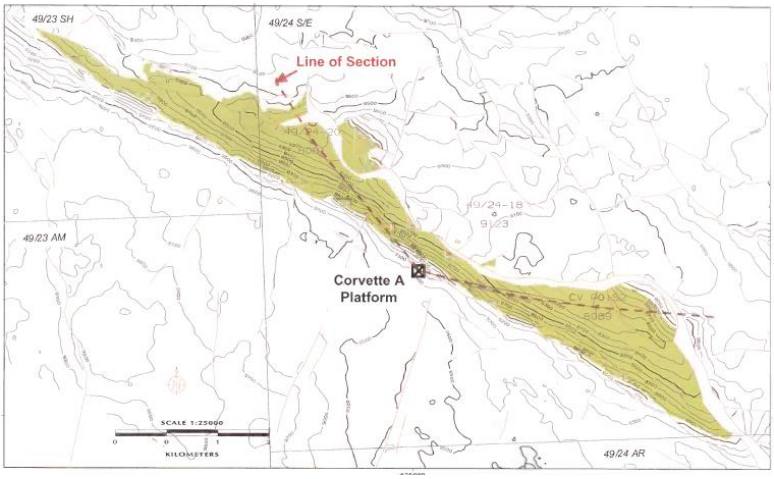

Corvette

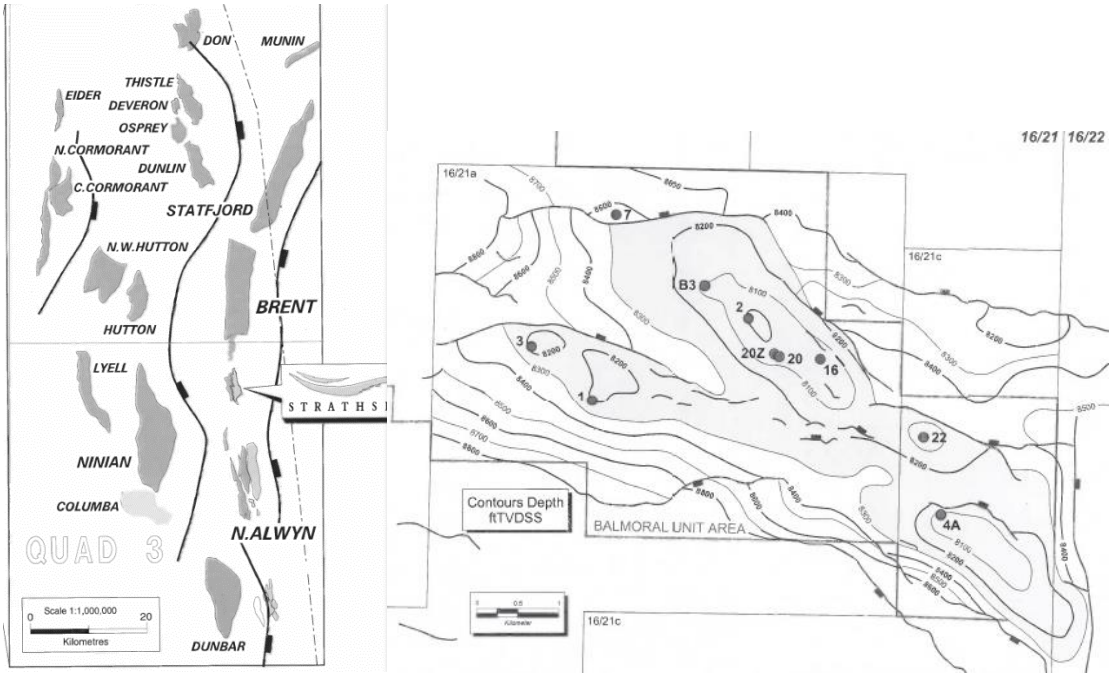

Straisphery Stirling

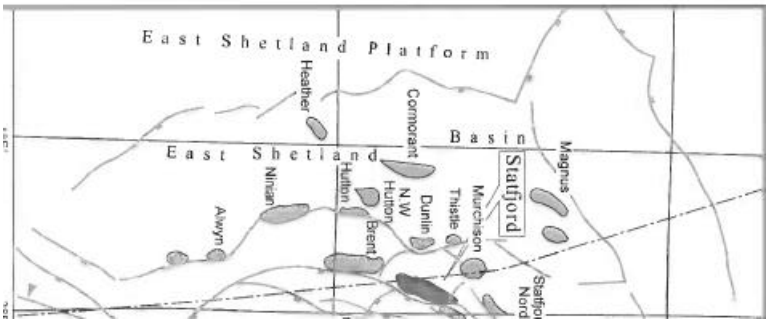

Statfjord

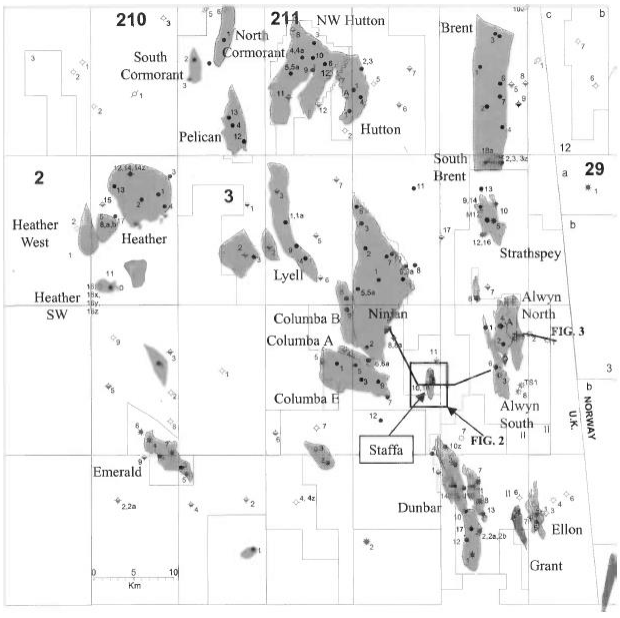

Stafa

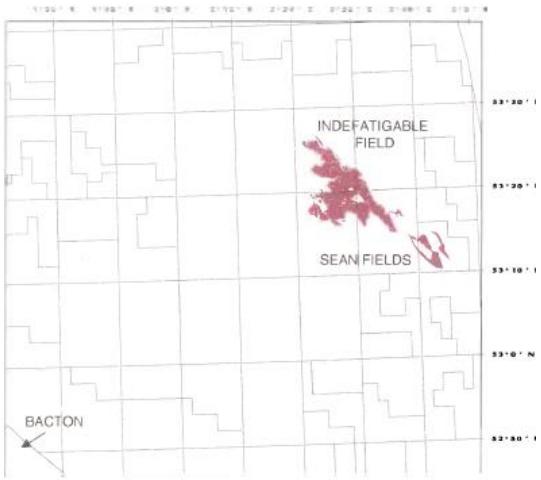

North-South Sean

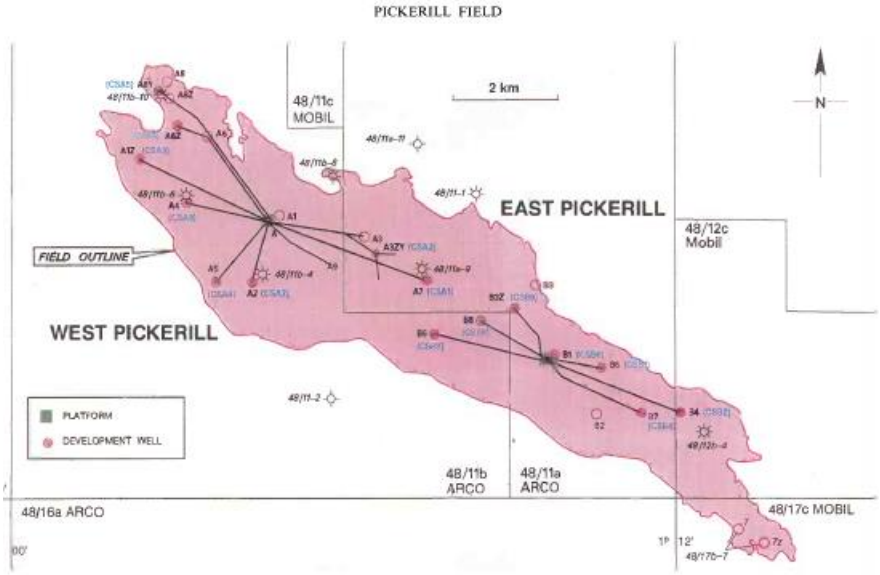

Pickerill

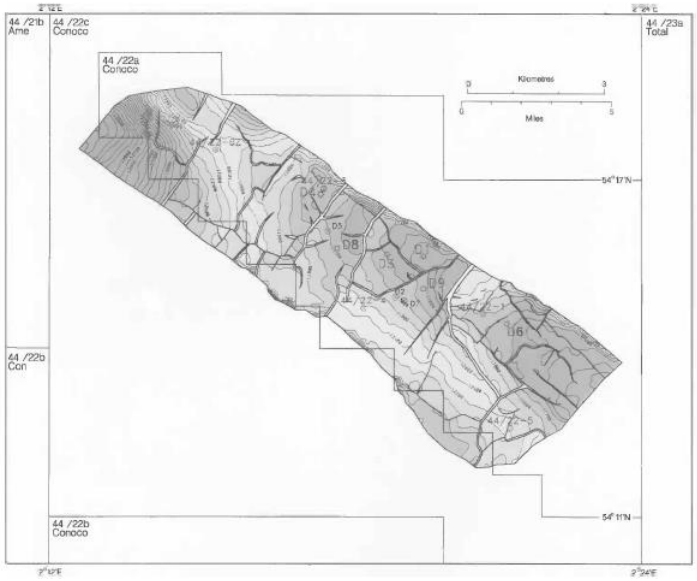

Murdoch

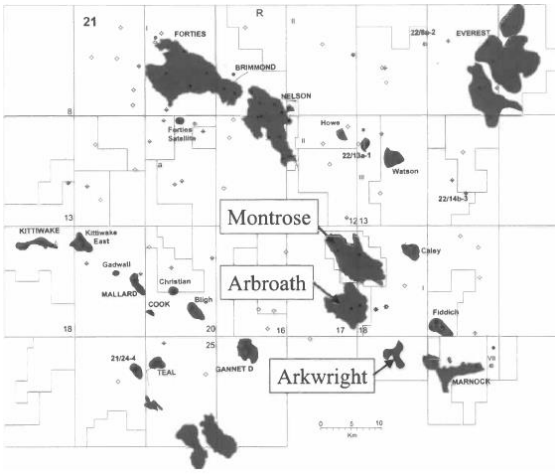

Montrose, Arboath, Arkwright

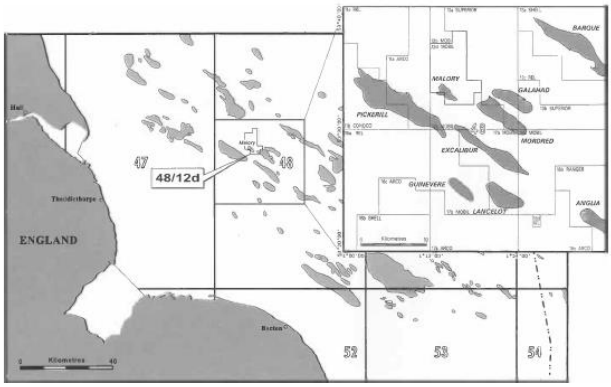

Malory

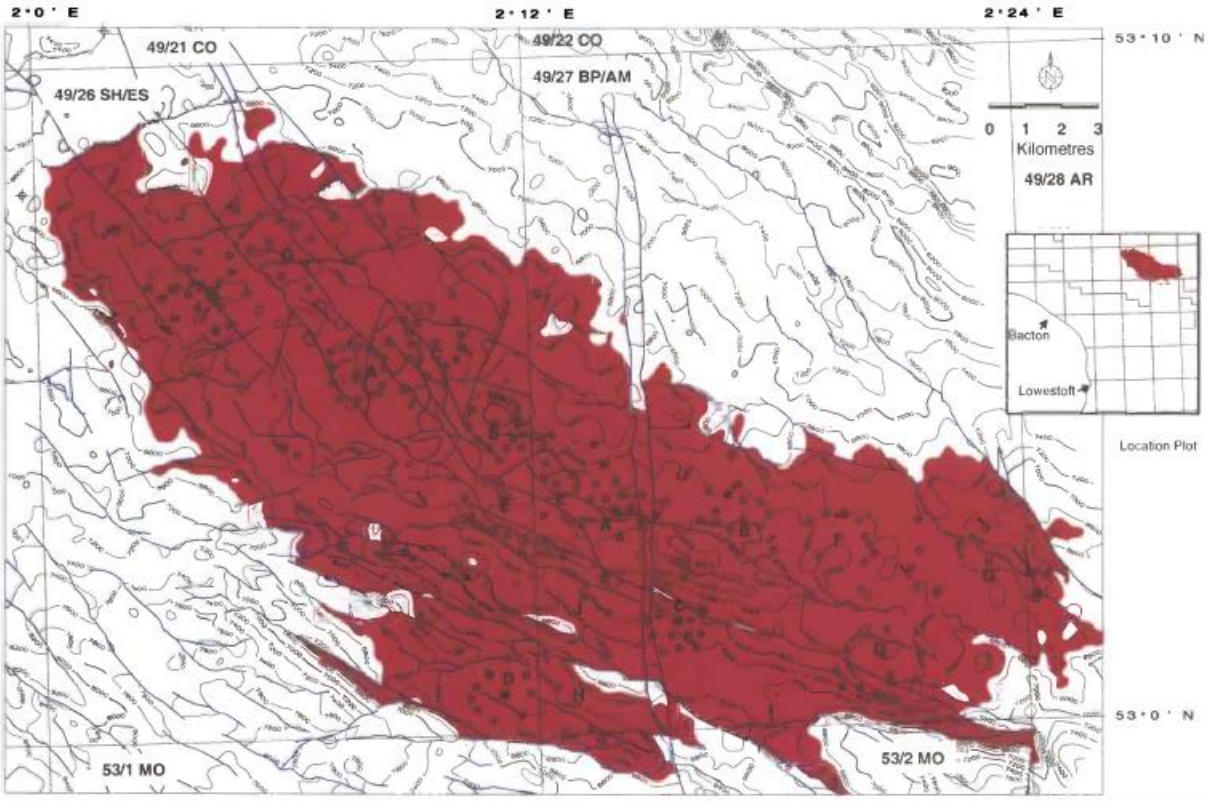

Leman

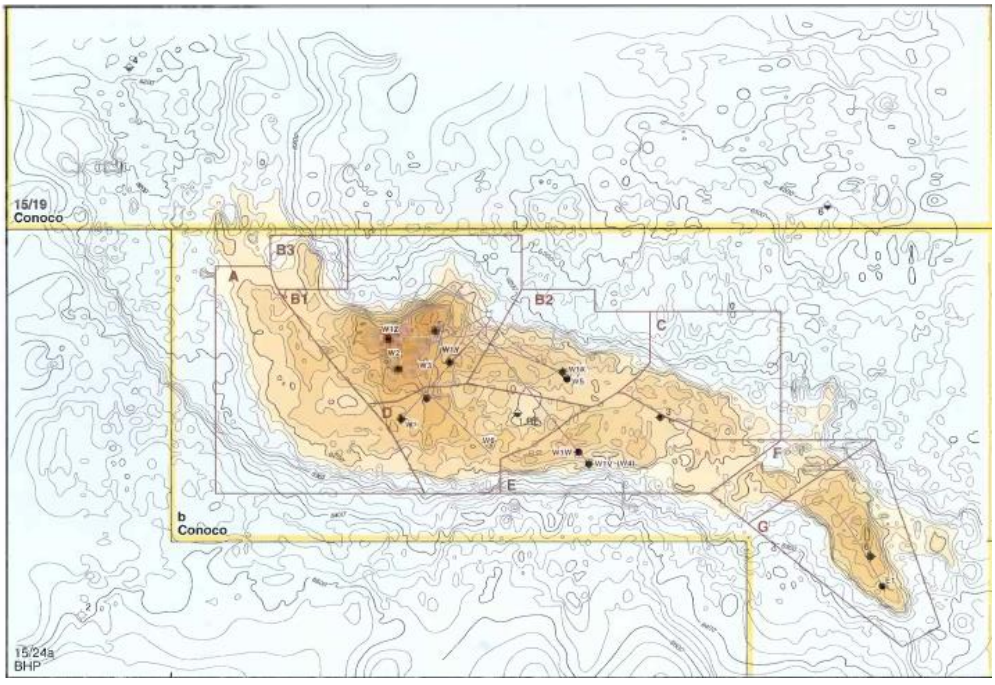

Mc Culloch

APPENDIX II

The extract of this project-thesis has been published at the per-reviewed journal International Journal of Greenhouse Gas Control, under the title: …

The database can be found at the following link:

Other work, that has been the product of the outstanding collaboration with professor Blunt has also been published in international literature under the titles:

…

…

REFERENCES

[1] IPCC, 2018: Summary for Policymakers. In: Global Warming of 1.5°C. An IPCC Special Report on the impacts of global warming of 1.5°C above pre-industrial levels and related global greenhouse gas emission pathways, in the context of strengthening the global response to the threat of climate change, sustainable development, and efforts to eradicate poverty [Masson-Delmotte, V., P. Zhai, H.-O. Pörtner, D. Roberts, et al.]. World Meteorological Organization, Geneva, Switzerland, 32 pp

[2] K. Riahi, D. P. van Vuuren, E. Kriegler, The Shared Socioeconomic Pathways and their energy, land use, and greenhouse gas emissions implications: An overview, Global Environmental Change, Volume 42, 2017, Pages 153-168.

[3] N. Bauer, K. Calvin, J. Emmerling, O. Fricko, S. Fujimori, et al., Shared Socio-Economic Pathways of the Energy Sector – Quantifying the Narratives, Global Environmental Change, Volume 42, 2017, Pages 316-330

[4] S. Ebrahimi, M. Mac Kinnon, J. Brouwer, California end-use electrification impacts on carbon neutrality and clean air, Applied Energy, Volume 213, 2018, Pages 435-449,

[5] IPCC, 2005 – B. Metz, O. Davidson, H. de Coninck, M. Loos and L. Meyer (Eds.) Cambridge University Press, UK. pp 431. Available from Cambridge University Press, The Edinburgh Building Shaftesbury Road, Cambridge CB2 2RU ENGLAND

[6] IEA (2020), CCUS in Clean Energy Transitions, IEA, Paris https://www.iea.org/reports/ccus-in-clean-energy-transitions

[7] IEA (2020), World Energy Model, IEA, Paris https://www.iea.org/reports/world-energy-model

[8] IEA (2020), The Covid-19 Crisis and Clean Energy Progress, IEA, Paris https://www.iea.org/reports/the-covid-19-crisis-and-clean-energy-progress

[9] A. Dias et al. EU coal regions: opportunities and challenges ahead, Office of the European Union, Luxemburg, 2018 ISBN 978-92-79-89884-6

[10] N. Heitmann, C. Bertram & D. Narita, Embedding CCS infrastructure into the European electricity system: a policy coordination problem, Mitigation and Adaptation Strategies for Global Change volume 17, pages669–686(2012)

[11] E. D. Schulze, S. Luyssaert, P. Ciais, A. Freibauer, I. A. Jassens et al. Importance of methane and nitrous oxide for Europe's terrestrial greenhouse-gas balance, Nature geoscience, vol.2, 2009

[12] P. Karvounis, M. J. Blunt, A Hubbert Analysis on Natural Gas Production of the Top Producers. How the Carbon Budget Is Affected Under Unconstrained Extraction, 5th World Congress on Civil, Structural, and Environmental Engineering (CSEE'20), DOI: 10.11159/iceptp20.154

[13] S. Giannaris , B. Jacobs , D. Janowczyk , C. Bruce , W. Srisanga, Y. Fenga, Reliability Improvements of SaskPower's BD3 Capture Facility Through Operational and Process Design

Changes: Experiencing the First Four Years of Operations, IEAGHG 5th Post Combustion Capture Conference 17 th -19th September 2019, Kyoto, Japan

[14] DIRECTIVE 2009/31/EC OF THE EUROPEAN PARLIAMENT AND OF THE COUNCIL of 23 April 2009 on the geological storage of carbon dioxide and amending Council Directive 85/337/EEC, European Parliament and Council Directives 2000/60/EC, 2001/80/EC, 2004/35/EC, 2006/12/EC, 2008/1/EC and Regulation (EC) No 1013/2006

[15] GREEN PAPER A 2030 framework for climate and energy policies https://eur-lex.europa.eu/legal-content/EN/TXT/PDF/?uri=CELEX:52013DC0169&from=EN

[16] The European Green Deal, https://eur-lex.europa.eu/resource.html?uri=cellar:b828d165-1c22-11ea-8c1f-01aa75ed71a1.0002.02/DOC_1&format=PDF

[17] Advanced Power Plant Materials, Design and Technology, A.D. Rao, 2010 ISBN: 978-1-84569-515-6

[18] Y. Zhu, H.C. Frey, 3 - Integrated gasification combined cycle (IGCC) power plant design and technology, Dermot Roddy, In Woodhead Publishing Series in Energy, Advanced Power Plant Materials, Design and Technology, Woodhead Publishing, 2010, Pages 54-88.

[19] P. Markewitz, W. Kuckshinrichs, W. Leitner, J. Linssen, P. Zapp, R. Bongartz, A. Schreiber and T. E. Muller. Worldwide innovations in the development of carbon capture technologies and the utilization of CO2, Energy & Environmental Science.

[20] O. Omoregbe, A. N. Mustapha, R. Steinberger-Wilckens, A. El-Kharouf, H. Onyeaka. Carbon capture technologies for climate change mitigation: A bibliometric analysis of the scientific discourse during 1998–2018, Energy Reports, Volume 6, November 2020, Pages 1200-1212

[21] Carbon capture by physical adsorption: Materials, experimental investigations and numerical modeling and simulations – A review, R. Ben-Mansour, M. A. Habib, O.E. Bamidele, M. Basha, N.A.A. Qasem, A. Peedikakkal, T. Laoui, M. Ali, Applied Energy, 161 (2016)

[22] M. Zhang and Y. Guo, Rate based modeling of absorption and regeneration for CO2 capture by aqueous ammonia solution, Appl Energy, 111 (x) (2013), pp. 142-152

[23] Y. Lv, X. Yu, J. Jia, S.-T. Tu, J. Yan and E. Dahlquist, Fabrication and characterization of superhydrophobic polypropylene hollow fiber membranes for carbon dioxide absorption, Appl Energy, 90 (1) (2012), pp. 167-174.

[24] C.F. Song, Y. Kitamura and S.H. Li, Evaluation of Stirling cooler system for cryogenic CO2 capture, Appl Energy, 98 (2012), pp. 491-501, Applied Energy, Volume 98, October 2012, Pages 491-501

[25] Nakamura T. Recovery and sequestration of CO2 from stationary combustion systems by photosynthesis of microalgae quarterly technical progress report # 9 reporting period start date: 1 October 2002

[26] H. Li, M. Ditaranto and J. Yan, Carbon capture with low energy penalty: supplementary fired natural gas combined cycles, Appl Energy, 97 (2012), pp. 164-169

[27] J.R. Li, J. Sculley and H.C. Zhou, Metal-organic frameworks for separations, Chem Rev, 112 (2) (2012), pp. 869-932

[28] R. Stanger, T. Wall, R. Spörl, M. Paneru, S. Grathwohl, M. Weidmann, G.Scheffknecht, D. McDonald, K. Myöhänen, J. Ritvanen, S. Rahiala, T. Hyppänen, J. Mletzko, A. Kather, S. Santos, Oxyfuel combustion for CO2capture in power plants, International Journal of Greenhouse Gas Control 40 (2015) 55–125

[29] B.J. Buhre, L.K. Elliott, C. Sheng, R.P. Gupta and T.F. Wall, Oxyfuel combustion technology for coal-fired power generation, Prog. Energy Combust. Sci., 31 (2005), pp. 283-307

[30] L. Chen, S.Z. Yong and A.F. Ghoniem, Oxyfuel combustion of pulverized coal: characterization, fundamentals, stabilization and CFD modeling, Prog. Energy Combust. Sci., 38 (2) (2012), pp. 156-214

[31] K. Myöhänen, T. Hyppänen, T. Eriksson and R. Kuivalainen, J. Li, F. Wei, X. Bao, W. Wang, Design and modeling of second generation oxygen-fired CFB, Proceedings of the 11th International Conference on Fluidized Bed Technology, Chemical Industry Press (2014) ISBN 978-7-122-20169-0

[32] Odenberger, M., Svensson, R., 2003. Transportation systems for CO2—application to carbon sequestration. Technical Report No. T2003-273. Department of Energy Conversion, Chalmers University of Technology, Göteborg, Sweden.

[33] A Shafeen, E. Croiset, P.L. Douglas, I. Chatzis, CO2 sequestration in Ontario, Canada. Part II: cost estimation, Energy Conversion and Management Volume 45, Issue 20, December 2004, Pages 3207-3217

[34] Z..X. Zhang, G.X. Wang, P. Massarotto, V. Rudolph, Optimization of pipeline transport for CO2 sequestration, Energy Conversion and Management, Volume 47, Issue 6, April 2006, Pages 702-715.

[35] V. Vandeginste, K. Piessens, Pipeline design for a least-cost router application for CO2transport in the CO_2 sequestration cycle, International journal of greenhouse gas control 2 (2008) 571–581

[36] IEA GHG, 2005. Building the cost curves for CO2 storage: European sector. Report Number 2005/2. International Energy Agency Greenhouse Gas R&D Programme.

[37] Heddle, G., Herzog, H., Klett, M., 2003. The economics of CO2 storage. Laboratory for Energy and the Environment, No. LFEE 2003-003 RP. Cambridge, MA

[38] Hamelinck, C.N., Faaij, A.P.C., Ruijg, G.J., Jansen, D., Pagnier, H., van Bergen, F., et al., 2001. Potential for CO2 Sequestration and Enhanced Coalbed Methane Production in the Netherlands. NOVEM Programma, Utrecht.

[39] U. Lee, Y. Lim, S. Lee, J. Jung, and C. Han, CO2 Storage Terminal for Ship Transportation, Ind. Eng. Chem. Res. 2012, 51, 389-397

[40] U.Lee, S. Yang, Yeong Su Jeong, Y. Lim, C. Seob Lee, and C. Han Carbon Dioxide Liquefaction Process for Ship Transportation, Ind. Eng. Chem. Res. 2012, 51, 15122−15131

[41] J. Alonso, V. Navarro, B. Calvo, Flow path development in different CO2storage reservoir scenarios. A critical state approach, Engineering geology, 127 54-64, 2012

[42] A. Antropov , A. Lavrov, B. Orlic, Effect of in-situ stress alterations on flow through faults and fractures in the cap rock, Energy Procedia 114 (2017) 3193 – 3201

[43] B. Orlic, Some geomechanical aspects of geological CO2 sequestration, KSCE Journal of Civil Engineering volume 13, pages225–232 (2009)

[44] J.P. Davies and D.K. Davies, Stress-dependent permeability: characterization and modeling, SPE Journal, 6 (2001), pp. 224-235

[45] Gutierrez M, Øino LE, Nygård R. Stress-dependent permeability of a de-mineralised fracture in shale. Marine and Petroleum Geology 2000; 17: 895-907

[46] https://zero.no/wp-content/uploads/2016/06/carbon-capture-and-storage.pdf

[47] Reservoir Engineering, M J Blunt, Volume 2 of the Imperial College Lectures in Petroleum Engineering, World Scientific Press (2017)

[48] Z. Song, Y. Song, Y. Li, B. Bai, K. Song, J. Hou, A critical review of CO2enhanced oil recovery in tight oil reservoirs of North America and China, Fuel, 276, 2020

[49] IEA (2018), World Energy Outlook 2018, IEA, Paris https://www.iea.org/reports/world-energy-outlook-2018

[50] IEA, EOR production in the New Policies Scenario, 2000-2040, IEA, Paris https://www.iea.org/data-and-statistics/charts/eor-production-in-the-new-policies-scenario-2000-2040

[51] Danish Energy Agency https://ens.dk/en

[52] Geological Survey of the Netherlands https://www.nlog.nl/en

[53] Eva K. Halland, W. T. Johansen, F. Riis, CO_2 storage atlas Norwegian North Sea, Norwegian Petroleum Directorate P O Box 600 NO-4003 Stavanger Norway.

[54] https://factpages.npd.no/en

[55] S. Grassmann, B. Cramer, G. Delisle, J. Messner & J. Winsemann, Geological history and petroleum system of the Mittelplate oil field, Northern Germany, International Journal of Earth Sciences volume 94, pages979–989(2005)

[56] Bulletin of the Geological Society of Denmark, Vol. 30,3-4, pp. 119-137

[57] CO2 stored database available at: http://www.co2stored.co.uk/home/index

[58] J. G. Gluyas, H. M. Hichens, United Kingdom Oil and Gas fields, Commemorative Millennium Volume, The Geological Society Publishing House Unit 7, Brassmill Enterprise Centre, Brassmill Lane, Bath BA, ISBN 1-86239-089-4

[59] R. W. Zimmerman, Compressibility of sandstones, ELSEVIER SCIENCE PUBLISHING COMPANY INC.655, Avenue of the Americas, New York, NY 10010, USA, ISBN 0-444-88325-8

[60] G. K. Batchelor, An introduction to fluid dynamics, Cambridge University Press, 2000 https://doi.org/10.1017/CBO9780511800955

[61] Ransohoff, T.C., Gauglitz, P.A. and Radke, C.J. (1987), Snap-off of gas bubbles in smoothly constricted noncircular capillaries. AIChE J., 33: 753-765. doi:10.1002/aic.690330508

[62] Wyckoff, R. D., Botset, H. G., & Muskat, M. The Mechanics of Porous Flow Applied to Water-flooding Problems. Society of Petroleum Engineers. (1933, December 1). doi:10.2118/933219-G

[63] Martin J. Blunt, Multiphase Flow in Permeable Media A Pore-Scale Perspective, Cambridge University press, February 2017, ISBN: 9781107093461

[64] K. L. Anthonsen. Bernstone, H. Feldrappe, Screening for CO2 storage sites in Southeast North Sea and Southwest Baltic Sea, Energy Procedia 63 (2014) 5083 – 5092

[65] Nordbotten, J.M., Celia, M.A. & Bachu, S. Injection and Storage of CO2 in Deep Saline Aquifers: Analytical Solution for CO2 Plume Evolution During Injection. Transp Porous Med 58, 339–360 (2005). https://doi.org/10.1007/s11242-004-0670-9

[66] Zoback, M. D. and Gorelick, S. M. (2012). Earthquake triggering and large-scale geologic storage of carbon dioxide. Proceedings of the National Academy of Sciences, 109(26):10164, 10168.

[67] Jaeger, J. C., Cook, N. G., and Zimmerman, R. (2009). Fundamentals of rock mechanics. John Wiley & Sons.

[68] M. L. Szulczewski, C. W. MacMinn, H. J. Herzog, and R. Juanes, Lifetime of carbon capture and storage as a climate-change mitigation technology, Proc. Natl. Acad. Sci. U.S.A., 109 (2012), pp. 5185-5189

[69] Blasing, T. J., Recent Greenhouse Gas Concentrations, Environmental System Science Data Infrastructure for a Virtual Ecosystem (ESS-DIVE) (United States); Carbon Dioxide Information Analysis Center (CDIAC), Oak Ridge National Laboratory (ORNL), Oak Ridge, TN (United States), doi:10.3334/CDIAC/atg.032.

[70] P.S. Ortiz, D. F-Orrego, S. de Oliveira J., R. M. Filho, P. Osseweijer, J. Posada, Unit exergy cost and specific CO2 emissions of the electricity generation in the Netherlands, Energy, 208, 2020

[71] P. Karvounis, M. J. Blunt, Unconstrained Extraction of Fossil Fuels and Implication for Carbon Budgets under Climate Change Scenarios. Journal of Fluid Flow, Heat and Mass Transfer

Volume 8, Year 2021, DOI: 10.11159/jffhmt.2021.009

[72] S. De Simone, S.J. Jackson, S. Krevor, The error using superposition to estimate pressure during multi-site subsurface CO_2 storage, Geophysical Research Letters, 46, 6525-6533

[73] M. Bentham, An assessment of carbon sequestration potential in the UK – Southern North Sea case study, Tyndall Centre for Climate Change Research Working Paper 85, January 2006

[74] N. Heinemann, M. Wilkinson, G.E. Pickup, R.S. Haszeldine, N.A. Cutler, CO2 storage in offshore UK Bunter Sandstone Formation, International Journal of Greenhouse Gas Control, 6, 210-219, 2012

[75] K.L. Anthonsen, P. Aagaard, P.E.S. Bergmo, M. Erlström, J.I. Fareide, S.R. Gislason, G.M. Mortensen, S.Ó. Snæbjörnsdottir, CO2 Storage Potential in the Nordic Region, Energy Procedia, Volume 37, 2013, Pages 5080-5092, ISSN 1876-6102, https://doi.org/10.1016/j.egypro.2013.06.421.

[76] Eva K. Halland, Ine Tørneng Gjeldvik, Wenche Tjelta Johansen, Christian Magnus, Ida Margrete Meling, Stig Pedersen, Fridtjof Riis, Terje Solbakk, Inge Tappel, CO_2 Atlas storage, Norwegian North Sea, Norwegian Petroleum Directorate, Norway

[77] Stefan Bachu, Review of CO2 storage efficiency in deep saline aquifers, International Journal of Greenhouse Gas Control 40 (2015) 188–202

[78] CO_2 thermodynamic properties available at: https://www.ohio.edu/mechanical/thermo/property_tables/co2/

[79] N. I. Gershenzon, R. W. Ritzi, D. F. Dominic, E. Mehnert, R. T. Okwen, Capillary trapping of CO2 in heterogeneous reservoirs during the injection period, International Journal of Greenhouse Gas Control, Volume 59, 2017, Pages 13-23,

[80] H. Emami-Meybodi, H. Hassanzadeh, Christopher P. Green, Jonathan Ennis-King, Convective dissolution of CO2 in saline aquifers: Progress in modeling and experiments, International Journal of Greenhouse Gas Control, Volume 40, 2015, Pages 238-266

[81] C. Xia, M. Wilkinson, The geological risks of exploring for a CO2storage reservoir, International Journal of Greenhouse Gas Control, Volume 63, 2017, Pages, 272-280

[82] P. Ringrose, Geological Storage of CO2: Processes, Capacity and Constraints In: How to Store CO2 Underground: Insights from early-mover CCS Projects. SpringerBriefs in Earth Sciences. (2020) Springer, Cham. https://doi.org/10.1007/978-3-030-33113-9_2

[83] Bergur Sigfusson, Sigurdur R. Gislason, Juerg M. Matter, Martin Stute, Einar Gunnlaugsson, Ingvi Gunnarsson, Edda S. Aradottir, Holmfridur Sigurdardottir, Kiflom Mesfin, Helgi A. Alfredsson, Domenik Wolff-Boenisch, Magnus T. Arnarsson, Eric H. Oelkers,

Solving the carbon-dioxide buoyancy challenge: The design and field testing of a dissolved CO2 injection system, International Journal of Greenhouse Gas Control, Volume 37, 2015, Pages 213-219,

[84] Aaron L. Goater, Branko Bijeljic, Martin J. Blunt, Dipping open aquifers—The effect of top-surface topography and heterogeneity on CO2 storage efficiency, International Journal of Greenhouse Gas Control, Volume 17, 2013, Pages 318-331,

[85] https://www.globalwarmingindex.org/

[86] M. D. Aminu, V. Manovic, A modelling study to evaluate the effect of impure CO2on reservoir performance in a sandstone saline aquifer, Helyion, Volume (6), 2020